Turning the tide: The effect of river discharge on estuary dynamics and equilibrium

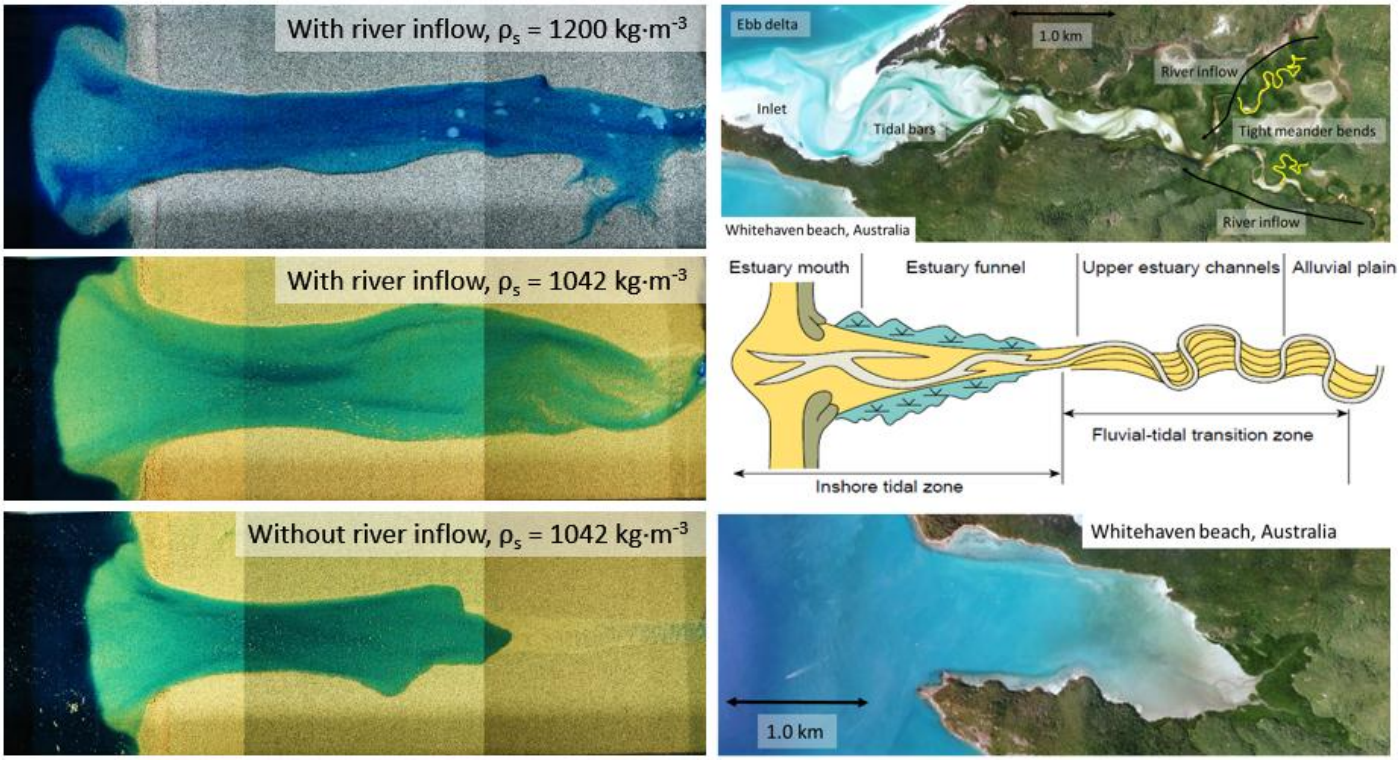

MSc thesis

Leuven, J.R.F.W.
Student number: 3471926
September 2013 – May 2014

Utrecht University, Department of Physical Geography
Utrecht, The Netherlands

Master: Earth surface and water
Track: Coastal dynamics and fluvial systems
Supervisors: Dr. M.G. Kleinhans & Dr. M. van der Vegt
Technical support: C. Roosendaal, H. Markies & M. van Maarseveen

Contents

Thesis outline

The most important terminology for this research is given in the definitions paragraph (1.1). After this, in the problem definition (1.2), I will state what my main target is – the effect of river flow on estuary morphodynamics – and describe the relevance of this topic (1.3). To assess this, I will first use a review of classifications and present knowledge on estuary dynamics to construct hypotheses (1.4-1.6). Thereafter, I elaborated on the hypotheses concerning large-scale estuary planform and dimensions for which I used a simplified behaviour-oriented model of an equilibrium estuary (2.2; 2.3). The results are presented in paragraph 2.4. Subsequently, all hypotheses were tested in scaled laboratory experiments. First previous laboratory experiments are reviewed (2.5) and the common problem with scaled laboratory experiments – scaling issues and approach – are addressed (2.6). Then the experimental method used in my research is described (2.7-2.10). Chapter 3, 4 and 5 comprise the experimental results, discussion and main conclusions. All chapters are stand alone and can thus be read separately.

For a reader with limited amount of time the following sections are suggested: problem definition and approach (1.2), qualitative hypotheses (1.6), methodology (2.1), hypotheses on gross properties of estuaries (2.4), experimental setup and conditions (2.8; 2.9), figures in the results (3), discussion (4.1; 4.2; 4.3) and conclusions (5).

For a reader with little knowledge on the subject the following sections are suggested: introduction (1), methodology (2.1), hypotheses on gross properties (2.4), experimental setup and conditions (2.8; 2.9), results (3) and conclusions (5).

Abstract

The impact of human intervention on long-term morphological evolution of estuaries is unknown. Numerical models fail to predict natural dynamics and are sensitive to constitutive parameters. On the other hand, physical models were hampered by scaling problems in the past century. Recently, is has been discovered that a periodically tilting flume generates dynamic tidal morphology. This enables experimental investigation to complement numerical modelling.

I studied the effects of upstream river discharge on the small-scale channel-shoal dynamics and large-scale equilibrium planform and dimensions of estuaries. A behaviour-oriented model was used to predict the effect of river discharge on equilibrium dimensions of estuaries. The model results were further tested in scaled laboratory experiments in which I systematically varied the amount of river inflow. Typical values of river flow velocity divided by tidal flow velocity were 0.015-0.030. Tilting amplitude was 3-4 mm with a flume of 3.8 m length.

River inflow increases the width of the upper estuary and estuary mouth, resulting in larger total surface area and larger tidal prism. Furthermore, river inflow increases small-scale dynamics of estuaries, particularly migration and shifting of channels and reversals in ebb and flood dominance of channels. This shows that river inflow is one of the key drivers for estuarine morphodynamics and must be included in any long term prediction. The results of this study have economic and ecological implications for management of estuaries, including dam construction, land reclamation and mining activities, as well as scientific implications for example for palaeoreconstruction of the Rhine-Meuse delta.

Key words: estuary; river; tides; tidal channel; tidal system; morphology; equilibrium; dynamics; experiment; scaling; behaviour-oriented model; tilting flume; scour holes.

Manuscript submitted: May 19th, 2014

1. Introduction

1.1 Definitions

Tidal systems and estuaries cause astonishing patterns (Fig. 1). An estuary is a partially enclosed body of water with at the landward boundary inflow of river water and at the seaward boundary an open connection to the sea where tides can enter. Estuaries from all over the world show a wide variety of shapes and patterns. Sediment transport causes the formation of channels, shoals and salt marshes (Fig. 1). All these features together are called the morphology of the system. The large amount of morphological processes involved in tidal systems and estuaries causes the variation in tidal systems. Among these processes are tidal currents, rivers, waves, ecology and humans (Karunarathna & Reeve, 2008; Reeve & Karunarathna, 2009; Coco et al., 2013; Kleinhans, 2013).

Different definitions and classifications were made over de past decades (Pritchard, 1967; Hume & Herdendorf, 1988; Davidson et al., 1991; Dalrymple et al., 1992; Perillo, 1995; Townend et al., 2000; Defra, 2002; EastSim Consortium, 2007). For example, the classification used for a geochemical analysis of estuaries is different from a geomorphological study. An example of a definition usable for biological and geochemical processes is the definition by Pritchard (1967), who defines an estuary based on salinities which are measurably diluted (ranging from 0.1% to 3.5%). This study regards the effect of river flow on the dynamics, equilibrium and morphology of estuaries. For this reason, the definition proposed by Perillo (1995) is better suitable:

> *An estuary is a semi-enclosed coastal body of water that extends to the effective limit of tidal influence, within which sea water entering from one or more free connections with the open sea, or any other saline coastal body of water, is significantly diluted with fresh water.*

This definition can be adjusted slightly based on the locations where estuarine deposits can be found (Dalrymple et al., 1992). Combining and stretching both definitions, I define the upstream end of the estuary as the limit of periodically flow reversal induced by tides. In the river reach upstream of the estuary, water movement is directed seaward, while in the estuary flow reverses over a tidal cycle. A reversal of water flow causes a periodically changing sediment transport direction, which influences the dynamics and morphology of the estuary.

Equilibrium is defined here as a state in which the large-scale gross properties of the estuary are constant. In such a state, the tidal prism, width and average estuary depth remain constant averaged over a long period of time. However, a dynamic equilibrium can exist between these fixed boundaries: small-scale dynamics of tidal channels and shoals can remain (Fig. 1), while the gross properties remain constant (Chorley & Kennedy, 1971).

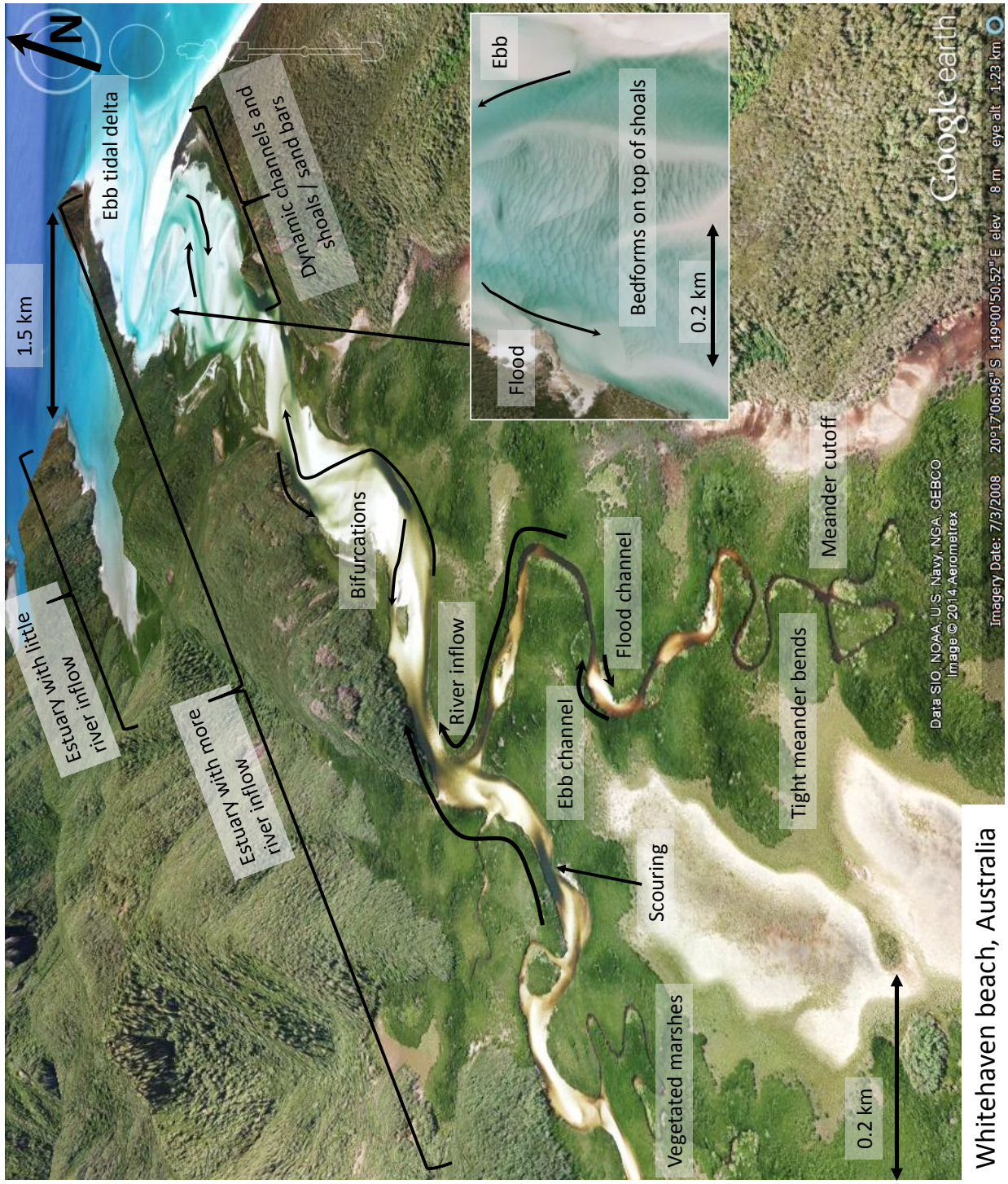

Fig. 1: Overview of definitions and morphological elements indicated on the estuary of Whitehaven beach (Australia) (Google Earth).

1.2 Problem definition and research approach

The prediction of the long-term evolution of tidal systems is still limited in mechanisms that describe the natural dynamics of channel-shoal systems and its response to human interference. This is due to (1) the large variety of drivers and their relative effect on the morphology, (2) a lack of analysis of dimensions and dynamics over a wide range of scales and systems, (3) theoretical and practical challenges in numerical models and scaled experimental approaches (Coco et al., 2013; Kleinhans, 2013; Kleinhans et al., 2014b).

Therefore, also the effect of river inflow on equilibrium morphology and dynamics of estuaries is unknown. Few studies regarded the role of river inflow on estuarine morphology and these studies showed contrasting results. For example Reeve & Karunarathna (2009) considered river inflow insignificant, because the final state of their model resembled the situation without river flow and the intermediate stages were only slightly different. Davies & Woodroffe (2010) analysed Australian estuaries and found that river discharge affects the convergence of the estuary channel, which corresponds to earlier ideas of Savenije (2005). Todeschini et al. (2005) also found in a 1D model approach that the estuary width profile was only exponential when the estuary received fluvial input upstream.

The alternative to field studies and modelling approach is experiments (Paola et al., 2009; Kleinhans et al., 2010c). About a century ago, Reynolds (1889, 1890, 1991) added river discharge to his scale experiments of tidal systems to create estuaries. He observed different patterns of shoals and channels compared to the experiments without river flow. More recently, more studies focussed on the morphology of tidal systems using an experimental approach (Mayor-Mora, 1977; Tambroni et al., 2005; Stefanon et al., 2010; Vlaswinkel & Cantelli, 2011; Kleinhans et al. 2012, 2014b; Iwasaki et al., 2013). While these laboratory experiments showed that it might be possible to reproduce aspects of natural behaviour, patterns and equilibrium states of tidal systems, major scaling issues remained.

Examples of scaling issues are the occurrence of scour holes and static equilibria. Scour holes dominate the morphology of experiments under hydraulic smooth conditions (Kleinhans et al., 2014c). The evolution to a static equilibrium without dynamic channels and shoals occurs when sediment mobility is too low during flood flows (Kleinhans et al., 2012). Kleinhans et al. (2012) solved these problems with a periodically tilting flume, which generates dynamic tidal morphology by periodic reversal of the bed sediment flux. This approach enables significant sediment transport in the flood direction, which was low in previous attempts in which the water level at the downstream boundary was periodically varied. Furthermore, Kleinhans et al. (2012) used light-weight sediments to increase sediment mobility, mixed with a coarse sediment fraction to prevent hydraulic smooth conditions from occurring. The novel approach opens up experimental investigation to complement numerical modelling for estuarine research.

This research focuses on the equilibrium conditions of estuaries and their bifurcating channels. The main question is: what is the effect of upstream river discharge on the small-scale channel-shoal dynamics and large-scale equilibrium planform and dimensions of the full estuary? I hypothesise that fluvial inflow (1) enhances dynamic shifting of ebb and flood tidal channels and (2) increases the width, depth and tidal prism of estuaries depending on the fluvial flow velocity relative to tidal flow velocity.

These hypotheses are elaborated after a review of present knowledge of large-scale and small-scale morphology of estuaries. A behaviour-oriented model is then used to extend the hypotheses on equilibrium morphology (Townend, 2010). Subsequently, hypotheses are tested, using the recent advances in the experimental approach (Kleinhans et al., 2012). In scaled laboratory experiments, I will systematically vary the amount of river discharge and the tidal tilting amplitude (tidal current velocity) to study the role of river discharge on estuary equilibrium and dynamics.

1.3 Relevance

Long-term understanding of estuarine morphology has a large societal as well as economic relevance (Wang et al., 2012; Coco et al., 2013). While the morphological patterns of rivers are relatively well understood, we lack knowledge of sediment transport and morphology in estuaries – probably because reversing flow (ebb and flood) causes complicated water flows. This resulted in a critical knowledge gap on the future development of these systems (Coco et al., 2013) and palaeoreconstruction of estuarine systems such as parts of the Rhine-Meuse delta and the Oer-IJ estuary (Berendsen & Stouthamer, 2000, 2001, 2002; Vos et al., 2011). Estuaries are valuable systems from various perspectives including ecology, shipping and land use (Wang et al., 2012; Coco et al., 2013). The core issue in all cases is long-term prediction of estuarine morphology.

Coastal environments host large urbanized settings, by which they became subject to intense anthropogenic pressure (Coco et al., 2013) and nowadays can be heavily engineered. Examples of human impact are: dam construction, land reclamation, mining activities resulting in land subsidence and dredging and dumping activities (Wang et al., 2012; Coco et al., 2013; Kleinhans, 2013). The economic and ecological value of estuaries conflict. Dredging activities to maintain shipping fairways and global sea level rise caused habitat losses and increased flooding risk (Wang et al., 2012). Meanwhile, the economic crisis reduced investments in nature rehabilitation (Kleinhans, 2013). Additionally, the effect of river flow on estuarine morphology is unknown. Future climate change, which modifies discharge regime (Van Vliet et al., 2013), might disturb system dynamics and pose additional flooding danger.

Concluding, there is a scientific, economic and ecological desire to understand the small-scale dynamics of channel-shoal systems and large-scale dimensions of estuaries. The key question in my research is: what is the effect of river inflow on these properties? To unravel this with field experiments, it would be required to control the amount of river discharge upstream of the Thames estuary (UK) or the Western Scheldt estuary (NL) (Fig. 2a). However, besides the impossibility to control river discharge, other major problems are:

- The time for a natural system to respond to a change in for example river discharge is in the order of a few human generations;
- The effects on the morphology of the estuary are unknown, which might cause problems related to shipping, harbours and land use;
- It is impossible to control all other natural factors, such as sea level rise, tidal conditions and vegetation growth and human influence. This makes isolation of boundary conditions (river discharge in this case) impossible.

To overcome these problems, I will use a simplified numerical model of an equilibrium estuary and experiments to study the effect of river discharge on estuarine morphology (Fig. 2bcde).

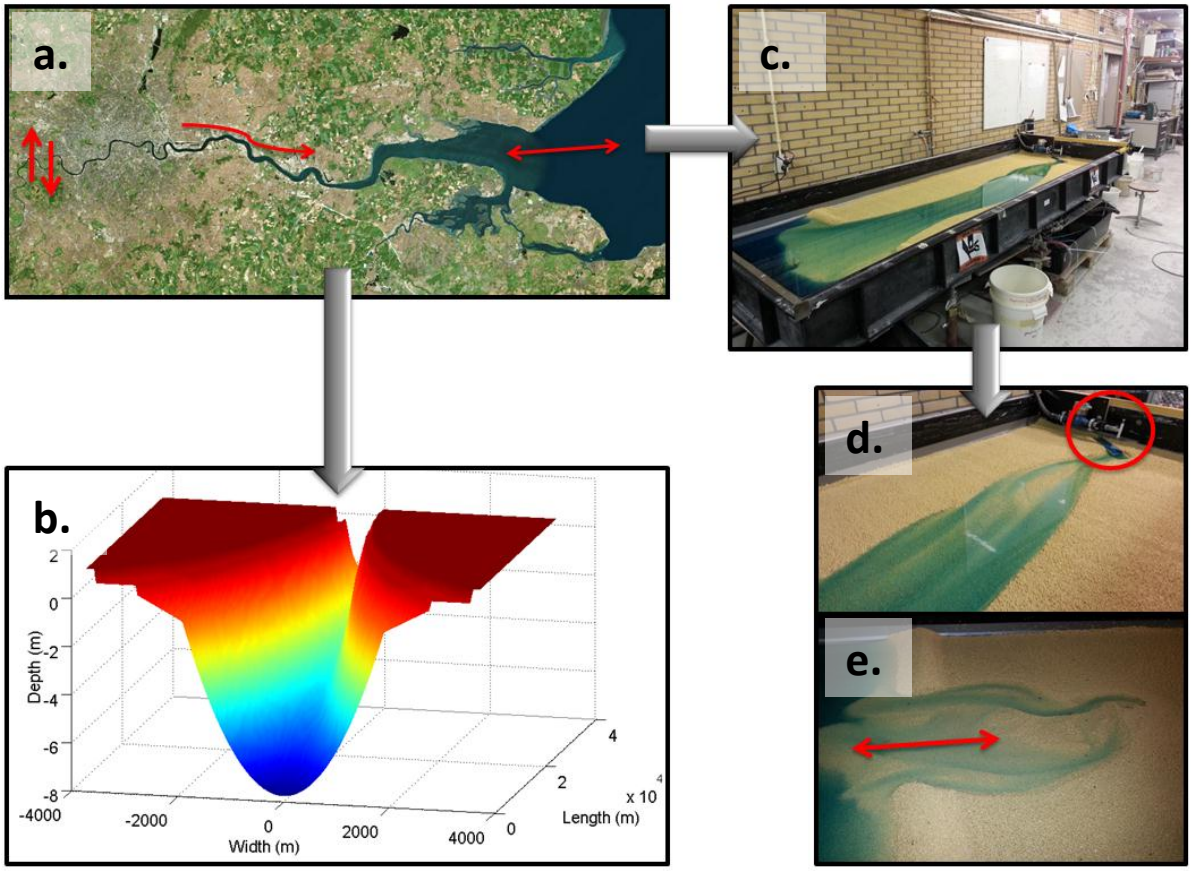

Fig. 2: Research approach. Increasing or decreasing river discharge in the Thames estuary (a) is impossible (Bing Maps Aerial © 2012 DigitalGlobe). For this reason I use a model approach (b) and scaled laboratory experiments in a flume (c) to determine the effect of river discharge on estuary dynamics and equilibrium. A tap determines river discharge in the experiments (d), while a tilting flume creates tides rushing in and out (e).

1.4 Review of large-scale planform, dimensions and equilibria

Many classification schemes exist for estuaries (Pritchard, 1967; Hume & Herdendorf, 1988; Davidson et al., 1991; Dalrymple et al., 1992; Townend et al., 2000; Defra, 2002; EastSim Consortium, 2007). Generally, the classes are based on one or more of the following: tides, waves, rivers, sediment types, vegetation, geology and time.

The main target of this research is the effect of river flow on estuary morphodynamics. A review of classifications will show the current knowledge of estuaries and the role of river discharge herein. I will assess the possible impacts of river inflow on large-scale planform, dimensions and equilibria in this section. The next section (1.5) focusses on the small-scale dynamics of channels and shoals. Together, these sections will provide a source of inspiration for qualitative hypotheses concerning the effect of river flow on estuarine patterns, dynamics and equilibrium.

These sections are required to interpret and discuss the results of the laboratory experiments. The classifications group and describe estuaries, which helps referring to these classes later on in this research. Besides, the discrimination between the different classes might be important if a mechanism or predictor works only for a specific range of estuary types. Finally, it will give a reference background which I will use to compare my experiments with natural systems.

Classifications

Most recent classifications only regarded river influence as the formative process of the valley, which flooded later to form an estuary (Hume & Herdendorf, 1988; Davidson et al., 1991). While in this case the present day influence of river flow is thus independent of estuary type, it is still relevant for this study: it shows the variety of planform patterns and helps to define the estuary type I will create in the experiments. Furthermore, the dataset with UK estuaries (Manning, 2012) used later on in this study is classified with the classification proposed by Davidson et al. (1991).

Davidson et al. (1991) described, based on formative process and topology, the following classes: fjord, fjard, ria, coastal plain, bar built, complex, embayment (Table 1; Fig. 3). All these classes of estuaries have characteristic shapes and patterns. For example fjords and complex estuaries are strongly bound by hard-rock geology (Fig. 3bf). Also the rias have a distinct dendritic pattern that reflects the river incision before the valley flooded by sea level rise (Fig. 3c). Most other systems are located in erodible low land areas, characterised by soft sediments in which channel and shoal patterns become visible (Fig. 3adeghi): the type of systems regarded in this research. From visual observation of soft sediment systems (Fig. 1; Fig. 3; Manning, 2012), I hypothesise that estuaries with minor influence of rivers are wide and short. River influenced systems tend to become more narrow and longer.

Table 1: Estuary classification based on formative processes and topology, adopted from Davidson et al. (1991).

Class	Geomorphology	Topology	Example
Fjord	Drowned glacial valleys	Deep inner basins, shallow entrance sills	Fig. 3b
Fjard	Glaciated lowland coasts	A more open coast and more irregular, short, shallow and wide than fjords	Fig. 3d
Ria	Drowned river valleys	Deep narrow channels, dendritic pattern of channels	Fig. 3c
Coastal plain	Flooding of pre-existing valleys	Very shallow, extensive salt marshes or mudflats	Fig. 3a
Bar built	Drowned river valleys	Bar across mouth because of high sedimentation rates	Fig. 3ei
Complex	Valleys drowned by a combination of factors including tectonics	Complex: much variation	Fig. 3fg
Embayment	Large natural areas formed between rocky headlands that naturally fill with soft sediments	-	Fig. 3h

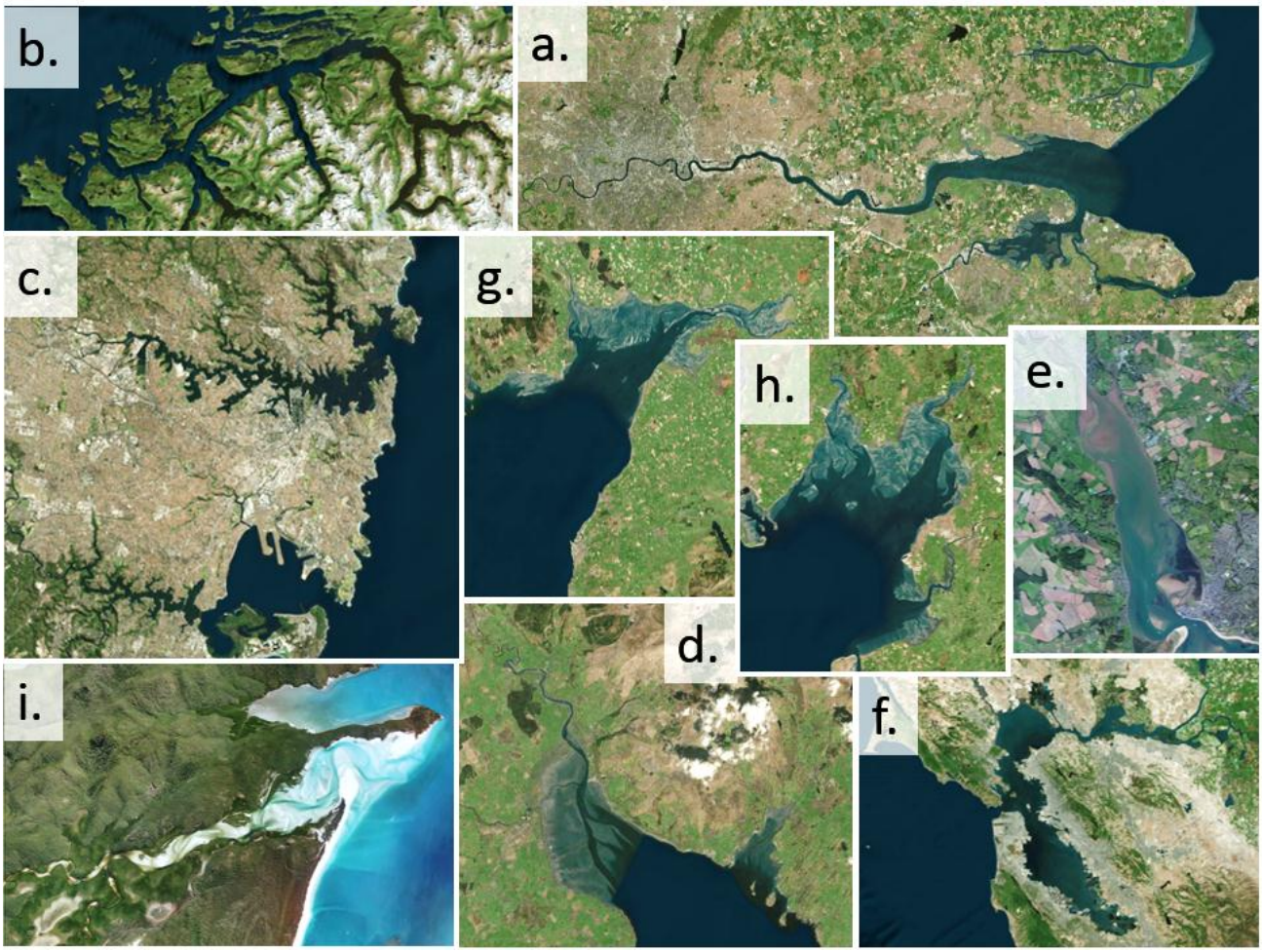

Fig. 3: Aerial photographs of (a) Thames estuary – Coastal plain; (b) Geiranger Fjord; (c) Sydney Harbour (upper) & Georges river (lower) - Rias; (d) River Cree (left) & Big water of fleet (right) UK – Fjards; (e) Exe estuary – Bar built (f) San Fransico Bay – Complex (g) Solway estuary (UK) – Complex; (h) Morecambe bay (UK) – Embayment; (i) Whitehaven beach, Australia – Bar built. (Source: (all exept (i)) Bing Maps Aerial © 2012 DigitalGlobe, (i) Google Earth © 2012 TerraMetrics (used February 2014).)

In contrast with recent classifications, the influence of rivers has been used in geological definitions of estuaries. For that reason, the geological classification is regarded here.

According to Curray (1969), most estuaries formed in river mouths flooded by the sea, which was caused by local sea level rise being larger than the sediment supply (transgression, Fig. 4a). Common geological classifications regard an estuary as a permanent sink for both terrestrial and marine sediments (Guilcher, 1967; Roy el al., 1980; Dalrymple et al., 1990). Therefore, it can be hypothesised that estuaries keep on filling under constant or slowly rising sea level. This also implies a sustained disequilibrium of estuaries. Geologists discriminate between a delta and an estuary, using the criterion that deltas have a net seaward sediment transport (Dalrymple et al., 1992).

Dalrymple et al. (1992) described physical and temporal forcing (Fig. 4). River, tides and waves are concerned physical forcing and sea level rise and sediment availability are concerned temporal. The relative importance of the physical forcing is represented with a triangle, using the system of Coleman and Wright (1975) and Galloway (1975). Deltas are positioned at the fluvial apex of the triangle, while non-deltaic coasts such as strand plains and tidal flats are at the bottom part of the triangle (waves and tides). While Dalrymple et al. (1992) further elaborate tidal and wave dominated estuaries, they leave fluvial dominated estuaries aside. Probably, fluvial dominated estuaries are considered deltas in this classification (Fig. 4b): the river only determines the filling rate of the system, without any influence on the morphology. I hypothesise that the relative role of river flow can be of significant importance: ebb and flood sediment transport may counteract each other, while sediment transport induced by the river might determine the net direction.

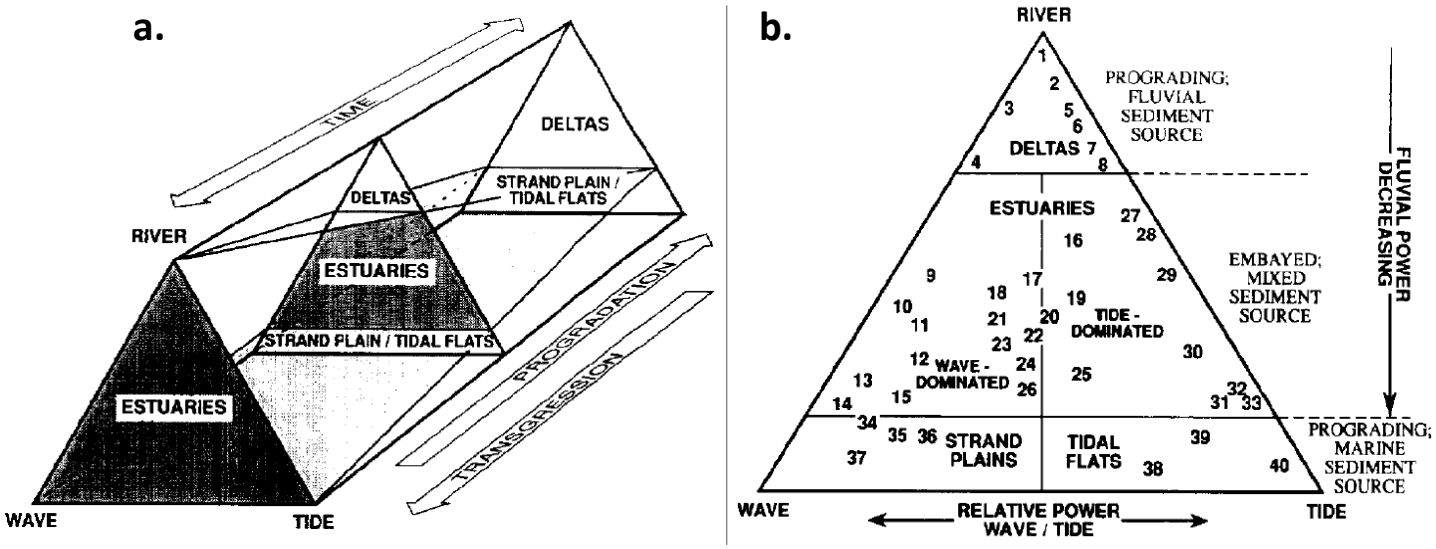

Fig. 4: Evolutionary classification of coastal environments. The edges of the triangle indicate the tree forcing mechanisms: river, tides and waves (Dalrymple et al., 1992). (a) Classification and alteration over time under transgression or progradation. The rate of sea level rise and sedimentation determine whether a system will shift to the back or front of the prism. (b) Classification of estuaries within the coastal triangle, which is in the middle of the prism. (a) Representative systems were projected on this triangle (Appendix 3, Dalrymple et al., 1992).

Recently, Martinius & Van den Berg (2011) adjusted the geological classification proposed by Dalrymple et al. (1992). Previous geological definitions implied that estuaries could only form under relative sea level rise. Furthermore, river mouths, deltas and estuaries were implied to be entirely different. The definition of an estuary was relaxed by Martinius & Van den Berg (2011):

> *The term 'estuary' principally refers to the water body (i.e. a river mouth); The term 'delta' refers to the body of accumulated sediment protruding into the water body; These two are not mutually exclusive;*
>
> *Estuaries develop during relative sea level rise and commonly occupy the seaward portions of drowned valleys. They receive sediment from both fluvial and marine sources. Accommodation is created by sea level rise and/or the removal of clastic sediment or peat by waves and currents in inshore basins.*

In contrast with the previous geological definition (Dalrymple et al., 1992), Martinius & Van den Berg (2011) hypothesised the possibility of an equilibrium estuary. An equilibrium estuary is regarded as a filled estuary (Fig. 5). The driving factor for the sedimentation of an estuary is the dissipation of (wave, tidal and river) energy in combination with the availability of sediment. An unfilled estuary has a low energy sub-tidal basin, where a lot of energy is dissipated. This results in high sedimentation rates in the central basin. In the filled estuary the time-averaged net cross-sectional sedimentation rate is very small compared to the amount of by-passing sediment. The classification of a wave-dominated mesotidal estuary is given as an example of this theory in Fig. 5.

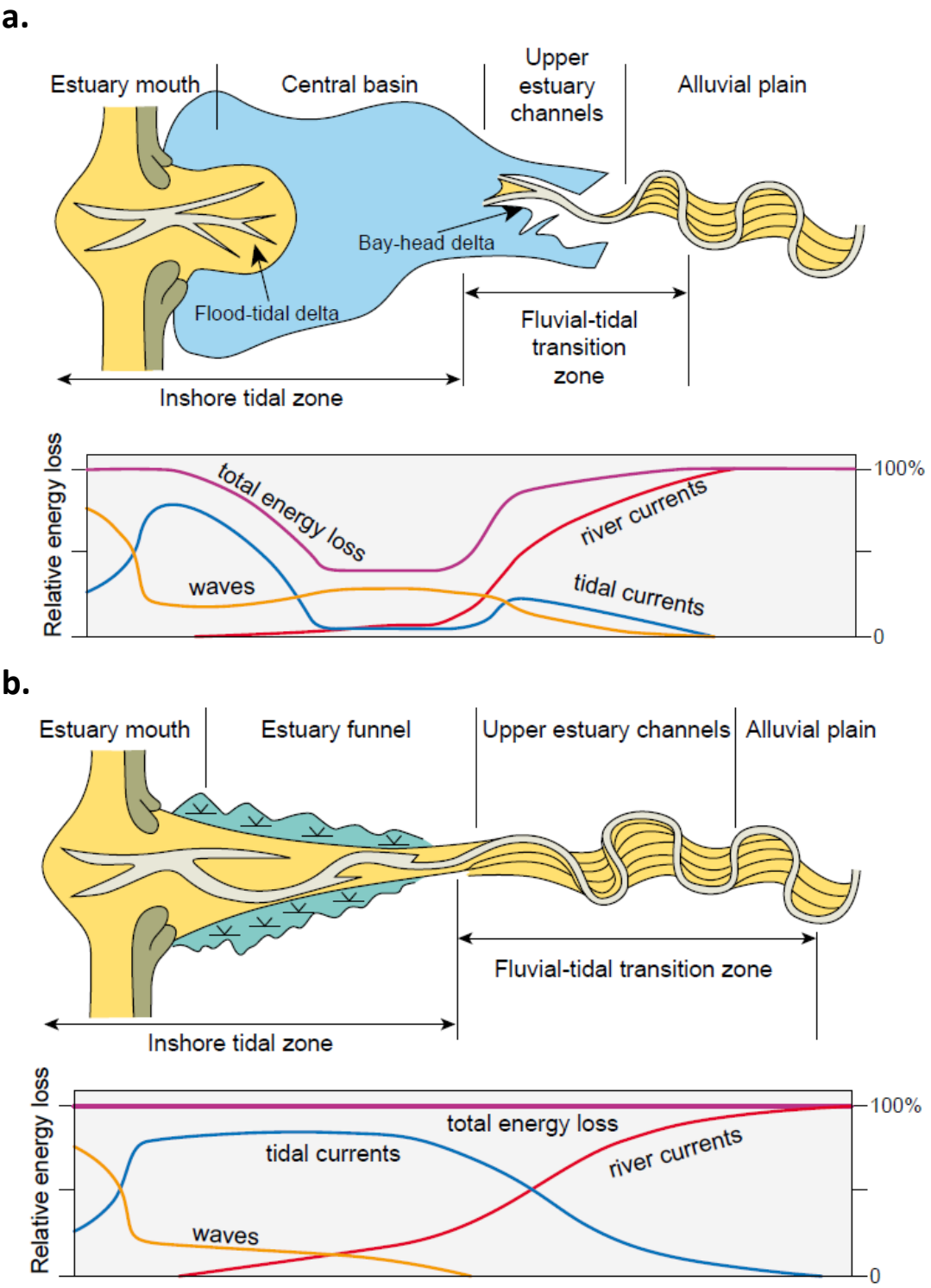

Fig. 5: Classification of morphological components in an idealized wave-dominated mesotidal (a) unfilled estuary and (b) filled estuary (Martinius & Van den Berg (2011), modified after Dalrymple et al. (1992), Boyd et al. (2006) and Van den Berg et al. (2007)). The morphology is related to the loss of hydraulic energy, because energy dissipation determines sediment dynamics rather than energy availability. Conservation of total energy results in a very small time-averaged sedimentation rate (b).

Dimensions

Previous research illustrated that river discharge can influence channel dimensions and planform of estuaries (Savenije, 2005; Todeschini et al., 2005; Davies & Woodroffe, 2010). For example Davies & Woodroffe (2010) found for Australian estuaries that river discharge affects the convergence of the channel. Likewise, river inflow might alter other large-scale dimensions – such as the total surface area – which enlarges the tidal prism. For this reason the factors that relate to estuary dimensions are discussed here.

Channel convergence and bottom friction control tidal amplitude, phase speed and relative phase difference between tidal velocity and elevation in most estuaries (Friedrichs, 2010). Convergence tends to increase the tidal amplitude, friction causes decay (Table 2; Fig. 6). When convergence dominates over friction, tidal amplitude increases along the estuary. The other way round, when friction dominates, tidal amplitude decreases along the estuary. Friedrichs (2010) described an equilibrium estuary case in which friction and convergence balance each other. He associated the uniform tidal velocity amplitude with a morphodynamic equilibrium (Friedrichs, 1995). The corresponding estuary shape is weakly to strongly funnel-shaped.

A measure of friction is the friction factor (*r*) (Friedrichs, 2010):

$$r = \frac{c_d}{<h>} \cdot \frac{8U}{3\pi} \qquad \text{(Eq. 1)}$$

In which *<h>* is the tidal average of the water depth, c_d is the bottom drag coefficient (depending on bottom roughness) and *U* is velocity amplitude.

A measure of convergence is the e-folding length (Townend, 2010). This is the length over which a variable (width, depth and area) changes by a multiple equal to the exponential function (*e*). This convergence length is calculated in:

$$W(x) = W_m \cdot exp(\frac{-x}{L_W}) \qquad \text{(Eq. 2)}$$

Where *W(x)* is the width at a specified location (*x*) from the estuary mouth. W_m is the width of the estuary at the mouth and L_W the e-folding length for width.

Friedrichs (2010) derived the balance between friction and convergence for long, intermediate depth, equilibrium estuaries:

$$\frac{r}{\omega} = \frac{{L_W}^{-1}}{k} \qquad \text{(Eq. 3)}$$

In which ω is tidal frequency and *k* is wavenumber.

Concluding, a balance between channel convergence and friction exists. River discharge can affect water depth and flow velocity, which determine the friction factor. For that reason, I hypothesise that river inflow can influence channel convergence. If the large-scale dimensions are altered – such as surface area, width and depth – also the tidal prism might be influenced by river flow. For example, Eysink (1990) described an empirical relation between cross-sectional area and the tidal prism (Eq. 22).

Table 2: Estuary classification based on a balance of friction and convergence (Nichols and Biggs 1985; Dyer, 1995).

Name	Characteristic	Reason	Example
Amplified (hypersynchronous)	Increasing tidal range in landward direction	Convergence > friction	Scheldt (Netherlands); Humber, Thames (UK)
Ideal (synchronous)	Constant tidal range up to river reach	Convergence = friction	Elbe (Germany); Delaware (UK)
Damped (hyposynchronous)	Decreasing tidal range in landward direction	Convergence < friction	Rotterdam Waterway (Netherlands); Mekong (Vietnam)

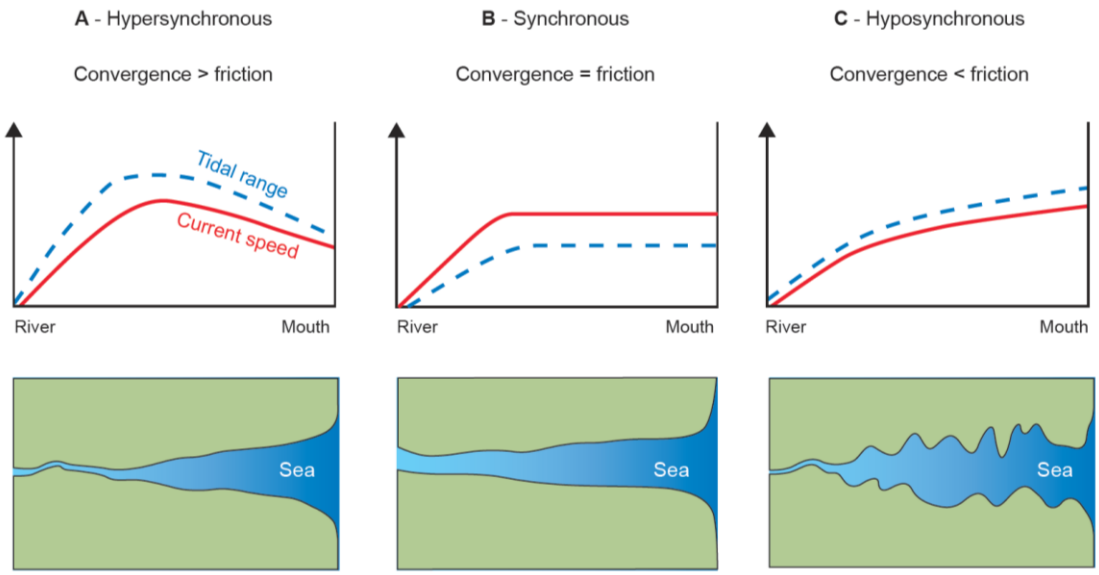

Fig. 6: The effect of friction and convergence on tidal range and velocity. Corresponding estuary shapes are indicated below the graphs (from Martinius & Van den Berg, 2011).An explanation of the terminology is given in Table 2.

1.5 Review of small-scale dynamics of channels and shoals

One of my targets is to assess the effect of river discharge on small-scale dynamics of estuaries. The first step is to describe the current theories for channels and shoals. Schramkowski et al. (2004) described a novel theory on estuarine channel-shoal patterns, which shows whether a system becomes meandering or braided. However, the theory for river channel and bar patterns is much further developed by Kleinhans & Van den Berg (2011) and it might contain key concepts for unraveling estuary channel-shoal dynamics and patterns. After all, both estuary and river patterns are determined by a balance between shoal or bar build-up and break-down

First, the characteristic ebb- and flood channels and extreme meanders observed in estuarine systems are described. Thereafter, the preliminary theory for esturary bar pattern and the more developed theory for river bar pattern are discussed.

Channel-shoal system patterns

Van Veen (1950) described ebb and flood channels ("ebschaar" and "vloedschaar"), which are tidal channels primarily open to either ebb or flood currents. A flood channel is characterised by a sill at the upstream end of the channel, while an ebb channel exhibits a sill at the seaward end (Fig. 7). The driving mechanism is still unknown, but Van Veen (1950) described that the sills were caused by opposing sand fluxes from the ebb and the flood channel. Van Veen (1950) remarks that it can be difficult to distinguish an ebb channel from a flood channel; it is possible that a channel has a sill on either side of it (landward and seaward). He hypothesises that such a channel is cut-off from the system and eventually may silt up.

The first hypothesis on the dynamics of tidal channels was based on tidal prism, meander action and sand transport. Nowadays, the meandering factor described by Van Veen (1950), might be described with a combination of the effects of spiral flow, transverse bed slope effect and non-linearity of sediment transport (Kleinhans & Van den Berg, 2011).

Tidal and estuarine networks have a channel network that respectively resembles the shape of an apple-tree and a slim poplar (Van Veen, 1950) (Fig. 8). Van Veen shows some interpretation on the difference between basins dominated by tides only (Fig. 8b) and both river and tide dominated (thus estuarine) systems (Fig. 8ac). The occurrence of ebb and flood tidal channels is visible in both type of systems. However, the mechanisms that drive the channel and shoal patterns might be very different (Green & Coco, 2007) and are relatively unknown compared to mechanisms in rivers.

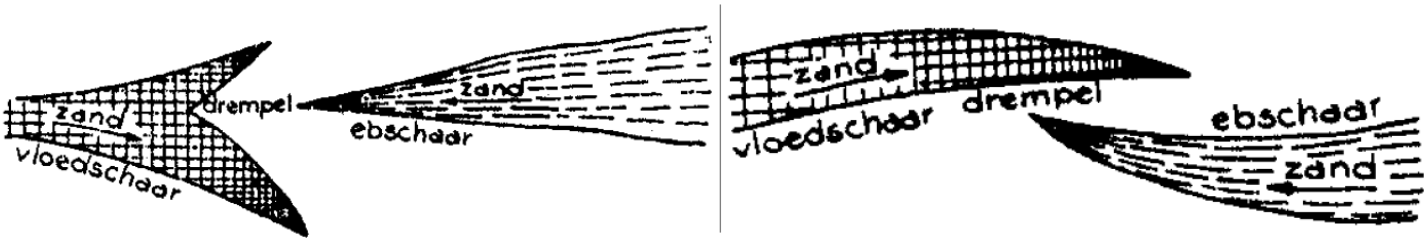

Fig. 7: Sketch of the mutual "evasion" of ebb and flood tidal channels by means of (a) a forked tongue and (b) flank attack (Van Veen, 1950) ('drempel' = sill).

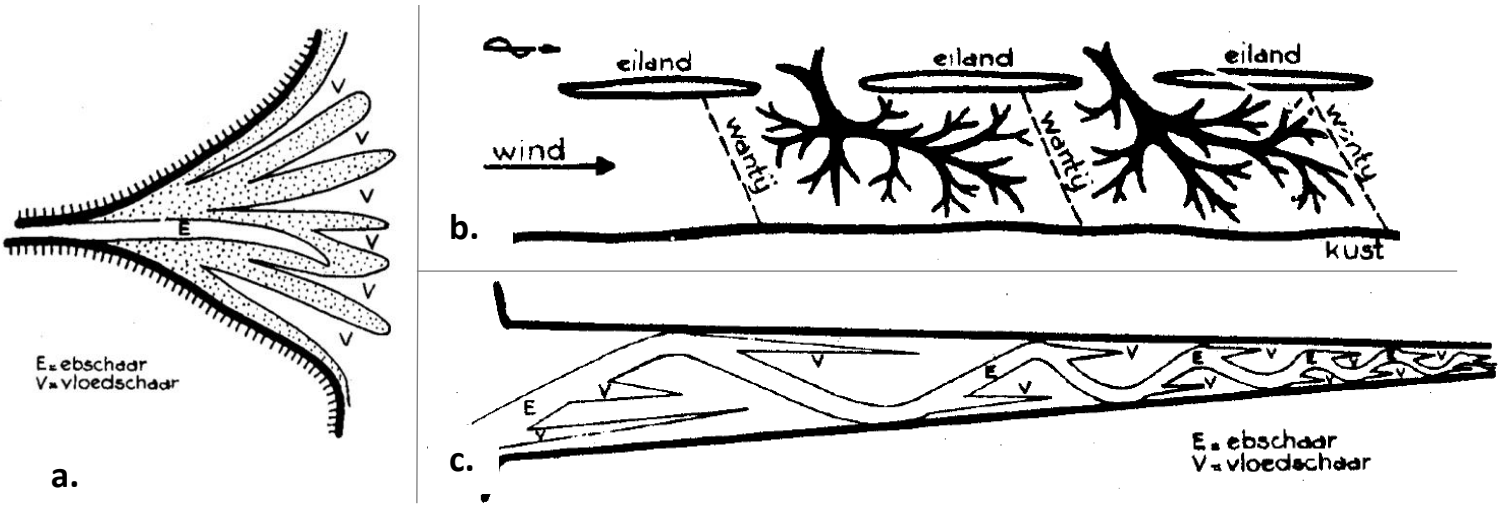

Fig. 8: Sketch of ebb and flood channels in (a) a wide estuary (e.g. the Thames or Wash). Channel migration may bring the ebb channel in connection with any of the flood channels. (b) The Frisian short tidal basins: apple-tree shaped channel system. (c) An ideal system of ebb and flood channels (Scheldt estuary): sine shaped main ebb channel, flood channels starting in each bend (Van Veen, 1950).

Dalrymple et al. (1992) described the morphology of the fluvial-tidal transition of an estuary. A sequence of fluvial patterns characterises this river reach: straight-meandering-straight (Fig. 9; Fig. 3a; Fig. 5). The meandering part consist of tight meanders with symmetrical point bars. Dalrymple et al. (1992) hypothesised that the meandering part relates to the location of net bedload convergence. They elaborated on the sediment grain sizes, which fine towards the meander bends from both directions, and channel gradient, which decreases in this zone.

Kleinhans (2013) identified the extreme meanders – far too large for the landward river – as a critical knowledge gap on estuaries. He seeks a theory for equilibrium dimensions of tidal bars, because these features affect how estuaries sedimentate and circulate. In addition to the discussion of Dalrymple et al. (1992), experiments of meandering rivers showed that cohesive floodplain formation is required for meandering (Van Dijk et al., 2012), which implies the importance of mud deposition. Kleinhans (2013) proposed to test the effect of channel dimensions (width to depth ratio), river discharge and mud deposition on the meandering pattern.

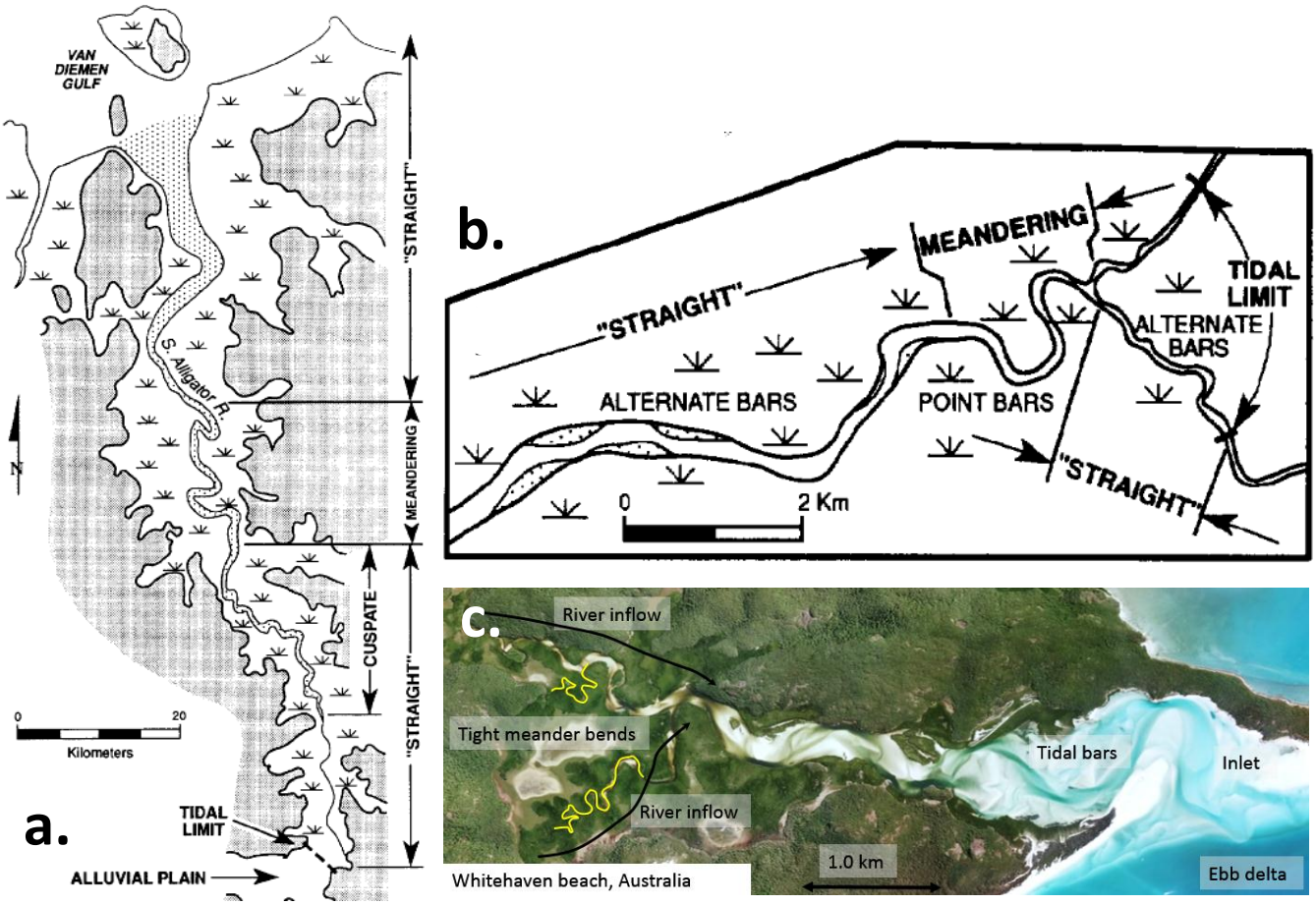

Fig. 9: (a) Map of the South Alligator River estuary shows the straight-meandering-straight channel pattern. The cuspate reach was formerly meandering, but the meanders moved seaward as a result of estuary filling (Dalrymple et al., 1992). (b) The inner portion of the Cobequid Bay-Salmon River estuary shows the longitudinal changes in channel morphology and bar type (Dalrymple et al., 1992). (c) Tight meanders bends in the Whitehaven beach estuary, Australia (Google Earth).

Bar pattern theory

Some pioneering theories are available on the occurrence of channel-shoal patterns in tidal channels. Schramkowski et al. (2002, 2004) performed a linear (2002) and a non-linear (2004) stability analysis to determine how initial perturbations behave under a tidal flow over a horizontal bed. They analysed whether initial perturbations grow or damp using a linear stability analysis (Scharmkowski et al., 2002). Morphological response to perturbations can be highly non-linear. Therefore, they used a non-linear morphological model to find out which patterns emerge as a result of initial perturbation and if they are stable (Scharmkowski et al., 2004). They assessed the sensitivity of channel and bar pattern to friction, channel width, channel depth and tidal excursion length (Schramkowski et al., 2002; Schramkowski et al., 2004). Generally, they found that wider channels result in more braided patterns. Lower friction and deeper channel resulted in more meandering patterns. The tidal excursion length – which is the distance a water particle travels in half a tidal cycle – appeared to be important for the distance between the locations of bar formation.

Concluding, it is possible to use stability analysis to determine whether the channel pattern is braided or meandering if the channel properties are known. However, so far it was assumed that channel banks are non-erodible in the models of Schramkowski et al. (2002, 2004). My study concerns the erodible soft sediment systems, which makes these theories partly unsatisfactory. Furthermore, the physics used in their models is simplified and it is impossible to predict the different types of bars found in estuaries. For these reasons, I will now regard the more developed theory for river patterns and use both theories to construct qualitative hypotheses on the effect of river flow on estuaries.

Width to depth ratio is an important factor to determine channel and bar patterns in rivers (Kleinhans & Van den Berg, 2011) and I hypothesise that this can also be an important factor in estuary patterns. The original theory for rivers (Kleinhans & Van den Berg, 2011) was based on an empirical classification and a theoretical predictor:

$$\omega_{pv} = \frac{\rho g Q S_v}{W_r} \qquad \text{with } W_r = \alpha\sqrt{Q} \qquad \text{(Eq. 4)}$$

In which ρ is water density, g is gravitational acceleration, S_v is valley slope, W_r is reference channel width, Q is channel-forming discharge (mean annual flood or bankfull discharge) and α is a constant (with a general value between 3 and 5) (Kleinhans & Van den Berg, 2011).

They concluded that an increase in potential-specific stream power results in more power to erode banks. This corresponds to the rivers with high width to depth ratio – relatively wide and shallow. From bar theory, it follows that relatively wide rivers develop more bars across the width and are classified as braided. In contrast, rivers with low stream power (and low width to depth ratios) hardly develop bars or meandering and are straight, sinuous or anastomosing. In between these two extremes, weakly braided and meandering rivers are found.

There is an empirical threshold for the transition of river patterns: a threshold value of potential stream power as a function of grain size (Fig. 10a). Fig. 10b compares the empirical stream power-based classification and physics-based bar pattern predictor.

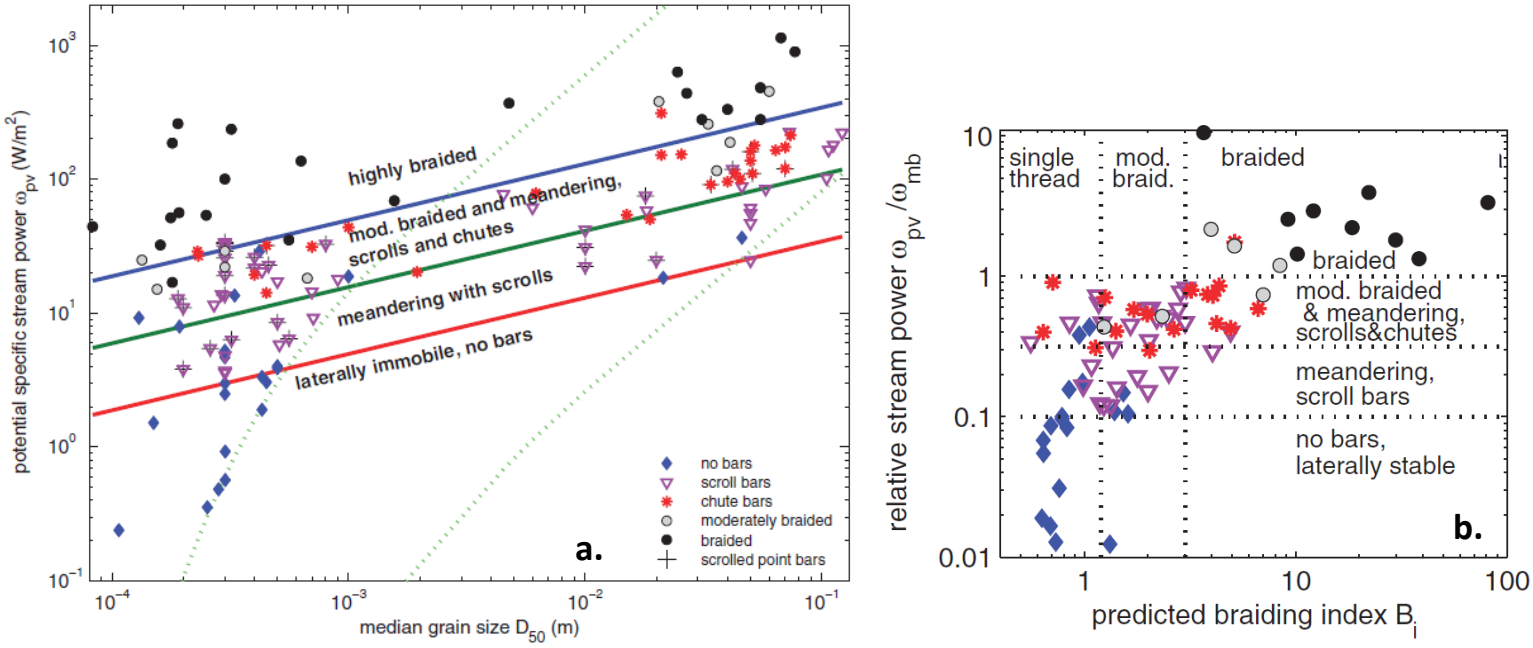

Fig. 10: (a) Classification of channel and bar pattern in rivers based on potential stream power as a function of grain size. (b) Comparison of theoretical and empirical bar pattern prediction. Stream power is divided by the empirical threshold for the meandering/braided transition on the vertical axis. The horizontal axis shows the number of parallel channels during channel-forming discharge (braiding index) predicted by bar theory (Kleinhans & Van den Berg, 2011).

1.6 Qualitative hypotheses

I constructed qualitative hypotheses based on a review and visual observations of estuaries. This extends the hypotheses proposed in the problem definition and research approach (1.2).

From visual observation of estuaries, I hypothesise that under the influence of rivers, estuaries become long and narrow, rather than wide and short (Fig. 1; Fig. 3). Davies & Woodroffe (2010) found for Australian estuaries that river discharge decreases channel convergence, which makes the estuary planform less squeezed. River discharge can affect water depth and flow velocity, which determine the friction factor. Based on the theory of Friedrichs (2010), I hypothesise that river inflow thus indeed can influence channel convergence. If the estuary length is fixed, a stronger channel convergence results in estuaries with a larger surface area.

Dalrymple et al. (1992) described that rivers, tides and waves are the physical forcing in estuaries. I hypothesise that river flow can enhance ebb flows and inhibit flood flows: a higher net seaward sediment transport is the result. Compared to the situation without river flow, I would expect that this results in larger, wider and deeper estuaries under influence of rivers. If the large-scale dimensions are altered, also the tidal prism might be influenced by river flow. The enlargement of estuary dimensions probably scales with the fluvial flow velocity relative to tidal flow velocity.

An alteration of large-scale planform and dimensions might also imply a modification of the smaller scale channel-shoal patterns. River influenced systems show more dynamic channels and bars (Fig. 1; Fig. 3). I would expect the same from bar theory for rivers and estuaries. Friction might increase if river discharge increases, because the channel becomes relatively wider and shallower. This could change the channel pattern to more braided, based on the results of Schramkowsi et al. (2004). Bar theory for river patterns also predicts more bars for wider channels (Kleinhans & Van den Berg, 2011). Bar theory thus supports the hypothesis that fluvial inflow enhances dynamic shifting of ebb and flood tidal channels.

Bank stability appeared to be an important factor for river patterns (Kleinhans & Van den Berg, 2011). A lack of cohesive floodplains and vegetation in my experiments might inhibit the formation of extreme meanders. Multiple channels and shoals will probably form in the softer erodible sediments. This opens up the posibillity to form mutually evasive ebb and flood channels in the experimental setup (Van Veen, 1950).

Waves, tides and rivers are the driving mechanisms that control estuarine morphology (Dalrymple et al., 1992). The relative role of river flow can be of significant importance on net sediment transport direction and can be determined by the amount of river discharge. If river flow induces a net seaward transport in the estuary, it is no longer a sink for both terrestrial and marine sediments (Guilcher, 1967; Roy el al., 1980; Dalrymple et al., 1990). From this, I hypothesise that fluvial input might keep the estuary open rather than silting up to become a short tidal basin.

2. Methods and materials

2.1 Methodology

So far I described the limited knowledge on the effect of river discharge on estuarine morphology – which has a large societal as well as economic relevance (Wang et al., 2012; Coco et al., 2013). In this research I determined the effect of upstream river discharge on the small-scale dynamics of channel-shoal systems and large-scale equilibrium planform and dimensions of the full estuary.

First, I elaborated on the hypotheses concerning large-scale estuary planform and dimensions. With a simplified numerical model of an equilibrium estuary, it is possible to model a wide range of conditions and study the effect of changing boundary condition, such as tides (Townend, 2010) (Fig. 2b). However, the present model of Townend (2010) excludes the effect of river discharge on estuarine morphology. The model is thus modified and used to derive hypotheses on gross properties. Subsequently, these hypotheses will be falsified with a large dataset on UK estuaries (Manning, 2012).

The hypotheses were tested in scaled laboratory experiments (Fig. 2). Novel in this research, compared to Kleinhans et al. (2014b) is the introduction of a river at the upstream boundary to create estuarine systems. While the numerical model only concerns gross properties, the experiments are also usable to study the small-scale dynamics of channels and shoals. Previous research showed that it is possible to reproduce natural behaviour of tidal systems in laboratory experiments (Reynolds, 1889, 1890, 1991; Mayor-Mora, 1977; Tambroni et al., 2005; Stefanon et al., 2010; Vlaswinkel & Cantelli, 2011; Kleinhans et al. 2012, 2014b; Iwasaki et al., 2013). Common findings and scaling problems are described in section 2.5. Thereafter, the scaling approach of this research is discussed (2.6).

One of the major scaling problems of scaled laboratory experiments is the occurrence of scour holes (Tambroni et al., 2005; Stefanon et al., 2010). For that reason, I performed scour hole experiments (Appendix 2) to determine the ideal sediment mixture for my tidal experiments (2.7). Subsequently, the experimental setup (2.8), experimental conditions (2.92.9) and the methodology for data collection, processing and data reduction (2.10) are given.

2.2 Model approach

Most behaviour-oriented models focus on predicting the end state or equilibrium of the system (Stive et al., 1998; Wang et al., 1998; Huthnance et al., 2007). Often a relationship between cross-sectional area or volume and tidal prism is used to predict equilibrium (Townend, 2010). Two challenges commonly occur: due to the empirical nature of these models, historical data is required for calibration (Coco et al., 2013) and the influence of wind generated waves and tidal flows is probably under predicted (Townend, 2010).

A behaviour-oriented model without time-stepping dynamics for the equilibrium end state of an estuary (Townend, 2010) was used in this research. Its results are based on properties that are independent of any response within the system and the intertidal flat as well as the effect of waves can be included. In short, the sediment balance equation is solved and related to a 3D estuary form that is itself a function of the hydraulics. Gross-properties, such as width and depth, are derived from the estuary 3D form.

I modified the model, such that I can study the effect of river discharge on equilibrium morphology. This model is only used for hypotheses on the large-scale dimensions, because it lacks detailed reproduction of channel networks and tidal flats. Models with faster scale interaction are used for the small-scale cases (Marciano et al., 2005; Van Maanen et al., 2013, decribed by Coco et al., 2013). I determined the hypotheses on three significant different scales: the scale of small-scale laboratory experiments, the Dutch Oer-IJ estuary and the Thames estuary (UK).

The original model (Townend, 2010)

I computed the state in which erosion and deposition balance each other – averaged over a full tidal cycle – using properties that are external to the system (Table 3). An initial premise is that estuaries have convergent channel systems and can be represented by a single convergent channel.

Table 3: Characteristic properties used to predict the gross properties of an equilibrium estuary, according to Townend (2010). The most right column describes the modifications I made to the model.

Property	**Symbol**	**Modification**
Basin area at high water	S_{hw}	
Length of the estuary (tidal limit)	L_e	
Tides		
- Tidal frequency	ω	
- Tidal amplitude (mouth)	a	
- Tidal period	T	
Grain size	D_{50}	
Dominant wind speed	U_w	Not used for predictions in this study
River discharge	Q_r	Induces a residual flow velocity that adds up to the tidal hydraulics
Critical bed shear stress	τ_{cr}	Predicted in the model based on Zanke (2003)
Average sediment concentration (supply)	c_n	Predicted in the model with Engelund and Hanssen (1967)
Erosion constant	m_e	

Three sets of equations need to be solved (Townend, 2010), to obtain an estuary depth and a flow velocity for which erosion and deposition balance each other:

I Hydraulic equations

Based on the assumptions that (1) the estuary is strongly convergent, (2) frictional damping balances the convergence of tidal energy, (3) the river flow is small compared to tidal flows and (4) the depth of the estuary (*h*) is constant; the following equations for tidal velocity (*u*) and amplitude of tidal current (*U*) are used, according to Friedrichs and Aubrey (1994):

$$u = -U \cdot sin(\omega \cdot t - k \cdot x) \quad \text{(Eq. 5)}$$

$$U = \frac{a \cdot \omega \cdot L_A}{h_s} \quad \text{(Eq. 6)}$$

In which *x* is this distance along the estuary from the mouth, *t* is time, *k* is wave number, *a* is tidal amplitude, L_A is the e-folding length of cross-sectional area and h_s is the average depth at mean tidal level including the influence of the tidal flats. See for all variables Table 3 or Appendix 1.

II Sediment balance equations

$$Erosion = deposition$$

$$m_e \cdot (\tau - \tau_{cr}) = -w_s \cdot c_n \quad \text{(Eq. 7)}$$

$$\tau = \rho \cdot c_d \cdot u^2 \quad \text{(Eq. 8)}$$

In which ρ is the density of water, τ is the bed shear stress due to the flow.

III Derivation of tidal prism equations

The tidal prism can be calculated using two different methods. The first method is integrating the discharge through the mouth of the estuary over a full tidal cycle, using the expression for flow for long channels with intermediate depth (Friedrichs, 2010):

$$P = \int_{LWS}^{HWS} Q(0,t)dt = \frac{U \cdot A_m}{2 \cdot \omega} \cdot (4 - \pi \frac{a}{h} sin(k \cdot L_A)) \quad \text{(Eq. 9)}$$

In which *HWS* is high water slack and *LWS* is low water slack.

The second method to calculate tidal prism uses the width at the mouth and the degree of convergence in combination with the tidal amplitude (Savenije, 2005):

$$P = 2acos(\varphi) \cdot \int_0^{L_e} W dx = 2a\, cos(\varphi) \cdot W_m \cdot L_W \cdot \left(1 - exp\left(\frac{-L_e}{L_W}\right)\right) \quad \text{(Eq. 10)}$$

In which φ is the phase lag between high water and high water slack. In Eq. 9, this phase lag was assumed to be zero.

Both calculations should result in the same tidal prism. Equating these two equations (Eq. 9; Eq. 10) a relation for the convergence of width of the estuary (Townend, 2010). Assuming that the channel is long compared to e-folding length scale, Townend (2010) obtains:

$$L_W = \frac{1}{k} \cdot tan^{-1}\left(\frac{2\frac{a}{h}}{1 - \frac{a^2}{h}}\right) \quad \text{(Eq. 11)}$$

The derivation uses the fact that the estuary is long relative to its scale of convergence. The convergence of width and depth should balance the convergence of cross-sectional area. The convergence of width equals the convergence of cross-sectional area. Thus if the depth along the estuary is constant:

$$L_A{}^{-1} = L_W{}^{-1} + L_h{}^{-1} \quad \text{(Eq. 12)}$$

$$L_A{}^{-1} = L_W{}^{-1} \qquad \text{if depth is constant} \quad \text{(Eq. 13)}$$

These three sets of equations have three unknowns: U, h, L_W. Three equations with three unknowns can be solved, for example by finding a water depth for which erosion and deposition balance each other.

So far the depth of the estuary was taken as constant along the channel, which might be incorrect (Eq. 12; Eq. 13). I will thus underestimate the convergence of cross-sectional area (Eq. 13). To correct, the convergence of cross-sectional area is recalculated. When the cross-sectional area at the mouth, the cross-sectional area at the upstream boundary (cross-sectional area of the river) and the length of the estuary are known, this can be calculated using the inverse of the following formula:

$$A(x) = A_m \cdot exp(\frac{-x}{L_A}) \qquad \text{(Eq. 14)}$$

The cross-sectional area of the river is calculated using a river regime equation (Cao and Knight, 1996). If the slope of the river is unknown, it is approximated by the ratio between the tidal range and the distance from the mouth to the tidal limit (Townend, 2010). The cross-sectional area at the mouth of the estuary is calculated by multiplying the average depth of the full estuary with the width at the mouth.

Once the hydraulics, the sediment balance and the length scales for convergence are known, the 3D shape of the estuary can be calculated for the channel, intertidal area and marshes. This profile is a function of the hydraulics.

The subtidal channel has a parabolic shape (based on the most probable distribution of the transverse bed slope, as proposed by Cao and Knight (1997) for fluvial systems). The tidal flat profile is based on the bathymetry described by Friedrich and Aubrey (1996). Their theory describes a linear slope below mean tide level and convex above this level, such that the maximum tidal velocity over the tidal flat is uniform. The saltmarsh is added to the sub tidal channel and tidal flat profile, based on biological guidelines (Townend, 2010), but since the properties of the marshes are not used in this study, they are not further discussed here. By integrating the channel equations over the relevant interval, gross properties of the system can be computed, such as the tidal prism and the dimensions (with, depth, volume) of the estuary.

The bed profile of the estuary can be modified by the influence of wind-generated waves. The method is similar to the method described before for the calculation of the tidal channel equilibrium. After all, the balance between erosion and deposition must still remain. For a full description of this process, see Townend (2010). The influence of waves is disabled in this study.

Modifications to the original model

The original model (Townend, 2010) as described before was modified in this study to be able to study the effect of river discharge on the equilibrium state of the estuary. Furthermore, the critical shear stress and sediment concentration were originally estimated or used as calibrating parameters. After my modification the critical shear stress is calculated as a function of sediment properties. Sediment suspension and induced sediment concentration are calculated with sediment properties and flow conditions. This makes the model insensitive to an initial estimation of the critical shear stress and sediment concentration. Finally, I altered the model to allow for computations at the scale of laboratory experiments. All modifications are described below.

The equilibrium 3D profile is determined based on a balance of erosion and deposition (Eq. 7). Since higher flow velocities enhance erosion, a significant river inflow at the upstream boundary might influence the equilibrium profile. I added this to the model by performing the following loop at least five consecutive times, after the original model has been used:

(1) The flow velocity induced by the river is calculated for all the different locations along the length of the estuary by dividing the river discharge by the cross-sectional area.
(2) The arithmetic along-channel mean of all these flow velocities is calculated.

(3) This flow velocity is added to the flow velocities induced by the ebb tides and subtracted from the flood tides.
(4) The hydraulic equations, sediment balance and tidal prism relation are recalculated with the new flow velocities.
(5) A new equilibrium profile is generated and the new estuary dimensions are used to repeat this loop.

It is essential that this loop is repeated for at least five times, since an alteration of the equilibrium profile will result in an alteration of the average flow velocities and a change in flow velocities will again influence the balance between erosion and deposition.

Now, a variation in river discharge would result in a different morphology for two reasons: (1) the upstream channel geometry is determined by a river regime equation (Cao and Knight, 1996), which influences the convergence length scales (Eq. 14) and thus gross properties of the system and (2) the solution for the three sets of hydraulic equations (Eq. 5-Eq. 11) are altered by the effect of river discharge I added to the original model. The latter is the effect of interest. So to study solely the effect of river flow on the gross parameters, I kept the channel geometry (width and depth) of the upstream river boundary fixed, while varying the river discharge.

The critical shear stress for erosion might be unknown in advance or there might be a desire to calculate the critical shear stress based on grain size and density rather than to estimate it. The critical shear stress can be calculated with the physical Zanke (2003) model, described in Kleinhans (2005):

$$\tau_{cr} = \left[0.145 \cdot \left\{D_{50}{}^{1.5}\frac{\sqrt{Rg}}{\nu}\right\}^{-0.333} + 0.045 \cdot 10^{-1100\left\{D_{50}{}^{1.5}\frac{\sqrt{Rg}}{\nu}\right\}^{-1.5}}\right] \cdot R\rho g D_{50} \qquad \text{(Eq. 15)}$$

In which R is the relative submerged density.

The sediment suspension and its induced average suspended sediment concentration (c_n; Eq. 7) can be calculated using the sediment transport predictor of Engelund and Hansen (1967). This predictor has been rewritten (Kleinhans, 2005) such that it is a function of flow velocity and the Chézy roughness coefficient.

$$q_s = \frac{0.05 \cdot U^5}{\sqrt{g} \cdot C^3 \cdot R^2 \cdot D_{50}} \qquad \text{(Eq. 16)}$$

$$C = \sqrt{\frac{g}{C_d}} \qquad \text{(Eq. 17)}$$

$$R = \frac{\rho_s - \rho_w}{\rho_w} \qquad \text{(Eq. 18)}$$

In which C is the Chézy roughness coefficient and c_d is the drag coefficient, which can be calculated using the maximum of the values for smooth and rough turbulent flow conditions (Soulsby & Clarke, 2004).

$$c_{d\,rough} = \left[\frac{0.4}{ln\left(\frac{h}{z_0}\right) - 1}\right]^2 \qquad \text{(Eq. 19)}$$

$$c_{d\,smooth} = 1.615 \cdot 10^{-4} \cdot exp(6 \cdot Re^{-0.08}) \qquad \text{using } Re = U \cdot \frac{h}{\nu} \qquad \text{(Eq. 20)}$$

Here z_0 is the bed roughness length (can be approximated using the grain size), Re is the Reynolds number and ν is the kinematic viscosity of water. If the sediment transport is known, the average suspended sediment concentration can be calculated with:

$$c_n = \frac{q_s}{U \cdot h} \qquad \text{(Eq. 21)}$$

The sediment transport and concentration are a function of the hydraulics and the water depth and its computation thus should be integrated in the sediment balance (Eq. 7) and likewise influence the outcome of U, h, and L_W. The suspended sediment is distributed uniform over the water column.

The same model as described so far, can also be used for small-scale laboratory experiments. The two differences with the original model are: (1) the sediment concentration in the model for laboratory experiments is not a function of the hydraulics but set to a constant value and (2) the computation of the hydraulic depth is started using an initial guess of 0.05 m.

For all three scales (experiment, Oer-IJ, Thames) models were run using a stepwise increase in river discharge (Table 4). Each run was repeated with a model run in which the effect of river flow was disabled. For comparison, the model results were plotted together with a large dataset of United Kingdom estuaries (Manning, 2012) and data gathered on Dutch estuaries (Western- and Eastern Scheldt (De Jong & Gerritsen, 1984; De Bok et al., 2001; Gourgue et al., 2013) and Ems estuary (Schuttelaars et al., 2013)).

Table 4: Model settings. The erosion constant was kept constant (0.002 $kg \cdot N^{-1} \cdot s^{-1}$) and wind speed was not used in this study and thus set to a value of 0 $m \cdot s^{-1}$. The grain size of the Thames was based on Whitehouse (1995).

Scale	**a (m)**	**T (s)**	**L_e (m)**	**S_{hw} (m^2)**	**D_{50} (mm)**	**ρ_s ($kg \cdot m^{-3}$)**	**Q ($m^3 \cdot s^{-1}$)**	**W_r (m)**	**h_r (m)**
Thames	2.1	44640	82500	$2.00 \cdot 10^8$	0.16	2650	25-1300	600	4
Oer-IJ	0.75	44640	30000	$4.39 \cdot 10^7$	0.2	2650	25-600	500	1.25
Experiment	0.006	30	3	1	2	1055	$1 \cdot 10^{-6}$-$1.5 \cdot 10^{-4}$	0.07	0.0039

2.3 Model results

Specifying attributes that are exogenous to the estuary as input for the model (Table 3) will result in a prediction of the idealised 3D form (Fig. 11) and its corresponding gross properties. The gross properties studied are: convergence length scales, tidal prism, hydraulic conditions (river flow velocities and tidal flow velocities), width and cross-sectional area at the mouth of the estuary and the average estuary depth.

In all cases the width, depth and cross-sectional area increased as a result of increased river discharge (Fig. 12). Fig. 12 shows that the ratio L_e/L – estuary length divided by convergence length scale – increases for all e-folding length scales (L_A, L_W, L_h). Since the length of the estuary (L_e) is kept constant (Table 4), increasing discharge indicate lower values for all e-folding length scales: this implies stronger convergence of width, depth and cross-sectional area. The total surface area and width of the estuary increase if the length of the estuary is kept constant. The dimensions increased more rapidly with increasing discharge, visible from the increasing slope of the L_e/L line (Fig. 12). In contrast, if river flow is neglected in the model, I cannot observe any change in geometry. The model run in that case gives the same estuary dimensions for every discharge, since factors that determine morphology remain constant.

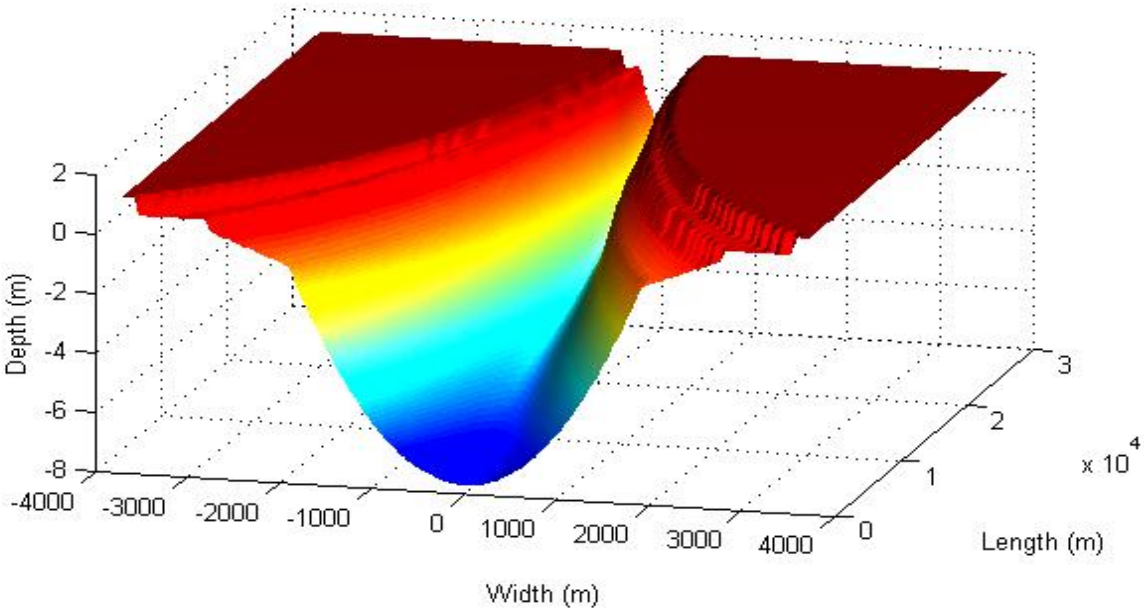

Fig. 11: Example of the 3D form model for the Oer-IJ estuary (Netherlands) with a river discharge of 250 m^3/s and a fixed geometry of the river at the upstream boundary. (See Table 4 for other input parameters.)

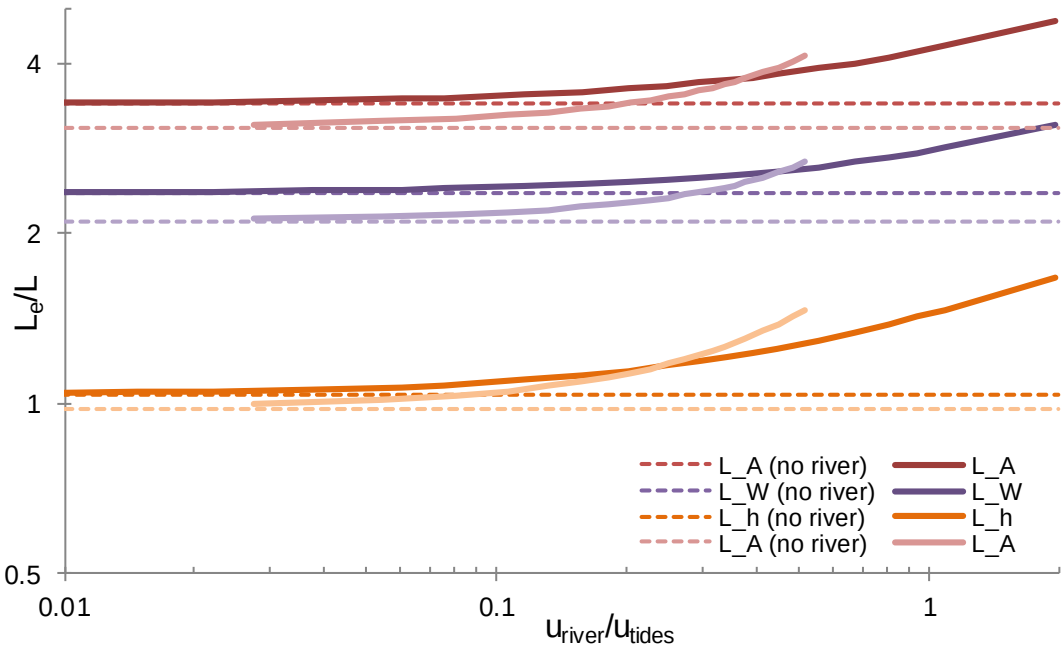

Fig. 12: The effect of river flow on convergence length scales. The length of the estuary is divided by the e-folding length scales for cross-sectional area (L_A), width (L_w) and depth (L_h). The higher the value of (L_e/L) the stronger the convergence is. The e-folding length scale for cross-sectional area is balanced by the e-folding length scale for width and depth (eq. 12). Model results for the Oer-IJ and experimental scale (lighter colours) are plotted: model results for the Thames are not shown because it shows the same trend. See for all model settings Table 4.

For rivers, the relation between river pattern and channel geometry is well known (Kleinhans & Van den Berg, 2001). For this reason, width to depth ratio of estuaries is here first compared with rivers. Fig. 13 shows that rivers occur on a large range of width to depth ratios. Sinuous and straight rivers show relatively low ratios, while braided rivers are relatively wide and shallow. For rivers, this has been related to an increase in potential-specific stream power (Kleinhans & Van den Berg, 2011). Estuaries in the UK and Netherlands, including model results, occur on a wide range of width to depth ratios and cross-sectional areas (Fig. 13). However, some data points and the model results seem to occur outside the common range of channel dimensions of rivers and estuaries. These estuaries appear to have relatively high river inflow (Fig. 14).

In fact, width to depth ratio increases with higher river discharge (Fig. 14): estuaries with relatively little input of river flow correspond to small width to depth ratios, while estuaries with high river input show larger ratios. This is in agreement with the model results, which also indicate higher ratios for increased river discharge. However, the model predicts much wider and shallower estuaries than the data indicate. From the data, I conclude that tide dominated estuaries have low cross-sectional areas and low width to depth ratios (Fig. 14). This resembles the geometry of meandering, sinuous and straight rivers. In contrast, river flow dominated estuaries have larger width to depth ratios, in the order of magnitude of braided rivers. The cross-sectional area of the river flow dominated estuaries can be much larger.

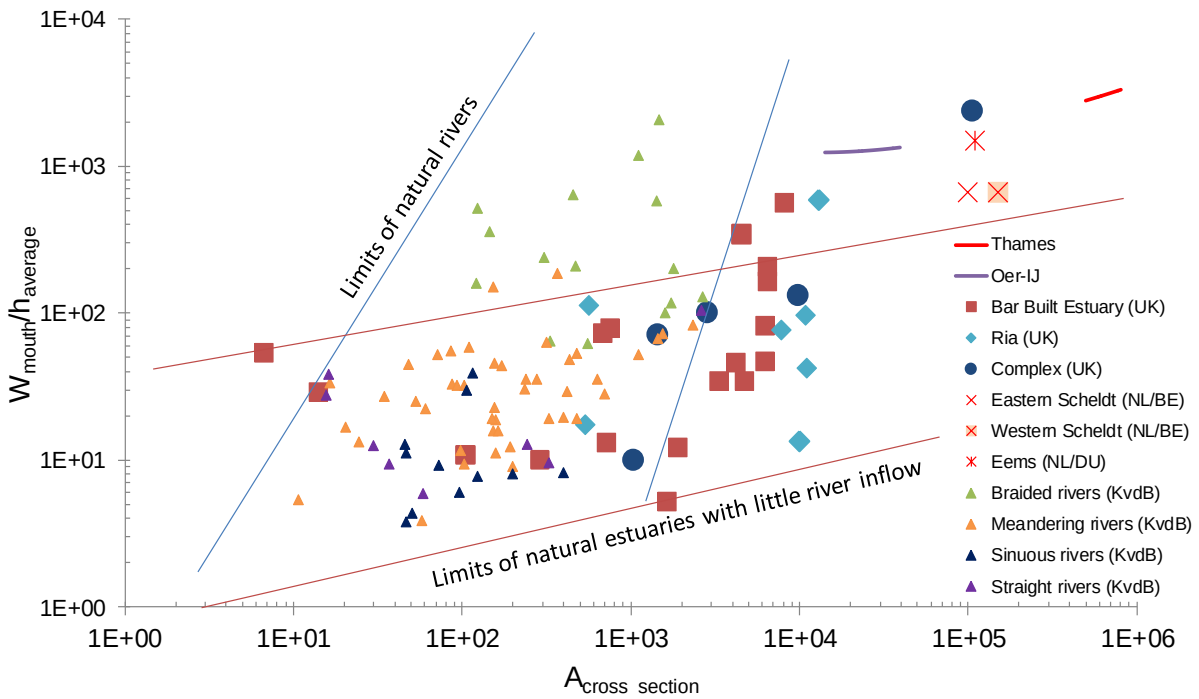

Fig. 13: Channel geometry of natural rivers and estuaries and model results. For estuaries, I used the width and cross-sectional area at the mouth of the estuary and the average estuary depth. The estuary dataset of Manning (2012), Dutch estuaries (De Jong & Gerritsen, 1984; De Bok et al., 2001; Gourgue et al., 2013; Schuttelaars et al., 2013) and rivers dataset of Kleinhans & Van den Berg (2011) are indicated.

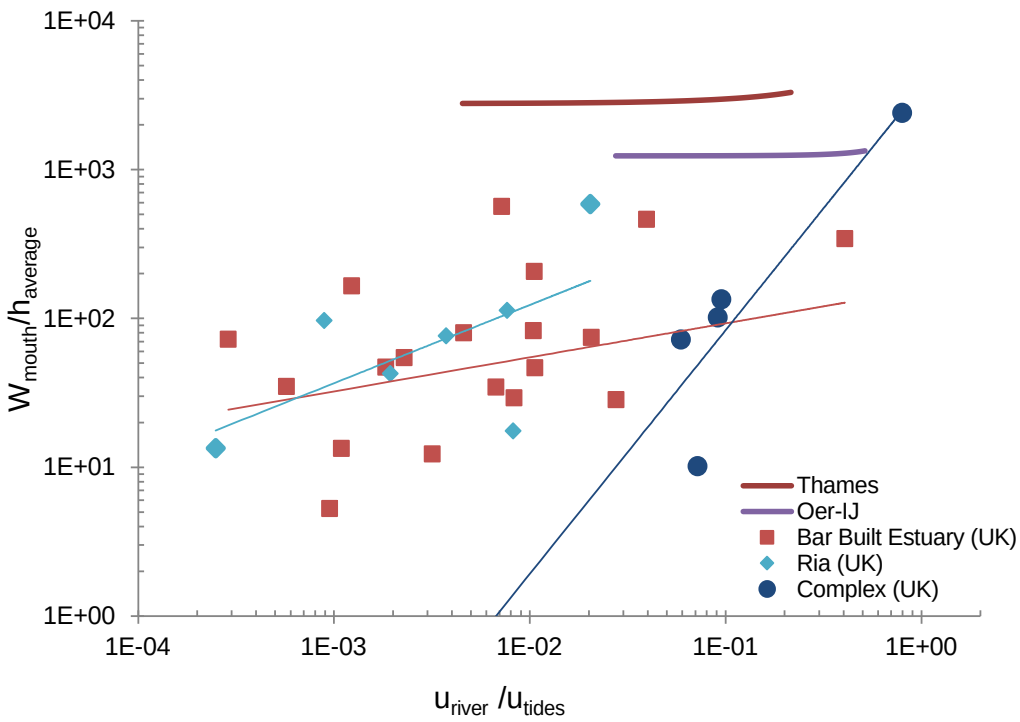

Fig. 14: Width to depth ratio as a function of relative flow velocities. Estuaries become relatively wider and shallower with increased flow velocities induced by the river: relations are given in Table 5. Model results for the experimental scale are not shown because it shows the same trend.

Table 5: Relation between relative flow velocities between river and tides for model results and data subsets. Corresponding R^2 values are given.

Group	Relation	R^2
Thames (model)	$\frac{W_m}{h} = 3362 \cdot \left(\frac{u_{river}}{u_{tides}}\right)^{0.04}$	0.76
Oer-IJ (model)	$\frac{W_m}{h} = 1310 \cdot \left(\frac{u_{river}}{u_{tides}}\right)^{0.02}$	0.59
Bar Built (data)	$\frac{W_m}{h} = 157 \cdot \left(\frac{u_{river}}{u_{tides}}\right)^{0.23}$	0.05
Ria (data)	$\frac{W_m}{h} = 1311 \cdot \left(\frac{u_{river}}{u_{tides}}\right)^{0.52}$	0.38
Complex (data)	$\frac{W_m}{h} = 3632 \cdot \left(\frac{u_{river}}{u_{tides}}\right)^{1.64}$	0.78

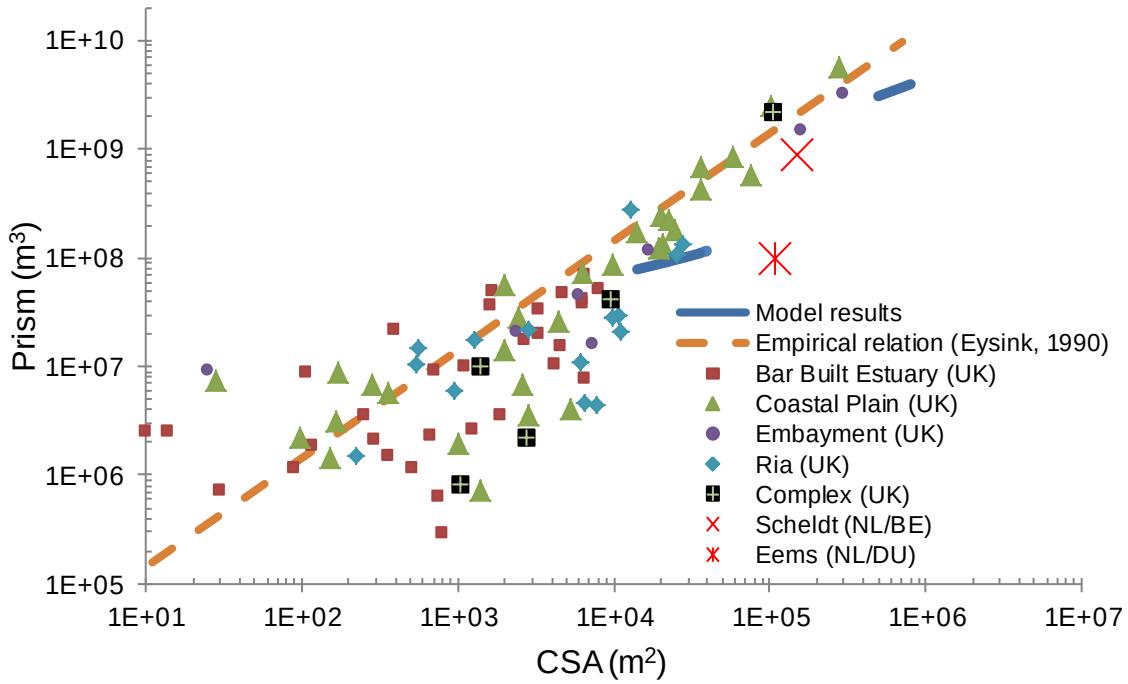

Fig. 15: The relation between cross-sectional area (CSA) at the mouth of the estuary and the tidal prism. Both the model results and the dataset show an increasing tidal prism with an increasing cross-sectional area at the mouth. Cross-sectional area at the mouth increases with increasing river discharge (Fig. 12). Higher river discharge also results in larger tidal prism.

The cross-sectional area at the mouth and the tidal prism increased as a result of increased river discharge (Fig. 12; Fig. 15). Both the model results and the datasets scatter around the empirical relation for tidal prism and cross-sectional area (Eysink, 1990: Eq. 22). For higher river discharge, cross-sectional area and tidal prism deviate more from the empirical relation (Fig. 15). This also implies that the empirical relation for tidal systems might lead to over predictions of the tidal prism when river flow is relatively large.

$$A_m = 7 \cdot 10^{-5} \cdot P \qquad \text{(Eq. 22)}$$

In which *P* is the tidal prism.

The UK estuaries dataset lacks information on grain size, which is required to calculate sediment mobility. To obtain this, friction was assumed to be equal in all estuaries (Chézy coefficient = 76.4 $m^{0.5} \cdot s^{-1}$ or f = 0.0135). Using the inverse of the White-Colebrook function, the Nikuradse roughness length (k_s) was estimated and converted to grain size (D_{50}) with $k_s = 2.5 \cdot D_{50}$. Fig. 16 shows the sediment mobility of UK and Dutch estuaries in the bedform stability diagram of Van den Berg & Van Gelder (1993). Most UK estuaries scatter around the beginning of motion and lower part of the dune regime. However, these results are sensitive to the grain size prediction. Dutch estuaries occur in the upper part of the ripple regime, close to the transition to dunes and upper plane bed.

Increasing the effect of river flow resulted in a decrease in average mobility of the sediment in the model results (Fig. 17). As discussed before, an increased river flow results in a deeper and wider estuary, together with a higher convergence. The net effect results in lower values of tidal velocity (Eq. 5; Eq. 6). Even if the average river flow velocity is added to the amplitude of tidal velocities, sediment mobility decreases due to increased river discharge (Fig. 17). This results in lower shear stresses and thus lower sediment mobility, as can be seen from (Kleinhans, 2005):

$$\tau = \frac{1}{8} \cdot \rho_w \cdot f \cdot U^2 \qquad \text{(Eq. 23)}$$

In which friction (*f*) can be predicted with the White-Colebrook function (Silberman et al., 1963).

While the model results indicate that sediment mobility decreases with increased river flow, there is a lot of scatter in the dataset (Fig. 17). Some types of estuaries show a weak relation between river flow and sediment mobility. In the dataset I found both increased and decreased mobility with increasing river flow (Fig. 17).

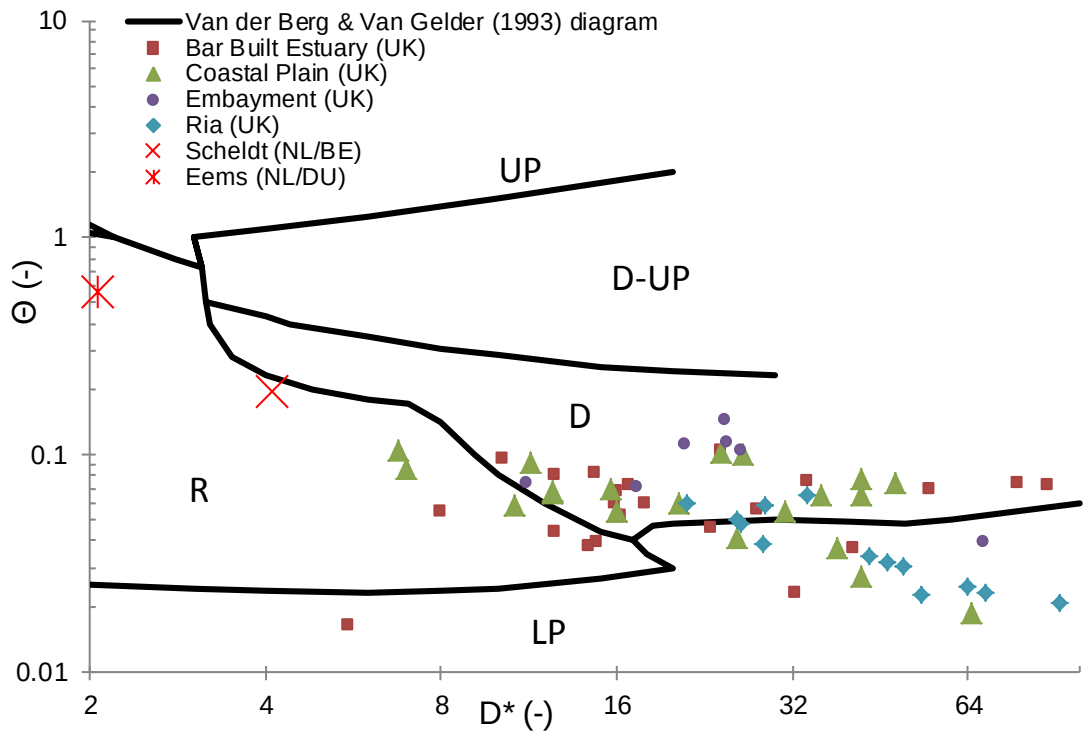

Fig. 16: Bedform stability diagram based on the Shields number and dimensionless grain size. Most of the UK data scatter around the beginning of motion, but this is sensitive to the estimation of the grain size. I calculated the grain size for all UK data (see text) assuming equal friction in all estuaries (which is of course not true). Chézy roughness coefficient was set to a value of 76.4 $m^{0.5} \cdot s^{-1}$. LP = lower stage plane bed, R = ripples, D = dunes, D-UP = transition from dunes to upper stage plan bed (UP).

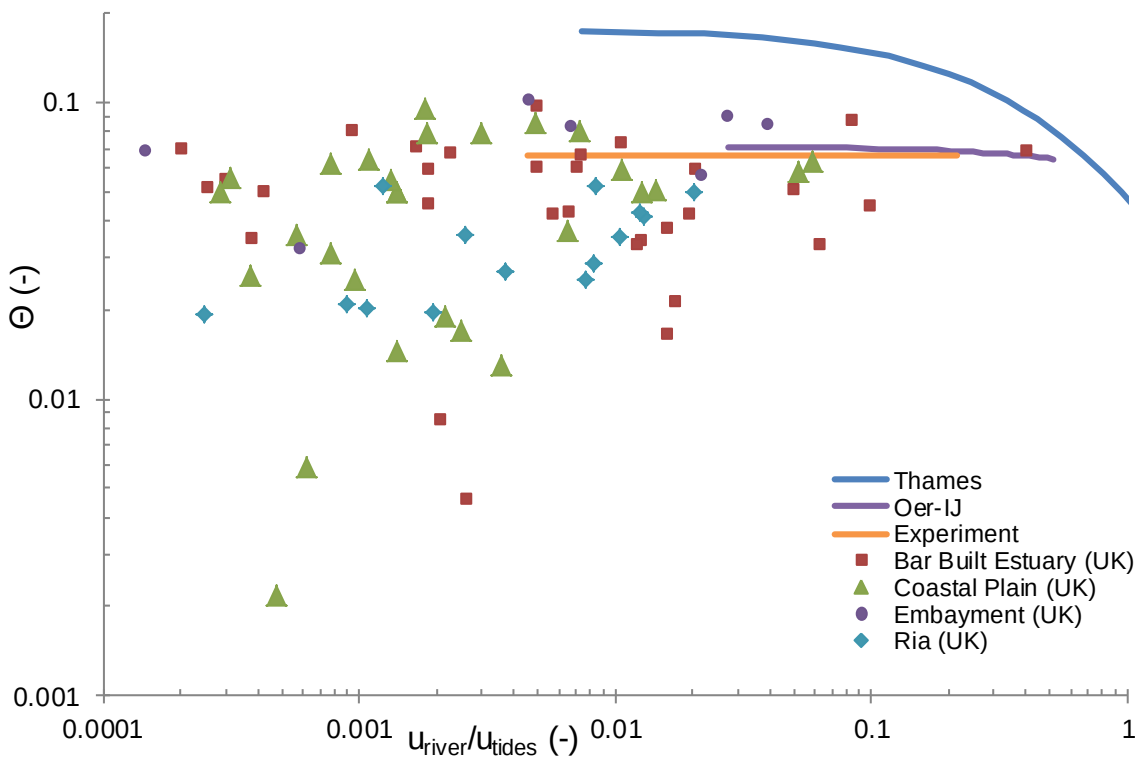

Fig. 17: Sediment mobility as a function of relative flow velocities for UK dataset and model results.

2.4 Hypotheses on gross properties

Based on the model results and data analysis – both focused on the effect river flow on the estuary hydraulics and dimensions – the hypotheses on the gross properties of estuarine systems are adjusted.

Model results do not support the hypothesis of Davies & Woodroffe (2010) that river discharge decreases channel convergence (Fig. 12): the model results imply stronger convergence. I found that river discharge increases width, depth and cross-sectional area if estuary length is fixed (Fig. 12). The estuarine channel has to converge to an upstream river geometry in my model. Total estuary surface area will increase with higher river discharge in the case the upstream geometry is fixed as well as when river dimensions increase by higher discharge. The river channel can widen in natural systems, possibly resulting in an estuary that stretches further landward. Tidal prism also increased together with cross-sectional area at the mouth (Fig. 15).

I found for both the model results and dataset that width to depth ratio increases for increasing river flow (Fig. 14). The resulting relations for rias and complex estuaries might be unreliable, because their geometry can be determined by geology. However, a similar – weaker – trend was found for bar built estuaries. To conclude, I hypothesise that width to depth ratio and channel width increase with increasing river discharge. According to theories of Schramkowski et al. (2002, 2004) and Kleinhans & Van den Berg (2011) this can result in a modification of the small-scale channel and shoal patterns.

So far I only used a simplified behaviour-oriented model with many assumptions and simplifications. For example, the sediment supply towards the estuary by the river, which is neglected in the model, is likely to affect sediment concentrations and sedimentation rates. The small-scale dynamics are also not included in this model approach. To include all these effects either a more process-based model (for example Van der Wegen & Roelvink, 2012) or experiments (for example Kleinhans et al., 2012) should be used. Therefore, I continued with experiments to test all the hypotheses constructed so far.

2.5 Review of previous laboratory experiments

As discussed before it is of obvious practical relevance for management strategies to understand whether tidal and estuarine systems are tending to an equilibrium state and if they are, what the gross properties under equilibrium are. Until 2005, little laboratory efforts have been made to unravel this. For this reason Tambroni et al. (2005) attempted to investigate the effect of boundary conditions on the mechanisms and evolution of tidal systems. A static equilibrium bed profile was found in this research: weakly concave in the seaward reach and convex more landward. Since then, further research attempts (Table 6) focused on decreasing the forming timescales and decreasing the scale effects. Time scale and space scale are usually inter-dependent (Cowell et al., 2003): time scale to reach equilibrium is generally strong related with the size of tidal basin (Vlaswinkel & Cantelli, 2011).

Recently, experiments have been addressed as one of the major challenges in the research field of tidal systems (Coco et al., 2013) and over the last decade more laboratory scale experiments focused on tidal morphology (Table 6). While these experiments resulted in some common findings, they also faced some similar problems, such as the occurrence of scour holes (Tambroni et al., 2005; Stefanon et al., 2010). No standard exists yet: one of the major challenges of tidal experiments is reducing the scaling issues (Coco et al., 2013).

Paola et al. (2009) discussed that scaling rules from engineering may be violated if direct comparison to a real world is not required. However, the significance of laboratory experiments increases when upscaling to this scale is possible. Different theories are known to transform these scales into each other, such as the theory of tidal wave motions and hydraulic similarity (Reynolds, 1889, 1890, 1891; Lanzoni en Seminara, 2002; Stefanon et al., 2010). Most of the present methods of upscaling are based on using dimensionless numbers for scales (Kleinhans et al., 2014b, 2014c).

Three of the fundamental problems of scaled laboratory experiments are addressed here (Kleinhans et al., 2012, 2014c; Coco et al., 2013):

1. The formation of unrealistically large scour holes and ripples, which where for example reported by Tambroni et al. (2005) and Stefanon et al. (2010). This alters the hydrodynamics to such extent that it is impossible to upscale the experiments to the real world scale.
2. A static equilibrium as end state rather than a dynamic equilibrium, such as found by Mayor-Mora (1977) and Stefanon et al. (2010). Since real tidal systems and estuaries are in dynamic equilibrium or disequilibrium, the sediment should be mobile in the end state of the experiment.
3. A net erosional behaviour of previous experiments (Stefanon et al., 2010). This can be explained by absence of significant flows and thus lack of sediment mobility.

According to Kleinhans et al. (2014b) the fundamental problem of previous tidal experiments is that a much steeper bed gradient is required than in natural systems, because the water depth and bed shear stress are much smaller in experiments. For river experiments this problem is rather minor, because sediment is transported in only one direction. In contrast, tidal experiments do require sediment transport also in landward (up-slope) direction. A steep seaward gradient in combination with periodic water level variations makes significant up-slope flood directed sediment transport in experiments impossible. Because the steep slopes flood and dry like a bath tub, sediment is exported out of the system until static equilibrium is reached (Kleinhans, 2013).

Table 6: Summary of previous tidal experiments and their setup. See for a more detailed description the review of experiments by Coco et al. (2013), Kleinhans et al. (2012) or the description of experiments itself.

Author	Basin size	D_{50} (mm)	ρ (kg·m^{-3})	Tide	Time to equilibrium	Remarks	Research goal
Reynolds (1889-1891)	4m × 1.2m	0.17	2650	Sinusoidal water level	6000·T	Tidal inlet and estuaries	Reproduce system
Mayor-Mora (1977)	28m × 19m	0.34	2650	Sinusoidal water level	4-7.5 hours	Tidal inlet and bay	Inlet hydraulics and stability
Tambroni et al. (2005)	24m × 0.3m	0.31	1480	Sinusoidal water level	2000·T	Fixed channel	Bed elevation
Stefanon et al. (2010, 2012)	5.3m × 4m	0.8	1041	Sinusoidal water level	~30-60 days	Variation at downstream boundary	Geometry, tidal prism
Vlaswinkel and Cantelli (2011)	3m × 2.5m	0.045 on top of gravel	2650	Sinusoidal water level	~5 days	Tidal network	Geometry
Iwasaki et al. (2013)	0.9m × 0.8m	0.12	1480	-	~2 hours	-	-
Kleinhans et al. (2012, 2014b)	1.2m × 1.2m 3.8m x 1.2m	0.48 1.2	2650 1042	Tilting basin	120-200 hours	Counteracts possible scale effects	Equilibrium and cyclic behaviour

2.6 Scaling approach and scaling parameters

Previous scale models of the real world had to adhere to strict similarity scale rules (Yalin, 1971; Hughes, 1993). These rules can be relaxed when a quantitative test of planned engineering measures is not required. I will take a pragmatic position concerning scaling issues and use the essential scaling rules, whilst relaxing others, similar to Kleinhans et al. (2014b) and based on Kleinhans et al. (2014c). Kleinhans et al. (2014c) described that several thresholds exist beyond which scale-independence breaks down. Crucial are the transitions from subcritical to supercritical flow, from hydraulic smooth to rough bed, initiation of sediment motion and bank stability. These parameters are thus strictly kept within thresholds. In addition, I will keep the relative flow velocity of river flow compared to tidal flow within the same order of magnitude as natural estuaries.

Recently, Kleinhans et al. (2012, 2014a, 2014b) presented a method that deals with a great amount of the scaling issues. The solution used for this novel setup is schematised in Table 7. This solution keeps the essential scaling parameters within the thresholds in which scale-independence of morphological processes still occurs. After solving these major issues (Table 7), two main differences between the real world and the experiment should be remarked:

1. The maximum bed slope is 10^3 times larger than in the real world, but this is compensated by a water depth which is proportionally smaller. The reduced sediment density compensates for the larger friction in the experiment (Kleinhans et al., 2012).
2. It is impossible to scale both the Reynolds number (a function of water depth) and Froude number (a function of the square root of water depth) at the same time (Eq. 25, Eq. 27). For this reason it is allowed for the Froude number to become larger than in real systems as long as the values are below the critical value (Kleinhans et al., 2010).

Afterwards, it is discussed how well the scaling approach succeeded with the method described Kleinhans et al. (2014c). The similarity between laboratory experiments and natural systems can be assessed in three ways: (1) compare hydrodynamic and morphodynamic conditions, (2) compare dimensionless values quantitatively and (3) compare morphology and dynamics.

Table 7: Solutions presented by Kleinhans et al. (2008, 2010, 2012, 2014b, 2014c) for the major scaling issues in laboratory experiments. The arrows indicate how single solutions create new scaling problems.

Observation	Main scaling issue	Solution	Why it works
	Hydraulics and sediment mobility must resemble real world processes	Use similar Froude, Shields and Reynolds number	
Scour holes and large ripples	Hydraulic smooth conditions	Use a unimodal sediment mix with a large D_{90} grain size	Creates hydraulic rough conditions
No/Little sediment transport with coarse grain size	Sediment below threshold of motion	Use larger bed slopes and use lightweight sediments	Slope increases sediment mobility
Ebb-dominance	Upslope (flood) transport is inhibited due to large slope	Tilt the flume to create tides	Creates same slope for ebb and flood phase

Scaling parameters

Flow conditions and sediment mobility are important factors for successful experiments. Froude and Reynolds numbers are dimensionless numbers used to describe flow conditions. Shields number is used for sediment mobility. To compare natural estuaries with experimental estuaries, the residual flow velocity at the inlet of the estuary is calculated. The relative contribution of river flow can then be assessed by dividing the residual river flow velocity by the characteristic tidal flow velocity:

$$u_{relative} = \frac{u_{river}}{u_{tides}} \quad \text{(Eq. 24)}$$

The Reynolds number indicates whether flow is turbulent or laminar. Turbulent flow is required for suspended sediment transport.

$$Re = \frac{u \cdot h}{\nu} \quad \text{(Eq. 25)}$$

For *Re* > 500 the flow is turbulent. All rivers on earth have turbulent flow (Kleinhans, 2005). At the bottom of this turbulent flow, a small layer of laminar flow occurs (Fig. 18). The conditions in this layer affect bed scouring tendency.

Kleinhans et al. (2014c) described the hydraulic conditions for the formation of scour holes. When the channel bed is hydraulic smooth, sediment particles are completely submerged in the laminar sublayer (Van Dijk et al., 2012). Under these conditions ripples and scour holes can form. Ripples form when the water depth is larger than 0.02 m (Mayor-Mora, 1977; Tambroni et al., 2005). Scour holes form in shallower water depth (Stefanon et al., 2010; Kleinhans et al., 2014c) (Table 8). The spontaneous formation of scour holes lacks a full explanation. So far a working hypothesis was used. It is assumed that the turbulence generated at the ripple top or scour hole rim penetrates the laminar sublayer (Kleinhans et al., 2014c), which maintains the scour hole.

Table 8: An indication of the conditions for the occurrence of scour holes, ripples and dunes.

Condition	Small water depth (<0.02 m)	Large water depth (>0.02 m)
Hydraulic smooth	Scour holes	Ripples
Hydraulic rough	Planar bed	Dunes

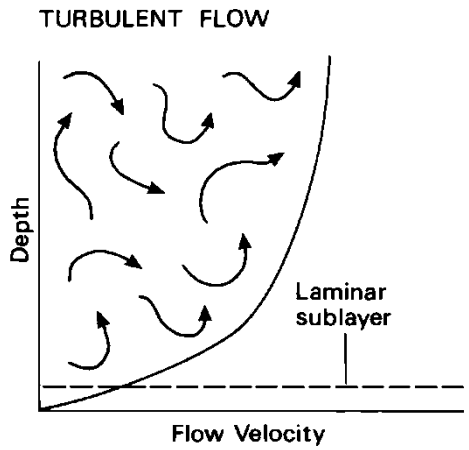

Fig. 18: Vertical profile of flow velocity for turbulent flow. Close to the bed, a small layer of laminar flow occurs: the laminar sublayer.

Whether the flow conditions are hydraulic smooth or rough can be determined by the Reynolds particle number: a dimensionless number that describes the balance between inertial and viscous forces at the bed surface. The particle size on the bed is compared with the thickness of the laminar sublayer above the bed. The Reynolds particle number is given by:

$$Re^* = \frac{u^* \cdot D_{50}}{\nu} \qquad \textit{with} \qquad u^* = \sqrt{\frac{\tau}{\rho}} \qquad \text{(Eq. 26)}$$

The transition from hydraulic smooth to rough occurs at Reynolds particle numbers between 3.5-70.

The Froude number is used to determine whether the flow is subcritical (Fr < 1) or supercritical (Fr > 1). Subcritical flow is affected by downstream roughness and obstruction, supercritical flow by the upstream.

$$Fr = \frac{u}{\sqrt{g \cdot h}} \qquad \text{(Eq. 27)}$$

Many gravel bed rivers occur around the critical (Fr = 1) transition or just below it (Kleinhans, 2005). Most of the sand bed rivers (Kleinhans, 2005) and estuaries (based on calculations with data of Manning, 2012) occur far below this transition.

For sediment mobility, the Shields number is a key indicator: a dimensionless number that describes the balance between bed shear stress and gravity. The higher the bed shear stress, the more mobile the sediment is.

$$\theta = \frac{\tau}{(\rho_s - \rho) \cdot g \cdot D_{50}} \qquad \text{(Eq. 28)}$$

In which the total shear stress (τ) is determined with:

$$\tau = \rho \cdot g \cdot \frac{u^2}{C^2} \qquad \text{(Eq. 29)}$$

For sediment transport, the grain (skin friction) related roughness should be used. According to Kleinhans et al. (2014b), the Keulegan equation can be used to estimate the skin friction-related Chézy roughness number (C'):

$$C' = 18 \cdot log \frac{12 \cdot h}{\alpha \cdot D_{90}} \qquad \text{(Eq. 30)}$$

For the multiplication parameter (α), Kleinhans et al. (2014b) used 3.

The dimensionless grain (D^*) size is calculated with:

$$D^* = D_{50} \cdot \sqrt[3]{\frac{R \cdot g}{\nu^2}} \qquad \text{(Eq. 31)}$$

2.7 Sediment selection for experiments

The first step towards the experimental setup is the selection of a suitable sediment type. I performed scour hole experiments to determine the range of hydraulic conditions and grain sizes under which scour holes occur in scaled laboratory experiments (Appendix 2). The scour hole experiments were used to select the sediment type that limits the occurrence of hydraulic smooth conditions and the associated scour holes or ripples (Table 8).

Particle size, shape and distribution effect roughness and turbulence (Kleinhans et al., 2014c). The occurrence of scour holes can thus be reduced when poorly sorted sediments are used (Van Dijk et al., 2012). When larger particle sizes are used, the Reynolds particle number can be far above the threshold below which scour holes and ripples form (Kleinhans et al., 2014c). Scour holes were prevented in previous experiments by using a poorly sorted unimodal sediment mixture.

Based on the scour hole experiments, I confirm the hypothesis of Kleinhans et al. (2014c) that autogenic scour holes form at the lower end of the transition from hydraulic rough to hydraulic smooth (Re* 3.5-70) and just above the beginning of motion in the ripple regime of the bedform stability diagram. However, critical Reynolds particle numbers (Re*) for the occurrence of scour holes seem dependent on grain size and sediment density for light-weight sediments.

Two types of sediments were selected for the estuary experiments: polystyrene particles and a mixture of poorly sorted blasting polymer with a coarse tail. The characteristic properties of these mixtures are given in Table 9 and Fig. 20.

Table 9: Characteristics of the sediment types used. Hydraulic conductivity of only the polystyrene sediment was measured with a constant head permeameter: 0.025 m·s^{-1}.

Sediment type	Density (kg·m^{-3})	D_{10} (mm)	D_{50} (mm)	D_{90} (mm)
Polystyrene	1042	1.0	2.1	2.8
Blasting polymer	1200	0.7	1.2	1.5
Blasting polymer - coarsened	1200	0.7	1.2	1.6

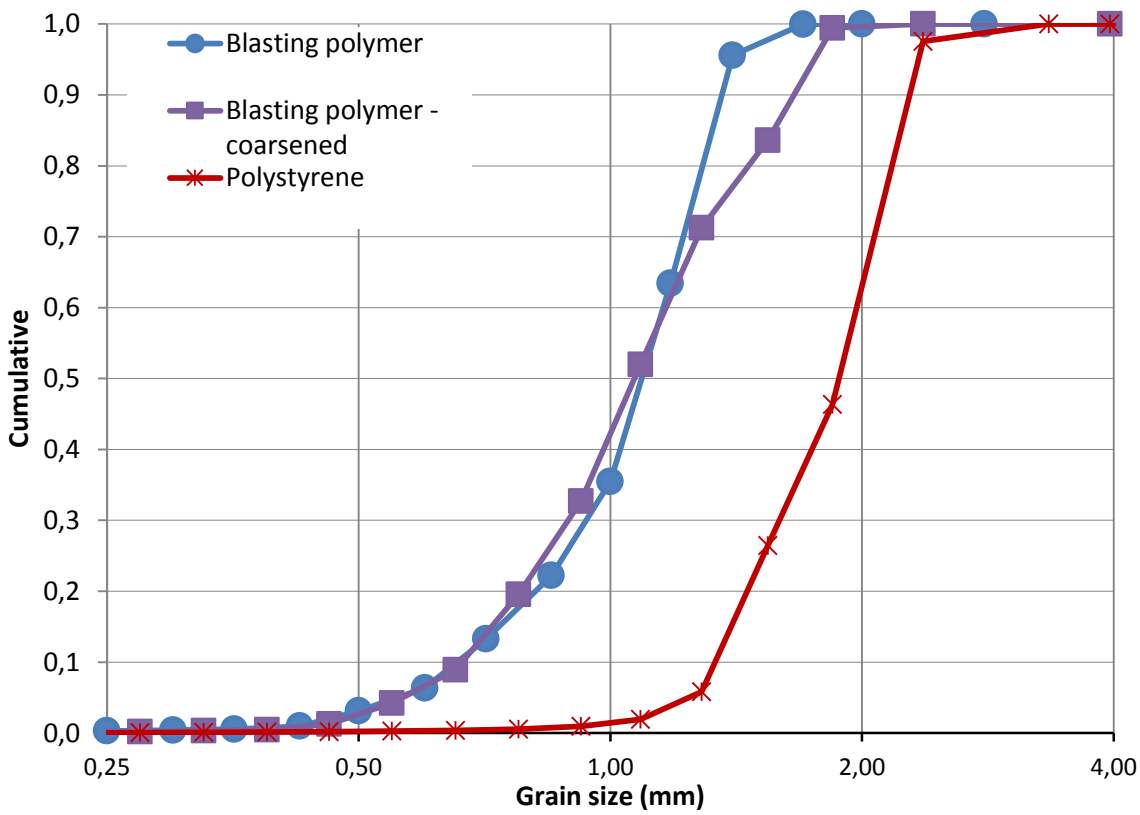

Fig. 19: Sediment distribution of the sediments used in this research.

2.8 Experimental setup

A tilting basin of 3.8 m by 1.2 m was used. The basin tilted over the short axis in the middle to produce tidal currents. A vertical threaded pole driven by a stepping motor with microcomputer control was used for a constant movement velocity (40 mm·min^{-1}). The maximum amplitudes has been varied. At maximum flume slope, there is a short pause (2 seconds) before the movement of the stepping motor changes direction (Fig. 20).

A constant water level at the seaward boundary was created by a constant head at the downstream boundary, allowing free in- and outflow of water. Water depth at the sea was set to a value of 0.054 m above the flume floor.

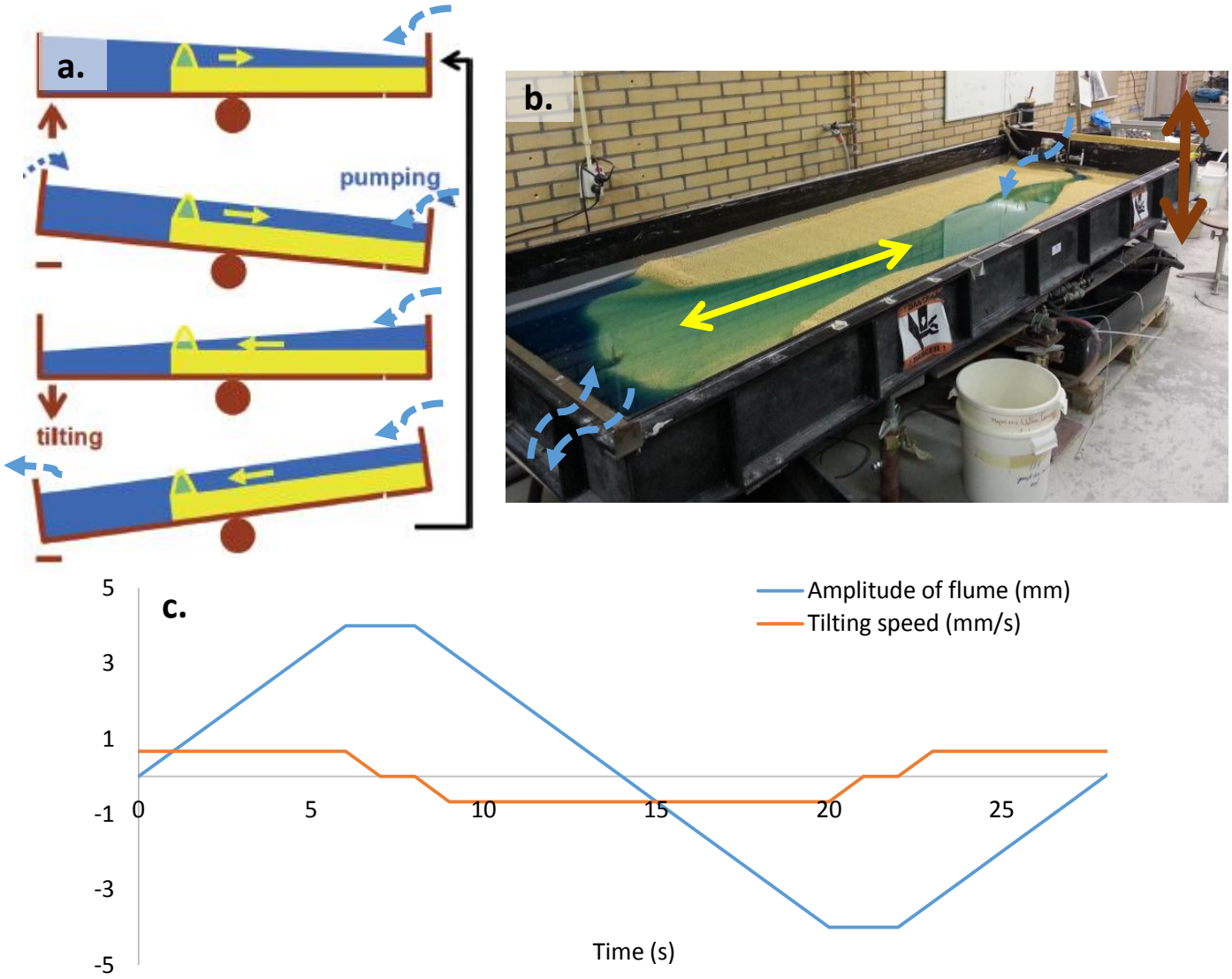

Fig. 20: Experimental setup. (a) Schematic drawing showing the principle (Kleinhans et al., 2012). Yellow arrows indicate sediment transport, blue arrows pumping direction and brown arrows tilting direction. (b) Photograph showing the experimental setup. (c) amplitude and tilting speed of right end of the flume during an experiment with 4.0 mm amplitude.

A plane bed of sediment (0.055 m height) was created in the basin, on top of a coarse grained mat. The bed was approximately 2.80 m long and 1.20 m wide. A barrier of erodible sediment (0.02 m height) was created at the border between the sea and the sediment bed (Fig. 21). At the upstream boundary water discharge was added to the flume (Fig. 21). The amount of discharge was varied from $6.0 \cdot 10^{-6}$ to $42 \cdot 10^{-6}$ $m^3 \cdot s^{-1}$. An initial channel was carved in the sediment bed of 0.02 m deep and 0.04 m wide to facilitate flow from the upstream boundary to the sea in the middle of the flume. This prevents the initiation of channels at the sidewalls of the flume. The inflow direction of water at the upstream boundary was under an angle with the initial channel (Fig. 21).

The sediment bed consisted of light-weight sediments. The use of the blasting polymer sediment limits the effect of ground water flow which is enhanced by the large permeability of the coarse polystyrene particles. The water was dyed blue with *Brilliant Blue FCF* colourant to enhance the visualisation of morphology.

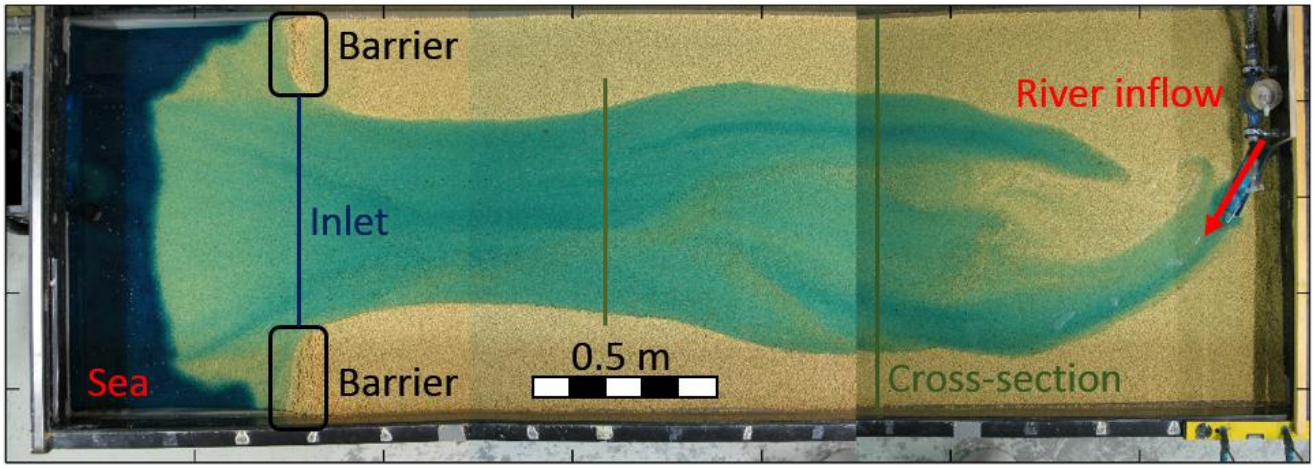

Fig. 21: Top view of experiment 26 after 900 tidal cycles. Location of cross-sectional profiles used in this study are indicated.

2.9 Experimental conditions

Approximately 45 experiments were performed in total. 9 experiments were selected for further analysis. These experiments appeared to be repeatable, because all initial and boundary conditions were fully controlled. Other experiments were not selected because (1) initial or boundary conditions were not kept constant, (2) experiments were hampered by scaling issues, such as sediment below the threshold of motion or (3) because recording hardware was not working or shut down during the experiments.

The first set of experiments consists of the polystyrene sediment experiments (26, 27, 29, 31 and 32), in which the tidal amplitude was kept constant (except for exp. 31) and river discharge was varied between 0 and $0.020 \cdot 10^{-3}$ $m^3 \cdot s^{-1}$. Experiment 32 was performed without river discharge. Accidentally the amplitude of experiment 31 was set to 2.8 mm. Nevertheless, the results were approximately similar to experiments 26, 27, 29 and 32.

The second set of experiments consists of the basting polymer sediment experiments (36, 39, 40 and 41), in which the tidal amplitude was kept constant at 4.0 mm and river discharge was varied between 0 and $0.042 \cdot 10^{-3}$ $m^3 \cdot s^{-1}$. A larger amplitude was used in these experiments, because the density of the blasting polymer sediment was higher than the polystyrene sediment. River discharge accidentally decreased during experiment 39 to approximately $0.010 \cdot 10^{-3}$ $m^3 \cdot s^{-1}$. It is unknown whether this was suddenly or gradual. In experiment 36, bed level at the upstream boundary was slightly higher (~ 1 mm) to prevent a tidal network from developing in the upper estuary. Experiment 41 was performed without river discharge.

Table 10: Summary of experimental conditions used in this study (Fig. 20c). See for properties of sediment types Table 12 and Fig. 19. Variations in tidal period (T) result from the variations in amplitude: the tidal period is determined by the amplitude, movement velocity of the stepping motor and pause duration (Fig. 20c).

Experiment	Amplitude (mm)	Q ($\cdot 10^{-3}$ $m^3 \cdot s^{-1}$)	T (s)	Sediment type	Duration (·T)
26	3.0	0.0200	22.0	Polystyrene	3564
27	3.0	0.0061	22.0	Polystyrene	3708
29	3.0	0.0093	22.0	Polystyrene	3336
31	2.8	0.0090	20.8	Polystyrene	8016
32	3.0	No river	22.0	Polystyrene	3636
36	4.0	0.0160	28.0	Polymer	2778
39	4.0	0.0420	28.0	Polymer	7272
40	4.0	0.0085	28.0	Polymer	5856
41	4.0	No river	28.0	Polymer	5904

2.10 Data collection, processing and data reduction

Three Canon Powershot cameras were used to record the evolution of the bed and channels over time. The images (3648 by 2736 pixels) were taken automatically with time-lapse photography in phase with the flume tilting. All images were taken under flood conditions (maximum landward gradient), each 6th tidal cycle. Point clouds with altitude data were made of the flume with a ViALUX 3D scanner at the end of each experiment. This scanner consists of a fringe projector and calibrated digital camera system ('Z-snapper'), which records dry bed elevation. The scanner and digital cameras were positioned at the ceiling on fixed locations. Cameras were located 2.0 m above the flume, which gives the true length of one pixel: 0.51 mm per pixel on the sediment bed. Flow velocity was measured by tracking floating particles.

A qualitative analysis and quantitative analysis of the experiments was based on the photographs taken over time. Qualitative analysis took place by visual analysis. Quantitative analysis was performed with colour bands extracted from the images.

Both RGB-bands and LAB-bands could be used as a proxy for water depth. RGB-bands contain number values for the intensity of red, green and blue. These images were converted to LAB (CIELAB) images, in which *L* represents light intensity, *A* represents red to green and *B* yellow to blue. The possibility to leave out the light intensity is the main advantage of an LAB image. Fig. 22 shows the different colour bands. The B-band of LAB results in the largest contrast between water and sediment and the widest range of values for the water depth (Fig. 22). The B-band indicates colour on a scale from 0 to 255. Lower values indicate yellow, higher values blue. A single B-band value thus indicates yellowness/blueness of a pixel, which was used as a proxy for water depth, width and total estuary area over time.

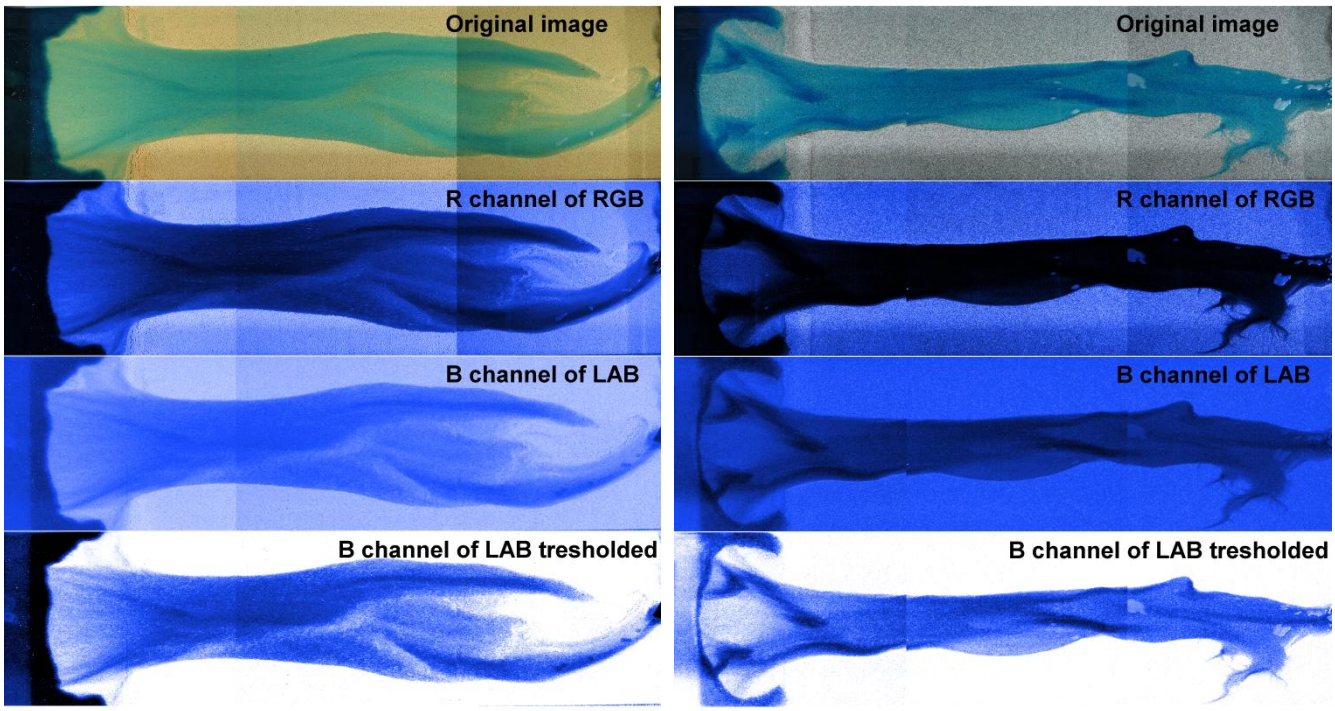

Fig. 22: Different colour bands, extracted from the original photo (top). All colour bands were converted to blue colour scale. For the R-band of RGB, values have been reversed to make deeper channels visible with darker (blue) colour. The bottom panel shows the thresholded images. The left panel shows experiment 26 after 900 tidal cycles. The right panel shows experiment 39 after 1500 tidal cycles. The B-band of the LAB image (bottom) was used for analysis in this research.

Cross-sectional areas (Fig. 21) of the images were studied over time. The median pixel value was used of the cross-sectional area and the cross-sectional areas 3, 6 and 9 pixels to the left and right to remove noise (such as floating particles or foam on the water). The morphology and channel dynamics remained the same after this correction. After correction, cross-sectional areas were plotted over time. This results in a time stack, which shows the dynamics of channels over a full experiment (see for example Fig. 26).

The location of maximum channel depth was calculated for each cross-section to visualise the channel dynamics over time. The full time stack was smoothened using a rectangular mean filter function (Reeves, 2009). This process made sure the maximum channel depth was located rather than an occasional pixel with a strong colour intensity.

A threshold was used to remove the dry morphology from the images and to narrow the range of colours present. This enhances the visibility of channels and their relative differences in depth. The threshold values were based on the intensity of the colours during different stages of the experiment. The colour variation was regarded for both the full surface area of the flume and for the time stacks (Fig. 23). After all, it is required that both in space and in time the thresholds are right for the recognition of channels and dry morphology. The colour limits used for experiments with yellow polystyrene sediments were 115 (lower) and 153 (upper). The colour limits used for experiments with blasting polymer sediments were 80 and 120.

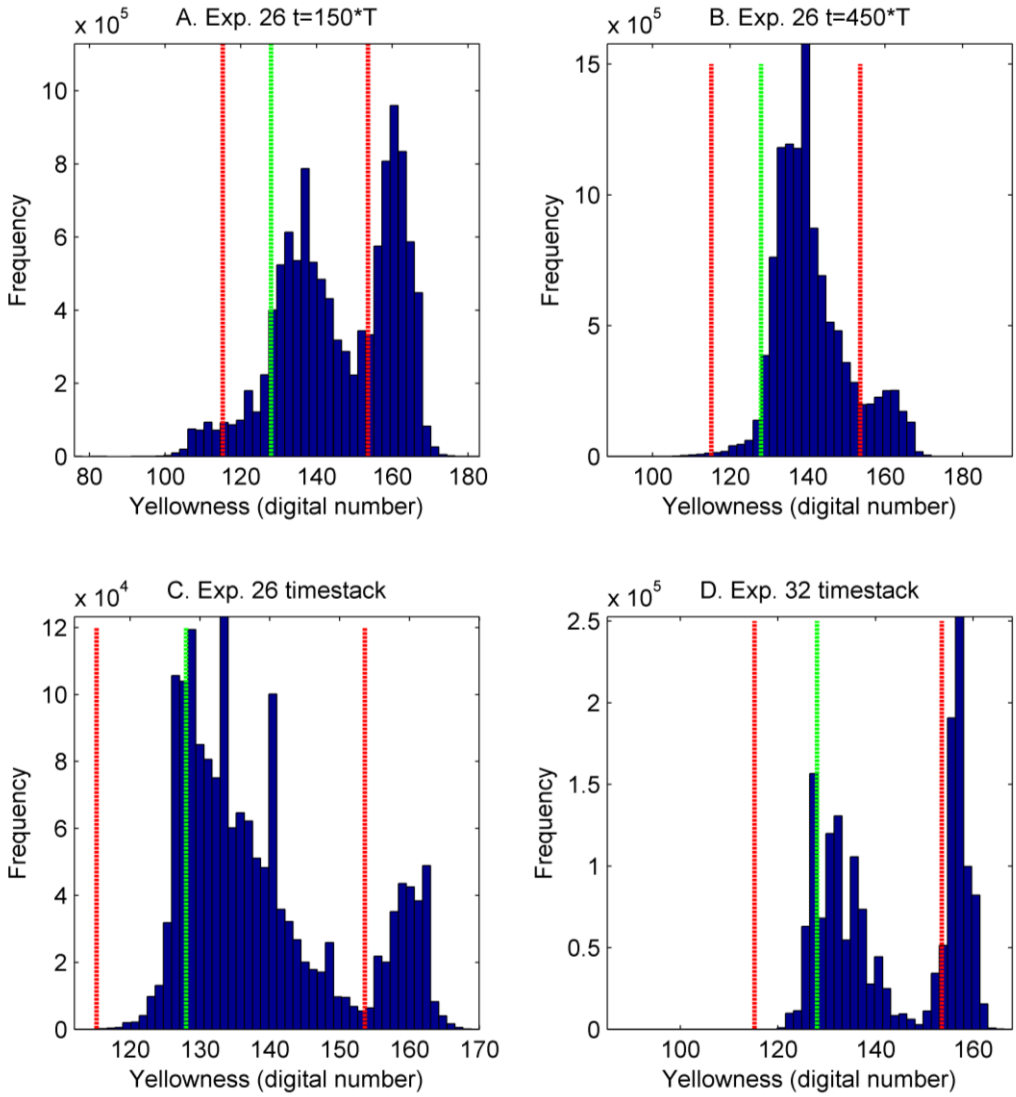

Fig. 23: Yellowness was used as a proxy for channel depth. Yellowness values in LAB-colour space range from 0 to 255. The green line indicates the middle value (127) – the transition from more blue to more yellow. Each histogram shows the frequency of yellow intensities: (a, b) the full flume at two stages of experiment 26; (c, d) upstream cross-sectional area (see Fig. 21) over time for the full experiment. Red lines indicate the thresholds used in this research to identify channels.

3. Results of experiments

3.1 Experiments with polystyrene sediment

The initial phase of all experiments (26, 27, 29, 31 and 32) was similar. At initiation, the ebb-tidal delta grew by export of sediment and the mouth of the estuary widened (Fig. 24). This resulted in a single converging channel. After approximately 120 tidal cycles, bars formed at the upstream boundary, but only under the condition of river water inflow. Without water inflow, the initial channel started to fill up upstream, shortening the tidal basin (Fig. 24; Fig. 25).
The initiation of a bar at the inner bend of the upstream river resulted in erosion and growth of the

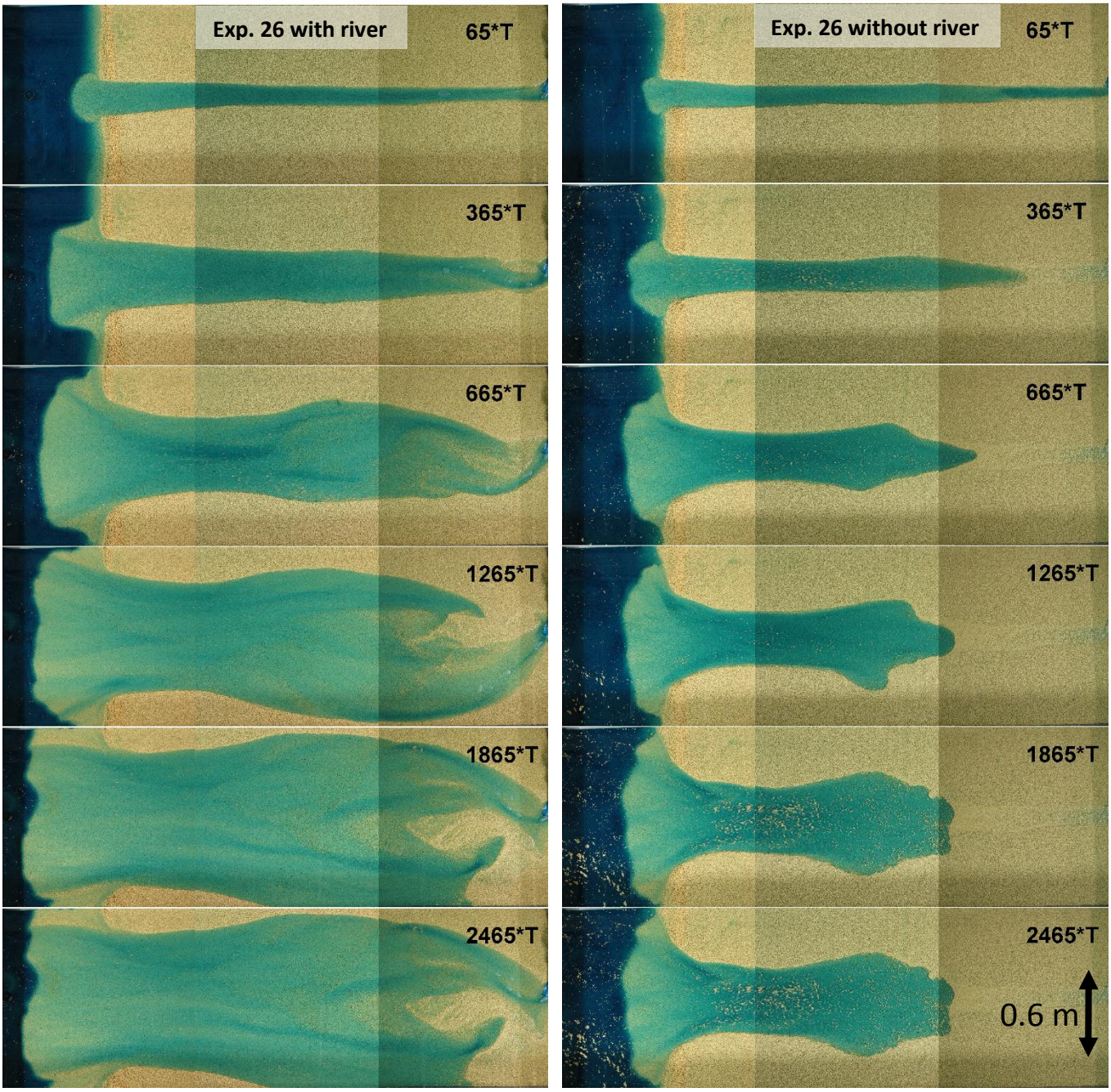

Fig. 24: Time series of images of experiment 26 with river discharge (left) and experiment 32 without river discharge (right). All other initial and boundary conditions correspond in these two experiments. T corresponds to the duration of one tidal cycle. (See Appendix 4 for QR-codes to the movies in the Online Supplementary Material.)

outer bend (Fig. 25). Multiple dynamic channels existed from this phase onward. At least one set of mutually evasive ebb and flood tidal channels was present after 600 tidal cycles, except for the experiment without river, which continued filling up (Fig. 24). Mid-channel bars formed together with the preferential ebb and flood channels.

The lateral migration and growth of these channels resulted in a widening of the estuary upstream and a growth of the surface area of the estuary. The total area and upstream width of the estuary grew faster for experiments with river inflow. Total area and width kept increasing fast until either the connection between river and estuary filled in (exp. 27 and 31) or further growth was constrained by the walls of the flume (exp. 29 and 32).

Upstream river inflow resulted in dynamic channels and bars. In contrast, I observed a rather stable single channel in the experiment without river inflow. This became visible from the time stack of the upstream cross-section of experiment 26 and 32 (Fig. 26) and a calculation of channel dynamics over the full area of the estuary (Fig. 27f). Initial and boundary conditions were the same in these experiments, except for river discharge which was only present in experiment 26.

Experiment 26 started with a single channel, which grew in width and migrated in the direction of river discharge inflow (Fig. 26). Fig. 26 shows that from t=500·T multiple channels exist. From then on, predominantly, two channels existed of which one was connected with the upstream river. The flood tidal channel occasionally cut off the bar built up in the inner bend of the ebb tidal channel (e.g. at 1860·T, Fig. 24-Fig. 26). Backward erosion and outflow of groundwater in the ebb phase probably caused the cut-off. A successful cut-off resulted in growth of the channel and eventually a reversing role of the ebb and flood tidal channel. Maximum channel depth shifted approximately 10 times in 2400 tidal cycles. This indicates a periodicity of 240 tidal cycles. After 2400 tidal cycles, the width of the estuary covered the full width of the flume. From this moment the maximum channel depth occurred most often close to the walls of the flume. However, migration of channels continued upstream of this location until the flume consisted of a big sea.

The rate of width increase was dependent on the amount of river inflow. The width of the estuary tended to increase for all experiments (Fig. 27a). In the cases with river inflow, the growth was much faster (Fig. 27ab). The higher the river discharge was, the higher the widening rate was for the first 900 tidal cycles (Fig. 27b; Fig. 27c). This rate decreased – and even became negative for a short period – when the river closed off in experiment 27 and 31 (t=1200·T, Fig. 27b). From that moment on, evolution of width seemed to coincide more with the evolution of width in experiment 32 (without river flow). Experiment 26 and 29 reached maximum width at approximately t=1800·T.

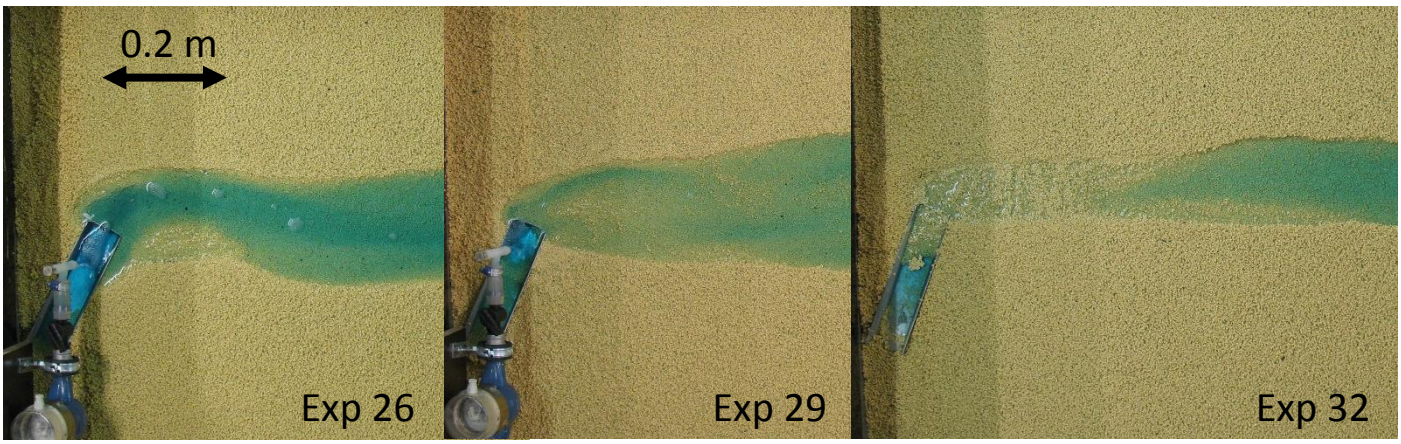

Fig. 25: Time-lapse photograph after 300 tidal cycles. The experiment without river inflow (32) filled up at the upstream boundary, while in the other experiments bars initiated.

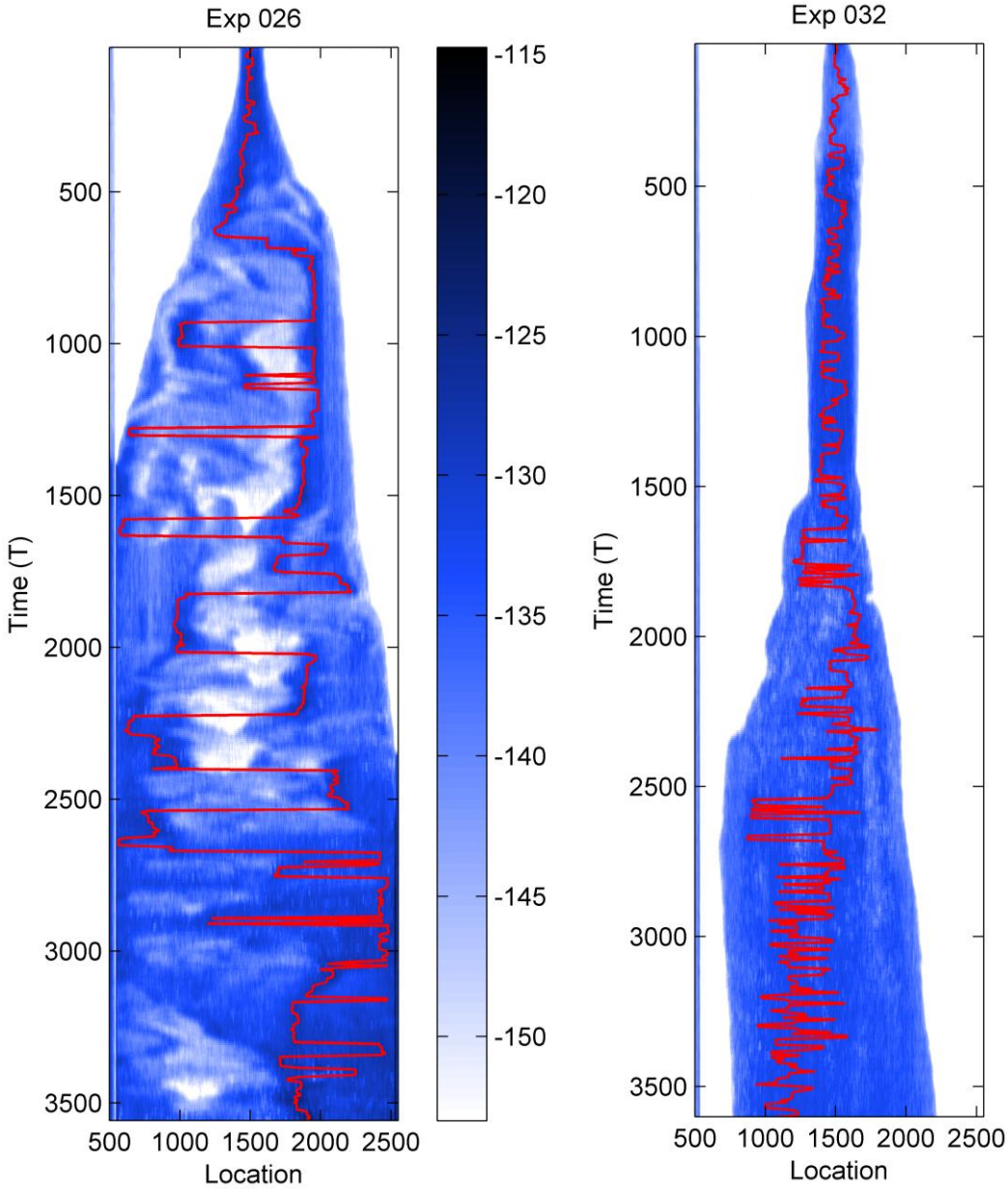

Fig. 26: Time stack of upstream cross-sectional area for experiment 26 and 32. Yellowness obtained from LAB colour space is used as a proxy for presence of channels and relative channel depth. The B-band (yellowness) is converted to blue colour scales – deeper channels are darker blue. Abscissa shows the location in amount of pixels. The width of a pixel is 0.51 mm. In all panels T corresponds to the duration of one tidal cycle. The red line indicates the location of the maximum channel depth. The direction of river inflow in this figure was to the left.

In experiment 26, the width of inlet and upstream estuary grew at similar rates until maximum width was reached (Fig. 27c). Without river flow (exp. 32), the growth of the inlet corresponds to the growth of the inlet with river flow for the initial phase. However, the width at the upstream location remained constant in this phase. Growth of the tidal basin from the seaward boundary in landward direction possibly triggered upstream growth (t=1400·T, Fig. 27c-Fig. 24). A constant width or area would suggest an equilibrium (steady state without trend): dynamic under the condition of channel and bar dynamics and otherwise static. The increase of width and total surface area decreased over time. For example the total area and width in experiment 32 flatten off in the final phase of the time series (Fig. 27cd). However, the time series are too short to prove constant gross properties. I am thus uncertain whether the final state of the experiments was a steady state.

A larger width (Fig. 27) and cross-sectional area (Fig. 30) of the inlet and larger total surface area suggested that the inflow of river discharge inflated the tidal system. The estuary (exp. 26) had a larger tidal prism compared to the short tidal basin (exp. 32): both the increased total surface area (Fig. 27d) and the increased cross-sectional area at the mouth (Fig. 30) suggested this.

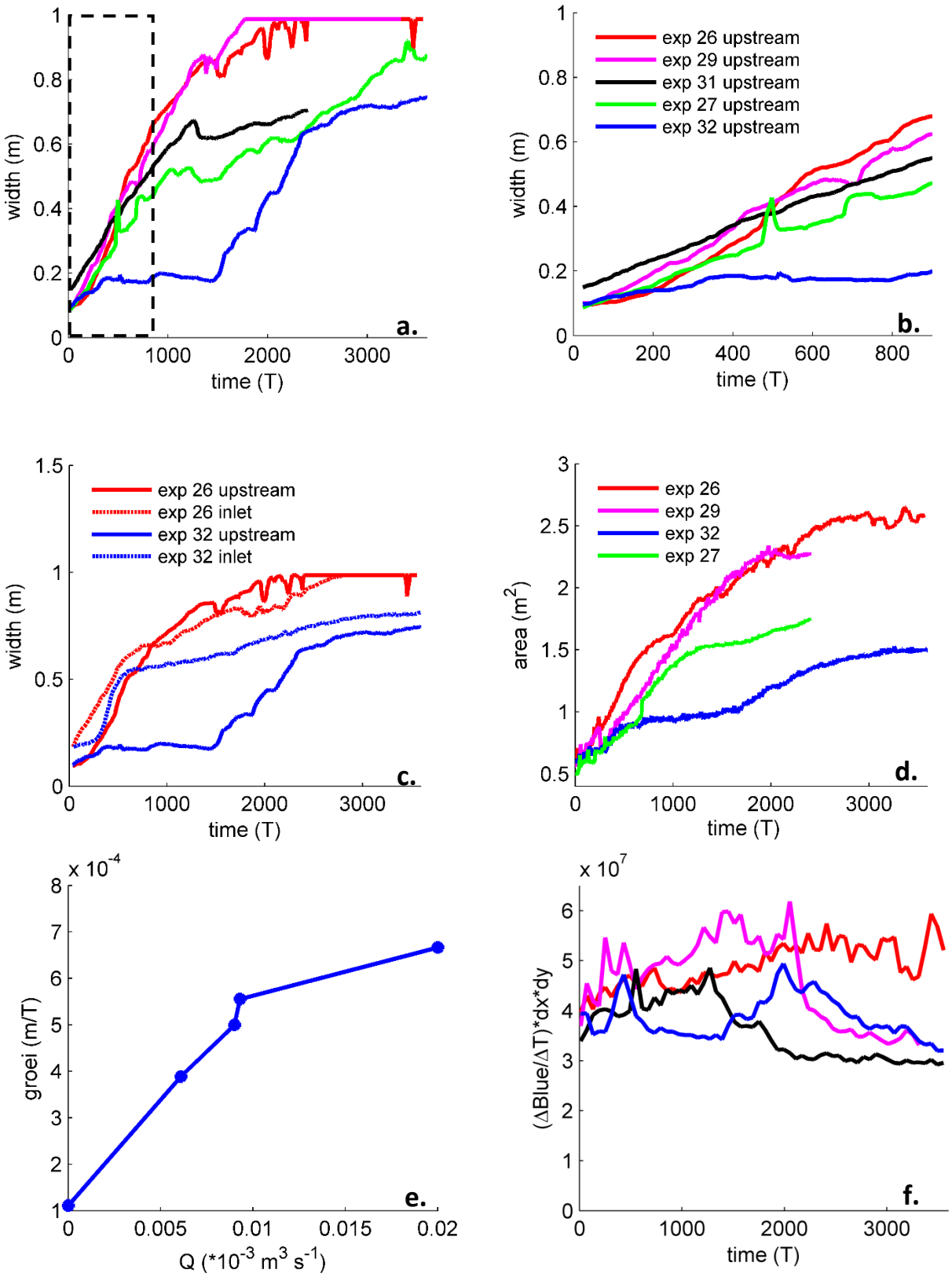

Fig. 27: (a) Time series of channel width at upstream cross-section. (b) Enlargement of the box shown in panel (a), showing the initial evolution of channel width. (c) Comparison of the evolution of inlet width and upstream channel width in experiments 26 and 32. (d) Time evolution of total estuary surface area in the experiments. (e) Growth of the width at the upstream cross-section in meters per tidal cycle as a function of river discharge. (f) Channel dynamics expressed as the variation in depth/colour in the full estuary over time. In all panels T corresponds to the duration of one tidal cycle.

In the other experiments (27, 29, 31), the dynamics of tidal channels over time resembled the dynamics of experiment 26 until the river was closed off (Fig. 28). The moment the river is closed off from the system by silting up is indicated with a green line in Fig. 28. Experiment 27 and 31 showed that after closure, channel dynamics ceased and bars disappeared. Experiment 29 showed the same tendency; the major difference was that closure of the river occurred after the width of the estuary covered the full flume. After the river was closed off from the system, bars vanished and the dynamics resembled experiment 32 without river discharge – a rather stable pattern of maximum channel depth and a constant channel width over time.

The final morphology of the estuaries in which the river closed off, correspond rather to the morphology of the tidal basin created in experiment 32 than to the high discharge experiment (26) (Fig. 29).

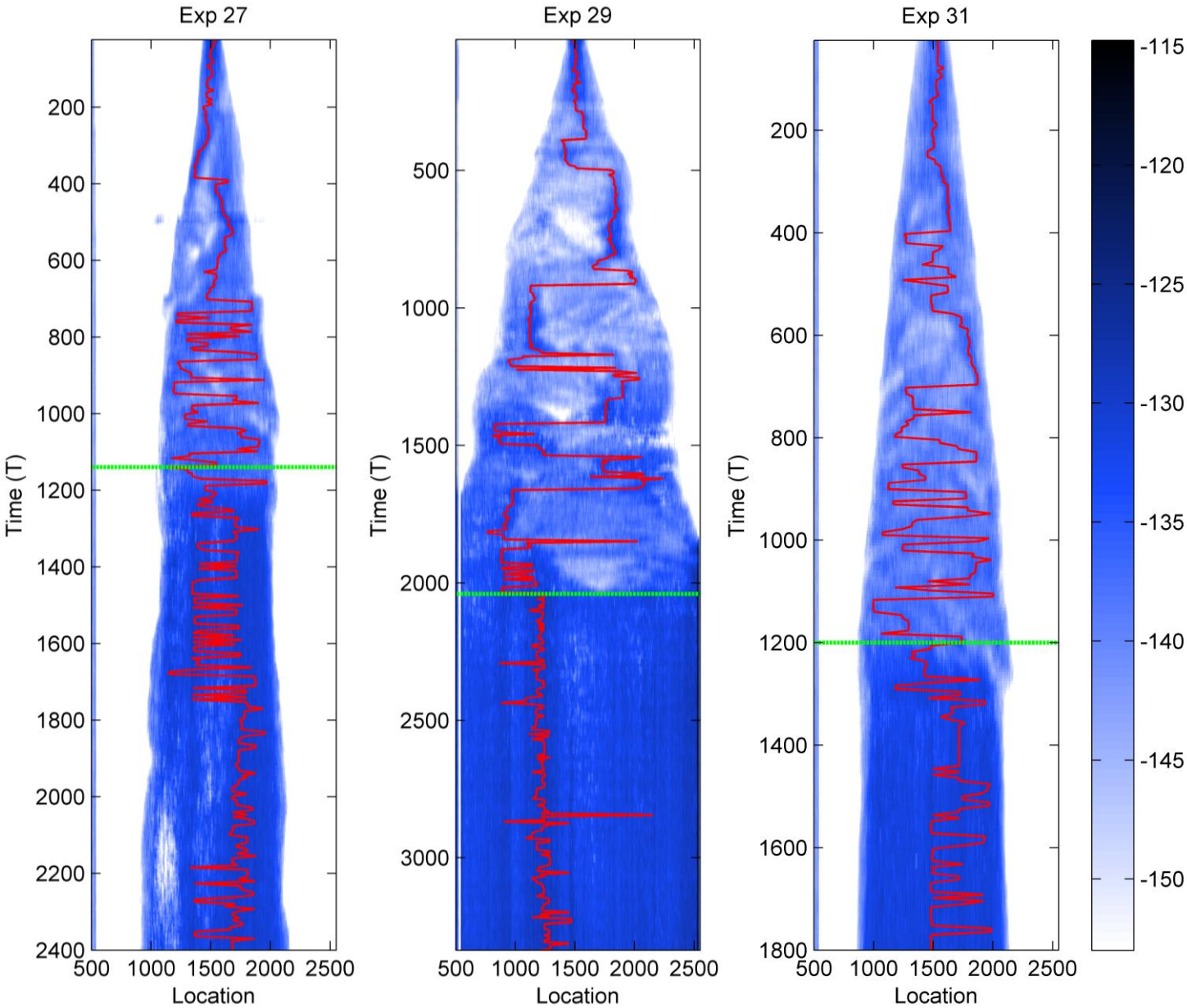

Fig. 28: Time stack of upstream cross-sectional area for experiment 27, 29 and 31. Yellowness obtained from LAB colour space is used as a proxy for presence of channels and relative channel depth. The B-band (yellowness) is converted to blue colour scales – deeper channels are darker blue. Abscissa shows the location in amount of pixels. The width of a pixel is 0.51 mm. In all panels T corresponds to the duration of one tidal cycle. The red line indicates the location of the maximum channel depth. Green lines indicate when the river closed off by infill of sediment at the upstream boundary. The direction of river inflow in this figure was to the left.

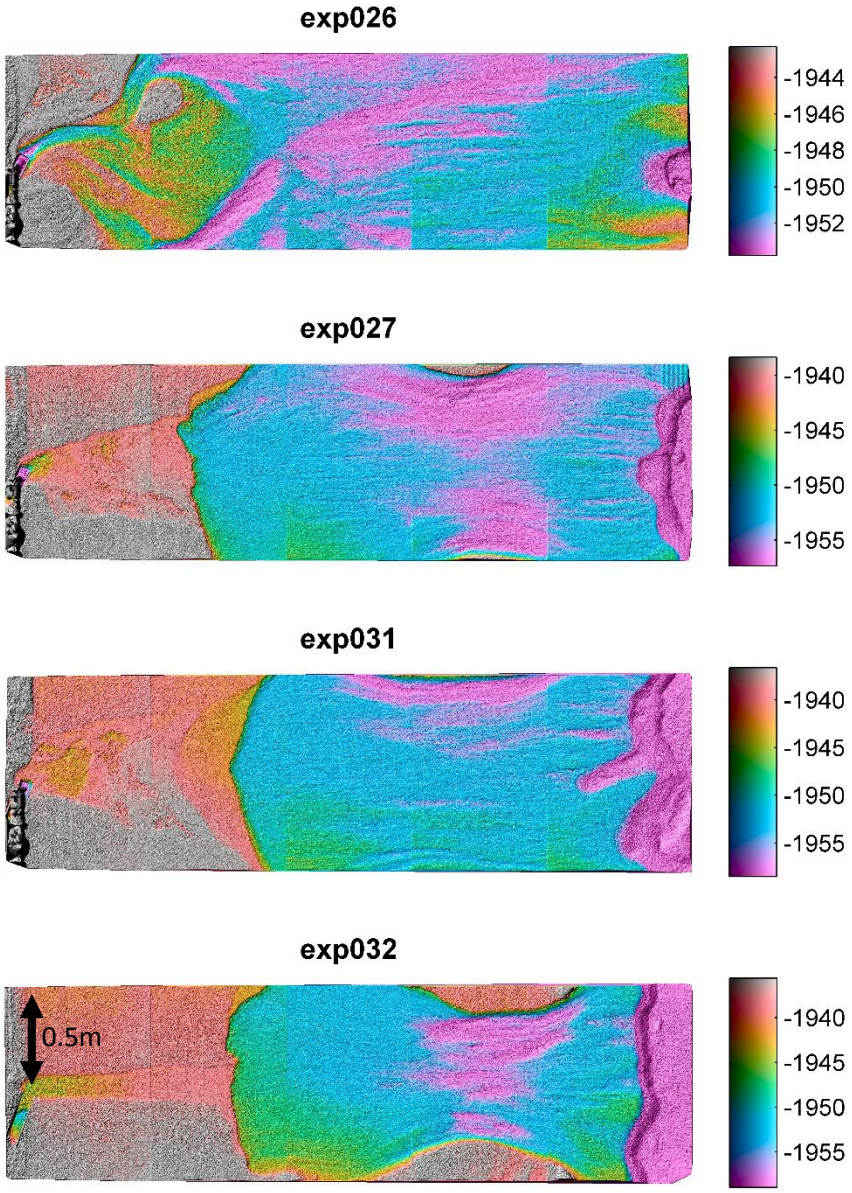

Fig. 29: Digital Elevation Model (DEM) of the final morphology of experiment 26, 27, 31 and 32. Colour bar indicates altitude in mm relative to the position of the camera. Higher values indicate lower areas.

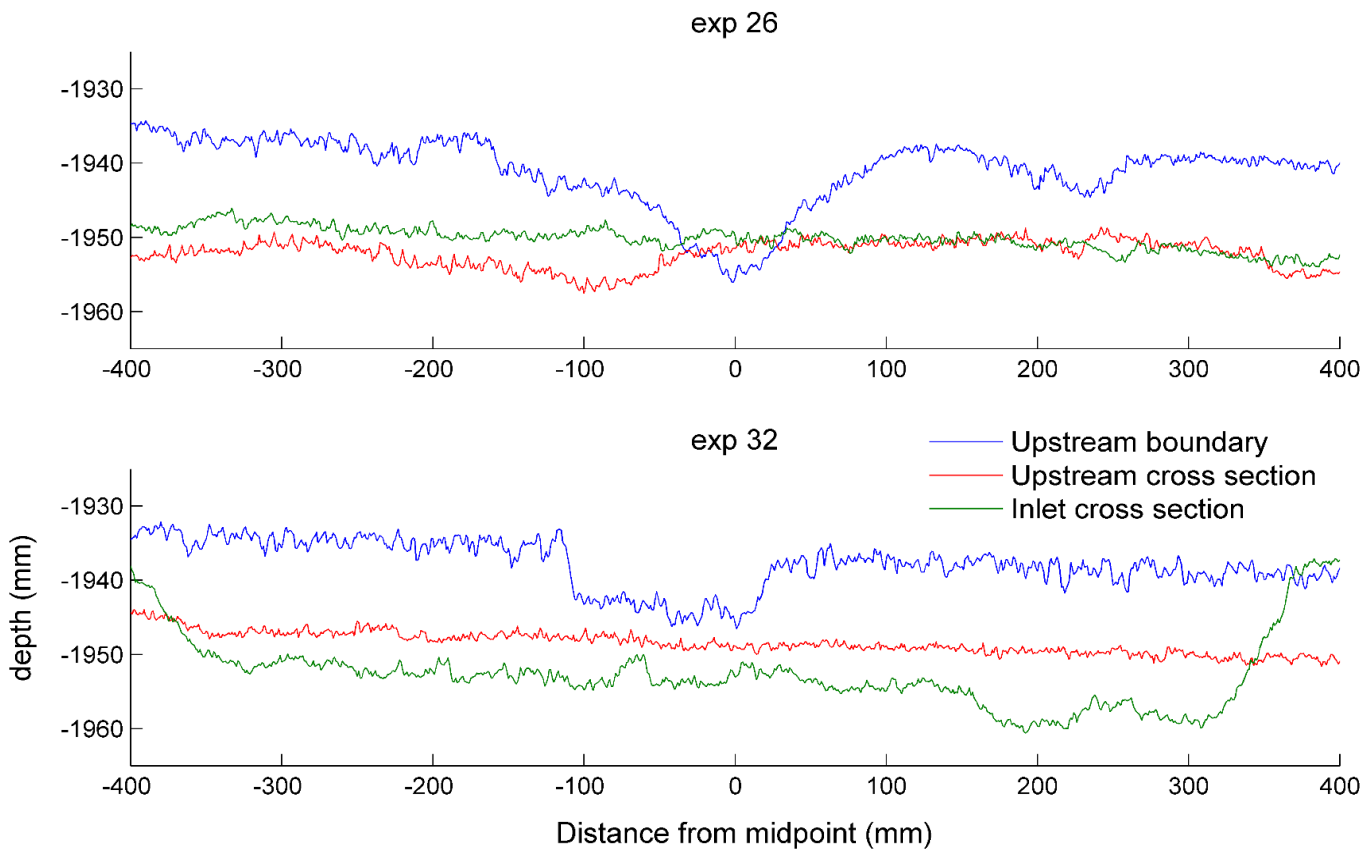

Fig. 30: Cross-sectional profiles obtained from the DEM (Fig. 29). The inlet and the upstream cross-section correspond to the locations indicated in Fig. 21. The cross-section at the upstream boundary was made as close to the upstream river as possible.

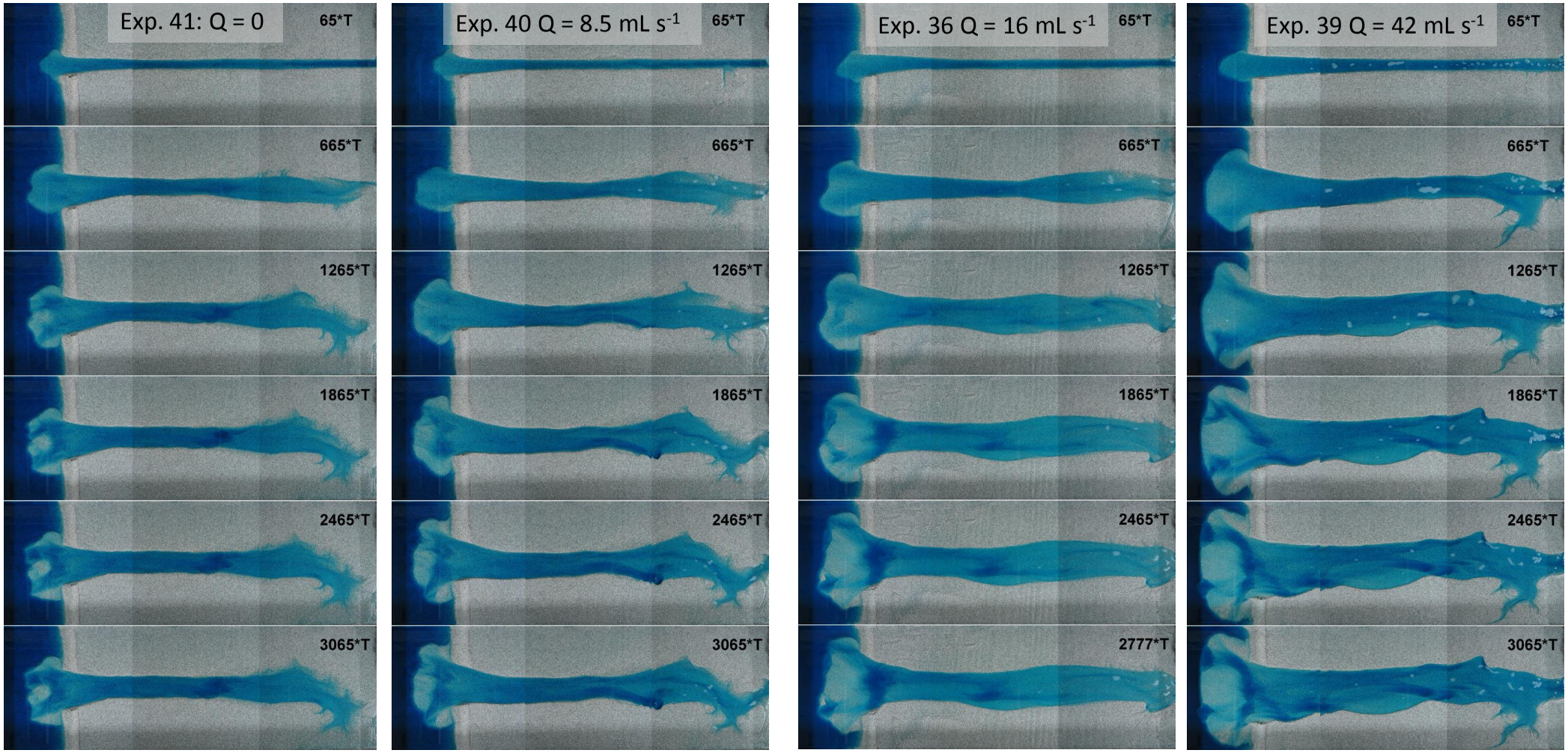

Fig. 31: Time series of images with increasing river discharge. The left panel shows the experiment without river discharge. All other initial and boundary conditions correspond in these experiments. In all panels T corresponds to the duration of one tidal cycle. (See Appendix 4 for QR-codes to the movie of experiment 39 in the Online Supplementary Material.)

3.2 Experiments with blasting polymer sediment

The initial phase of these experiments (36, 39, 40 and 41) resembled the experiments with the yellow polystyrene sediment, which was characterised by growth of the ebb-tidal delta and a single converging channel (Fig. 31). In contrast with the previous experiments, no bar developed in the inner bend of the upstream boundary, except for experiment 40 in a later stage (Fig. 32).

After approximately 120 tidal cycles the flood flow initiated a bifurcation at the upstream boundary. During flood phases, the sediment bed at the upstream boundary flooded. The following drainage, during the ebb phase, caused some initial depressions in the upstream surface area. Preferential flow in the lower areas of the perturbated surface, created new channels by backward erosion. This eventually caused a tidal network at the upstream boundary (Fig. 33).

In some cases (exp. 36, 39 and 40), the formation of the tidal network caused dynamic channels and shoals with mutually evasive ebb and flood tidal channels (t=665·T) (Fig. 32, Fig. 33). Mid-channel bars formed together with the preferential ebb and flood channels.

During the growth of the tidal network upstream, flow bifurcated on the ebb-tidal delta (t=665·T in exp. 36 and 39, somewhat later, t=1000·T for exp. 41 and 40). After the bifurcation of the ebb-tidal delta, scour holes formed at the ebb tidal delta or slightly landward (t=1200·T) (Fig. 34). After t=1865·T scour holes were found also in the estuary channel. Initial scours grew and were mobile. In the final stage of the experiments, scours probably reached equilibrium: dimensions were constant and locations remained fixed (compare t=2465·T with t=3065·T, Fig. 31). The formation of scour holes altered the hydrodynamics such that the dynamics of tidal channels vanished. However, sediment remained mobile until the end of the experiments.

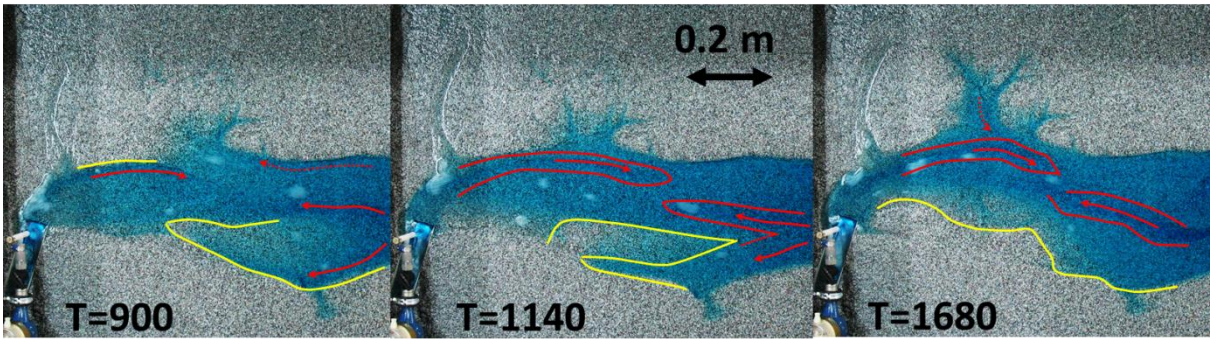

Fig. 32: Evolution of the upper estuary in experiment 40. Preferential ebb and flood channels developed and a bar built up at the inner bend of the river inflow. Red lines indicate the channels, red arrows flow direction, yellow lines the contours of the bars.

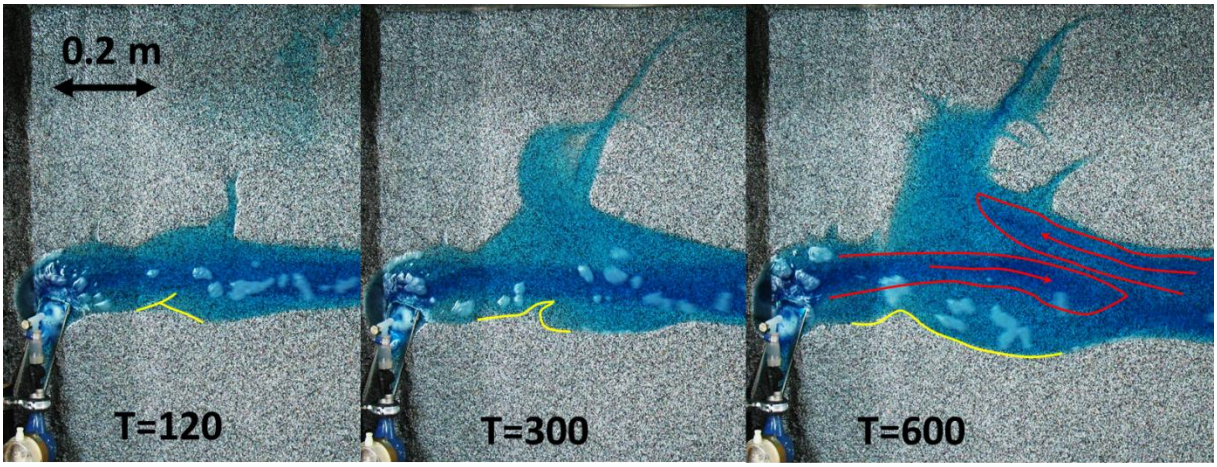

Fig. 33: Initiation of bifurcation at the upstream boundary in experiment 39. An initial perturbation (left) evolved to a tidal network (right). Red lines indicate the channels, red arrows flow direction, yellow lines the contours of the bars.

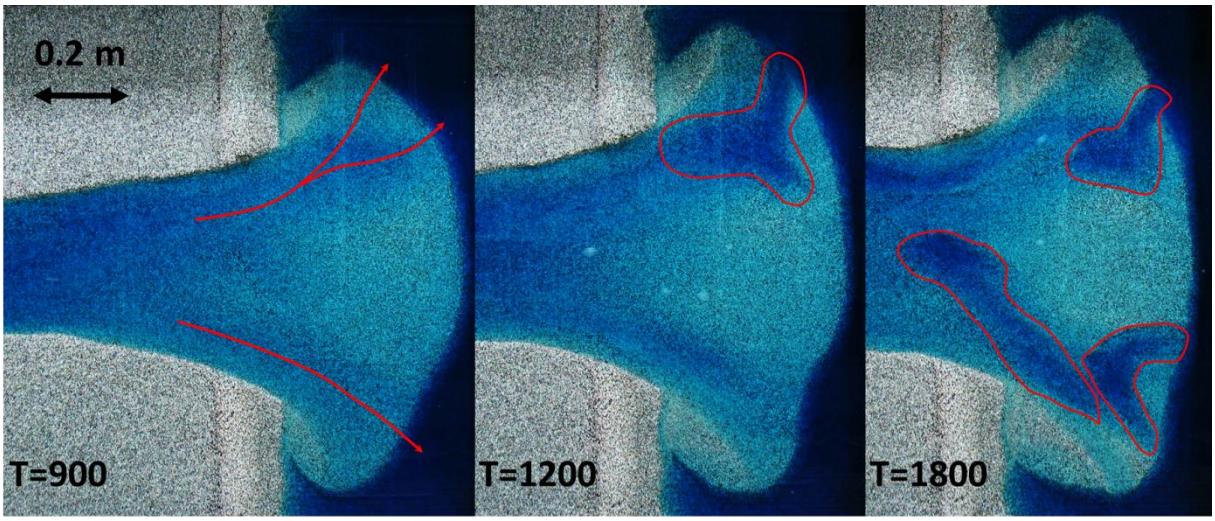

Fig. 34: Evolution of the ebb-tidal delta in experiment 39. Scour holes initiated in this experiment after 1200 tidal cycles. Red lines indicate the contours of scours, red arrows flow direction.

The width of the upper estuary increased similarly for all experiments, with approximately equal rates. The terminal width was the smallest for the experiment without river. Equilibrium width was reached after 1000 tidal cycles (Fig. 36a). Maximum terminal width in the upper estuary was found for experiment 36 (Fig. 36a). The decrease in river flow in the highest discharge experiment possibly (exp. 39) affected the final width.

At approximately t=1700·T, the width of the upper estuary was in equilibrium for experiments 36, 39 and 41 – for experiment 40 somewhat later (t=2000·T). Total estuary area was constant after 1800 tidal cycles in all experiments. Both the constant width and total estuary surface area suggested equilibrium state after 1700 tidal cycles (Fig. 36bc).

The width of the inlet grew fast at the start of all experiments (during the first 100·T), after this period, growth declined (Fig. 36a). The rate of growth from that phase onward was dependent on river discharge: the higher the river discharge, the stronger the growth was (Fig. 36d). Inlet width reached equilibrium at the same time as the width at the upper cross-section in experiment 40 and 41. For the other two experiments, width kept increasing after 2400 tidal cycles. This corresponds with the phase that large scours were present at the exact location of the inlet (Fig. 31).

Differences in width between the upper cross-section and the cross-section in the middle of the flume were very small. Width was generally a bit smaller in the middle of the flume, compared to the upper estuary (Fig. 36b). In the final state, total estuary surface area was largest for the experiment with highest river discharge (exp. 39) and smallest for the case without river flow (exp. 41) (Fig. 36c). Increased river discharge caused a larger tidal prism compared to the experiments with lower river discharge and without river discharge. The increased total surface area of the upper estuary (Fig. 35) and the increased cross-sectional area of the inlet (Table 11) suggested this.

The final morphology of all experiments was characterised by a large amount of scour holes in a convergent channel (Fig. 35; Fig. 37). The strongest channel width convergence was found in the experiment without river discharge and with the most river discharge (Table 11). There is no trend between river discharge and channel convergence.

Since in most cases the scours covered only a part of the channel width, it was still possible to determine the average channel depth of the cross-sections (Fig. 37). I neglected scours in the calculation of average depth. After all, scours formed in the main estuary channel after equilibrium conditions set in, so width and depth were already constant before the scouring phase.

From calculations of width to depth ratio, I found that an increase of river discharge resulted in larger width to depth ratios in both the upper estuary and the estuary mouth (Table 11). Only the upstream width to depth ratio of experiment 39 deviates from the trend. This can be explained by the lower upstream width, which was caused by a decreasing river discharge during the experiment.

Table 11: Width to depth ratios, convergence length scales (see Eq. 2) and cross-sectional area at the mouth. Data on width and depth were obtained from the cross-sectional profiles (Fig. 37). Scour holes, indicated in Fig. 37, were excluded in the calculation of the average channel depth. Higher values of convergence length (L_W^{-1}) indicate stronger convergence.

Experiment	W/h_{inlet}	$W/h_{upstream}$	A_{inlet} (m^2)	Convergence length (L_W^{-1})
39	35.3	34.3	0.0098	0.294
36	26.7	36.0	0.0060	0.079
40	24.6	20.4	0.0044	0.141
41	19.2	13.3	0.0053	0.356

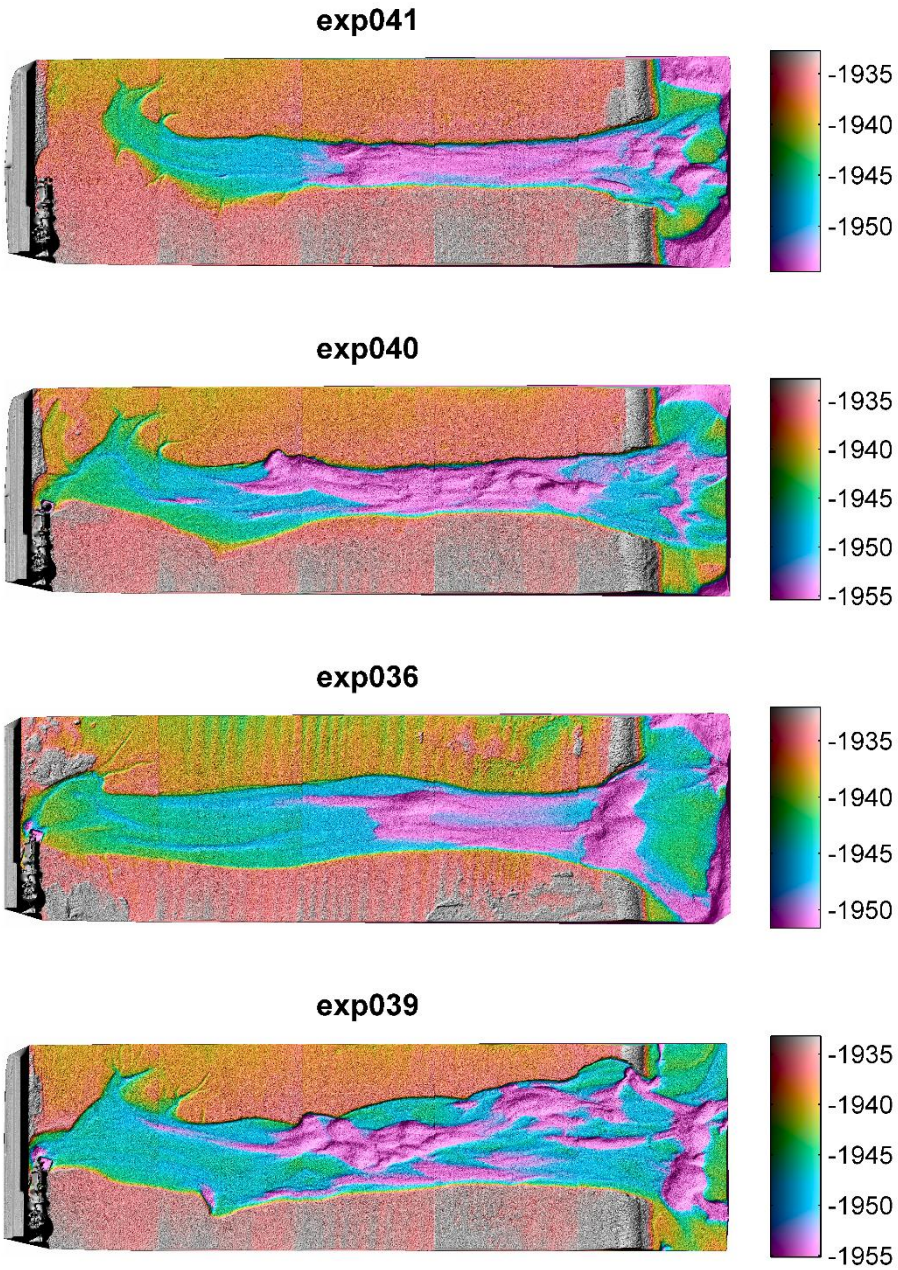

Fig. 35: Digital Elevation Model (DEM) of the final morphology of experiment 41, 40, 36 and 39. Colour bar indicates altitude in mm relative to the position of the camera. Higher values indicate lower areas.

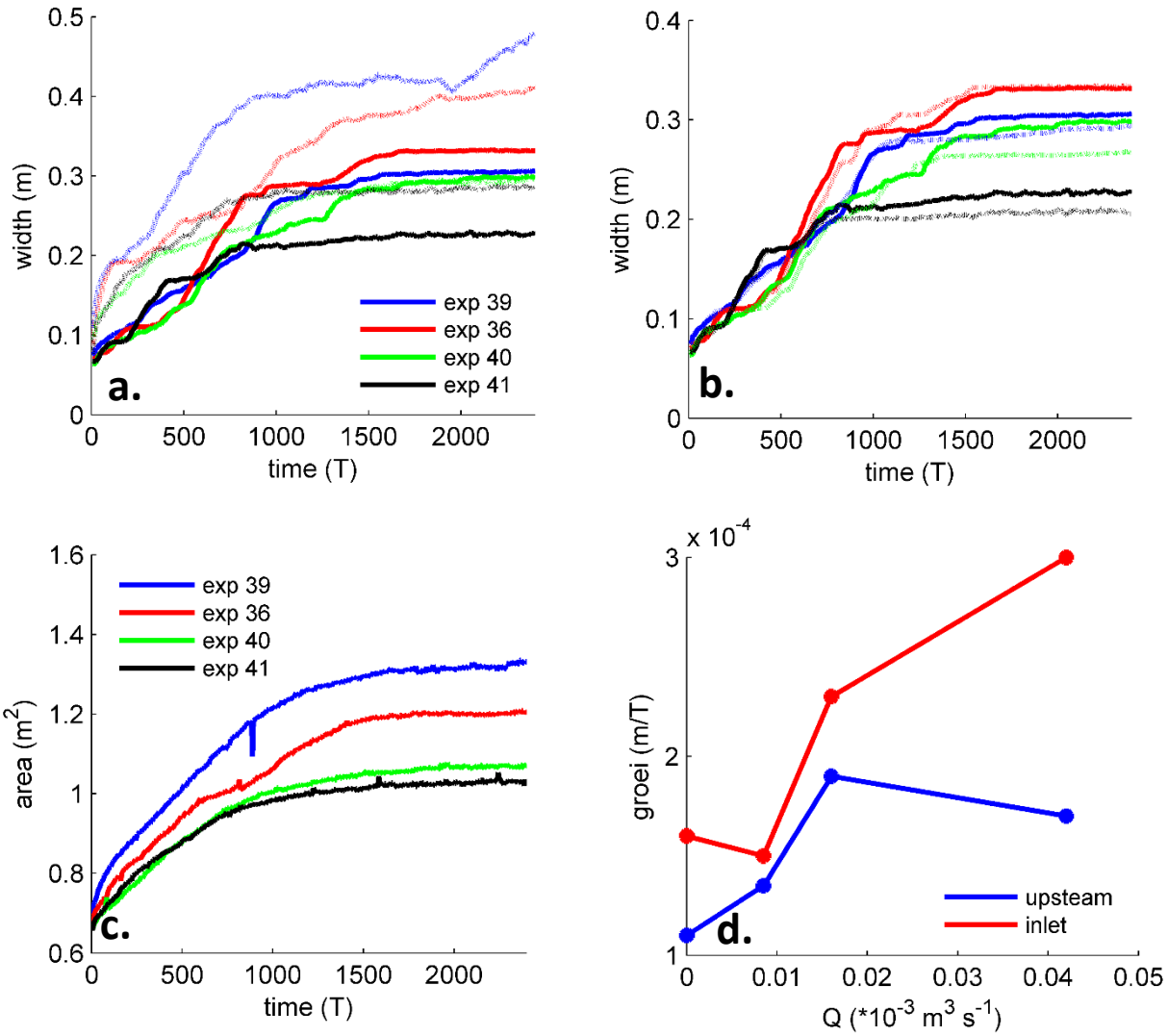

Fig. 36: (a) Time series of channel width at upstream cross-section (solid line) and inlet (dotted line). (a) Time series of channel width at upstream cross-section (solid line) and cross-section made in the middle of the flume (dotted line) (See Fig. 21). (c) Time evolution of total estuary surface area in the experiments. In all panels T corresponds to the duration of one tidal cycle. (d) Growth of the width at the upstream cross-section and inlet in meters per tidal cycle as a function of river discharge.

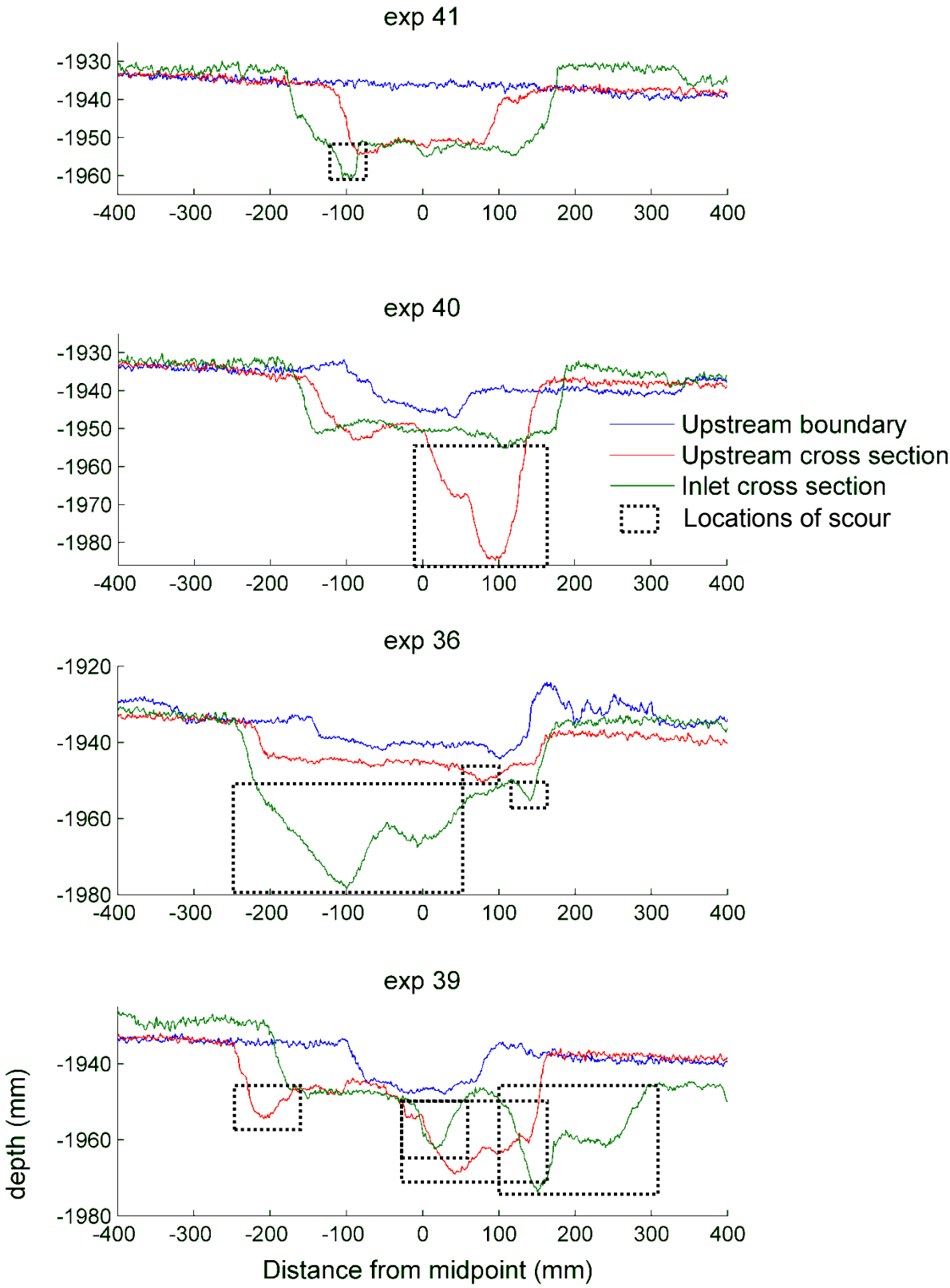

Fig. 37: Cross-sectional profiles obtained from the DEM (Fig. 35). The inlet and the upstream cross-section correspond to the locations in Fig. 21. The cross-section at the upstream boundary was made as close to the upstream river as possible. The locations of scour holes are indicated. The scour holes modified the altitude data in the final stage of the experiment.

3.3 Effect of river flow on relative width increase

Both the width of the upper estuary and inlet increased over time for all experiments. However, its behaviour seemed dependent on the amount of river inflow (Fig. 38). Results for experiments with both sediment types (polystyrene and polymer) are included in this section.

In the experiments with high river discharge, first large increase in inlet width occurred, followed by increase in upstream width (exp. 39, 26) (Fig. 38). For low or no river discharge, initially the inlet grew faster than the upper estuary, but only for a short period (until the inlet was ~0.2 m). From then on, upstream area increased faster. For low flow conditions, growth stops after upper estuary grew to the maximum estuary width – a slightly convergent equilibrium state.

The initial evolution of experiment 36 and 40 is similar (Fig. 38). Contrasting was that, when experiment 40 reached equilibrium dimensions, the inlet grew again in experiment 36. Growth of the upper estuary followed, after which the inlet grew again to reach equilibrium conditions. I observed the same tendency for the highest discharge case (exp. 39): a sudden growth of the inlet after it appeared that equilibrium set in.

Concluding, the cases with highest discharge (exp. 39 and 26) show counterclockwise hysteresis, while the experiments with lower discharge show more clockwise hysteresis (exp. 36 and 32) (Fig. 38). Continuous growth of the inlet width in experiment 32 eventually resulted in upstream widening of the estuary. Experiment 36 and 39 were characterized by an alternating stepwise increase of downstream and upstream width (staircase graph).

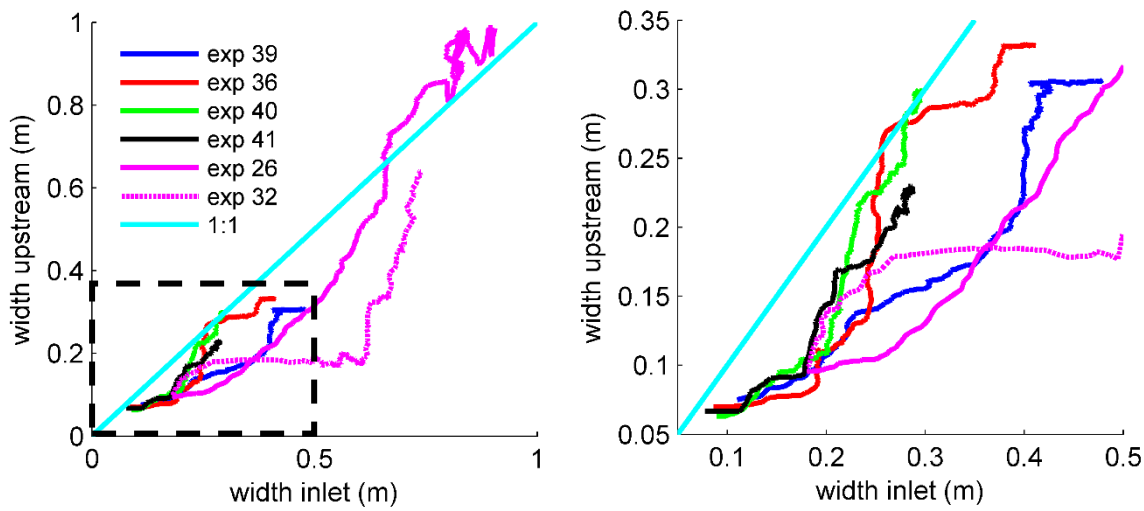

Fig. 38: (a) Comparison of widening at the upstream cross-section and inlet. (b) Enlargement of the box shown in (a).

4. Discussion

4.1 Large-scale equilibrium properties

River inflow increases the width of the upper estuary and estuary mouth resulting in larger total estuary surface area and larger tidal prisms (Fig. 27; Fig. 36). This is in agreement with the model results, which showed that river discharge widens estuaries (Fig. 12) and increases tidal prism (Fig. 15). The experiments with polystyrene sediment also showed that higher river inflow possibly causes deeper estuaries (Fig. 37). However, the experiment without river discharge resulted in approximately the same depth at the inlet as the experiment with the highest discharge.

From empirical relations on river channel geometry, it is known that width and depth depend on discharge (Lacey, 1929; Hey & Thorne, 1986; Parker et al., 2007). Hydraulic geometry relations for rivers are difficult to apply on estuaries, because (1) discharge varies over a tidal cycle, (2) flow direction reverses and (3) discharge comprises tidal discharge and river discharge. Nevertheless, empirical hydraulic channel geometry relations can explain why larger total discharge results in wider and possibly deeper channels.

Width to depth ratios increased due to river inflow. Model results, data from UK estuaries and the experiments confirmed this (Fig. 14; Fig. 37; Table 11). If estuary channel and bar pattern is dependent on width to depth ratio – just as with rivers (Kleinhans & Van den Berg, 2011) – river flow possibly influences estuary patterns. The mechanism for the increase in width to depth ratios comprises possibly of three steps. River discharge increases estuary width, which causes larger tidal prisms. The increased tidal prism results in higher tidal discharge, causing wider and deeper channels with a higher width to depth ratio.

The estuary kept growing in the experiments with blasting polymer sediment (Fig. 27). Kleinhans et al. (2014b) recognised the higher erodibility of sediment at the banks also in their experiments of tidal basins. The concept of 'threshold channels' (Parker, 1978) describes that entrainment of sediment continues until mobility is below critical values for motion in the full basin – after all, bank slope is higher than bed slope, which causes lower critical values at the banks. Experiments in this research with blasting polymer showed that dynamic equilibrium dimensions can be reached in the experimental setup. Whether I should address this to the higher density, higher cohesion, lower permeability or a combination of these factors is uncertain.

Davies & Woodroffe (2010) obtained from analysis of estuaries in Australia that river discharge causes estuaries with larger e-folding length scales, indicating estuaries in which width ceases less over distance. Results in this study indicated that convergence is independent of river discharge in experimental estuaries (Table 11). However, asuming constant estuary length, a stronger estuary convergence results in larger channel width on all locations along the estuary. Davies & Woodroffe (2010) conclude that fluvial discharge tends to promote wider channels, which is in agreement with my experimental results.

Surprisingly, the evolution of estuary width over time showed hysteresis (Fig. 38). High river inflow caused staircase patterns in the evolution of width, which characterises distinct phases of inlet and upper estuary growth. These results also showed that the morphological response to high river inflow initially may resemble the response to low flow cases, but in the final state result in a sudden increase of the inlet width.

Besides inflation of gross properties by river inflow, I found that without river inflow a tidal system evolves into a short tidal basin. Experiments with polystyrene sediment implied that a threshold of river discharge was required to keep the estuary open. This is in agreement with the hypothesis that Davies & Woodroffe (2010) propose for estuaries in Northern Australia in where wave energy is generally low (Porter-Smith et al., 2004).

Experimental results form a strong contrast with previous studies of estuaries in which river discharge was considered insignificant. The results of this study imply that river inflow is one of the key drivers for estuarine morphodynamics and must be included in any long term prediction.

4.2 Small-scale dynamics of channels and shoals

I found that river inflow enhances small scale dynamics of estuaries – particularly migration and shifting of channels and reversals in ebb and flood dominance of channels. Dynamic bars formed and active channel migration occurred only under the condition of river inflow (Fig. 26; Fig. 27f; Fig. 28). Dynamics and bars instantaneously vanished when the river disconnected from the estuary by infill of sediment (Fig. 27f; Fig. 28).

River inflow probably stabilises the ebb tidal channel by enhancing the flow and seaward sediment transport in this channel. Without sufficient river discharge, flood flows eventually disconnect the ebb tidal channel that starts at the upstream boundary by forming a plug bar. Schramkowski et al. (2002, 2004) described theory on the occurrence and stability of tidal bars, which is related to channel width, depth and friction. Based on the theory of Schramkowski et al. (2002, 2004) and Kleinhans & Van den Berg (2011), I expected a more braided bar pattern with higher river discharge – because river discharge increases width to depth ratios and probably bottom friction. Hibma et al. (2003) found the same trends as Schramkowski et al. (2002). Hibma et al. (2003) reproduced the dynamics of mutually evasive ebb and flood tidal channels in a 2D depth-averaged model. A full physical explanation for these features still lacks (Scharmkowski et al., 2004). However, Hibma et al. (2003) showed that non-linear interactions on an initially perturbated surface can reproduce the channel-shoal patterns observed by Van Veen (1950). In addition, I found that continuous flow through the ebb tidal channel – in this case by river inflow – might be required for this mechanism to work.

Kleinhans et al. (2014a) reproduced the ebb and flood-dominant channels in experiments. They described that mutually evasive channels occur with the onset of tidal bar formation: one flow direction evades the heads of bars formed by the flow in opposite direction. I performed two sets of experiments in this research of which only the first set (with polystyrene sediment) showed this behaviour. Experiments without river flow and with blasting polymer sediment lacked dynamic ebb and flood tidal channels. This might be related to the width of the estuary: the channel in the polystyrene experiments with river flow was rather wide and shallow, while in the other experiments, the channel was more narrow. Upstream perturbation by means of river inflow is possibly required to obtain sufficiently large width to depth ratios in which mutually evasive channels form.

Bar theory for estuaries has an analogy with rivers, for which it was described by Kleinhans & Van den Berg (2011). Channels migrated towards the outer bend of the upstream ebb tidal channel in experiments 26, 27, 29 and 31. This resulted in a sharper bend and eventually chute cutoff by landward erosion of the flood tidal channel. When the cutoff occurred, the upstream part of the original ebb tidal channel filled in with sediment. The channel was then temporarily deserted, after which it became a flood tidal channel. In river morphology, chute cutoffs indicate the transition from meandering to braided river pattern (Kleinhans et al., 2014b). Similar cutoffs in estuaries may indicate a change of estuary pattern. So far we only have precarious theory for estuary bar and channel patterns as given by Schramkowski et al. (2002, 2004) and Hibma et al. (2003).

Concluding, previous research pointed yet out that width, depth, friction and width to depth ratio determine the occurrence of tidal bars. I showed for the first time that river discharge might be required to create sufficiently wide and shallow estuaries in which dynamic channels and bars can occur. The effect of river discharge may even explain why ebb and flood dominance of tidal channels reversed and channels changed course over time.

4.3 Similarity of morphology and dynamics with natural systems

Comparison of general morphology and dynamics observed in nature can be used to assess the similarity between scaled experiments and natural systems (Kleinhans et al., 2014b, 2014c). Both the full estuary scale and characteristic features are compared to the Whitehaven beach estuary (Australia) and the theoretical model of Martinius & Van den Berg (2011) (Fig. 39).

I observed much similarity between the experiments and natural systems. The estuary is characterised by a main converging channel and an ebb tidal delta at the seaward boundary (Fig. 39abcde). While dynamic channels and mutually evasive ebb and flood tidal channels where very similar (Fig. 39bde), the tight meanders – characteristic for the fluvial-tidal transition zone (Fig. 39de) – were absent in the experiments (Fig. 39abc). Particularly the experiments with polystyrene sediments showed the tendency to form scroll bars. Tight meanders were absent because floodplain formation and bank strength were probably too low to build these up (Van Dijk et al., 2012). A small tidal network formed in my experiments at the upstream boundary (Fig. 39a). This resembles tidal networks commonly observed on salt marshes (Fig. 39d). I conclude that the experiments resembled natural estuaries reasonably well for both the cases with river discharge (Fig. 39abde) and without river inflow (Fig. 39cf).

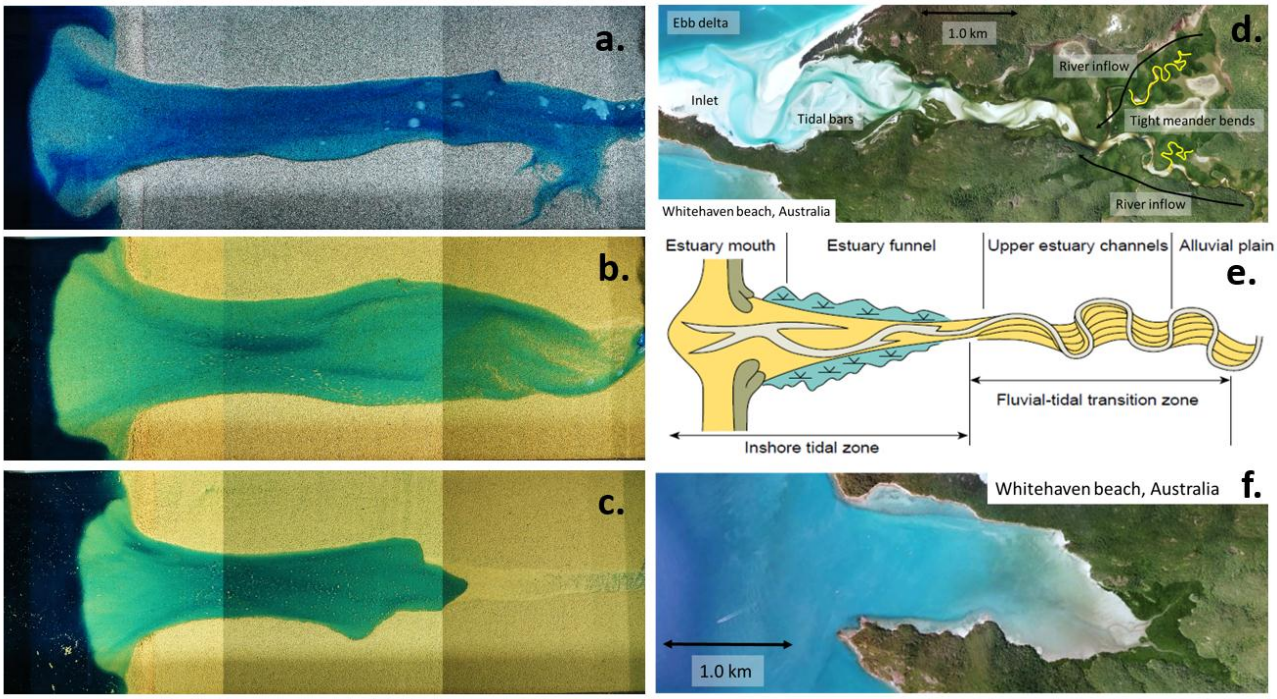

Fig. 39: Comparison of theory, natural systems and experiments. Boxes with the same colour indicate similar features. (a) Experiment 39 after 1350 tidal cycles. (b) Experiment 26 after 900 tidal cycles. (c) Experiment 32 after 900 tidal cycles. (d) Whitehaven beach estuary, Australia with significant river inflow (Google Earth). (e) filled equilibrium estuary (Martinius & Van den Berg (2011), modified after Dalrymple et al. (1992), Boyd et al. (2006) and Van den Berg et al. (2007)). (f) Whitehaven beach estuary, Australia with low river inflow (Google Earth).

Another way to assess the similarity between scaled experiments and natural systems is by comparison of dimensionless numbers that characterise the system (Kleinhans et al., 2014b, 2014c). I calculated characteristic values of hydrodynamics and sediment mobility for the laboratory experiments and for the Oer-IJ, Western Scheldt, Thames, Tweed and Coquet estuary (Table 12). Typical values for the experiments correspond to the final state of the experiments.

Table 12: Comparison of dimensional and dimensionless numbers for scaled laboratory experiments and natural estuaries. The Coquet estuary is a bar built estuary and the Tweed estuary is a complex estuary. These estuaries were selected from the dataset with United Kingdom estuaries (Manning, 2012), based on the relative flow velocity of the river (hypothetical flow velocity of the river at the inlet of the estuary divided by tidal flow velocity). Data for the Thames, Tweed and Coquet estuary were adopted from Manning (2012). Grain size for the Thames was obtained from Whitehouse (1995) and for Tweed/Coquet estimated to be 0.18 mm. Data for Western Scheldt were adopted from De Bok et al. (2001), Gourgue et al. (2013) and De Jong & Gerritsen (1984). Data for the Oer-IJ were based on Vos et al. (2011).

Variable	Exp. 26	Exp. 39	Western Scheldt	Thames	Coquet (UK)	Tweed (UK)	Oer-IJ	Explanation
u ($m \cdot s^{-1}$)	0.10	0.15	1.5	1.02	0.60	0.66	1.0	Velocity
h (m)	0.012	0.014	10	6.4	4	5.4	2	Depth
T (s)	22	28	44640	44640	44640	44640	44640	Tidal period
a (m)	0.006	0.008	1.50	2.10	1.06	1.32	0.75	Tidal amplitude
L_e (m)	2.8	2.8	$160 \cdot 10^3$	$82.5 \cdot 10^3$	$5.0 \cdot 10^3$	$9.9 \cdot 10^3$	$30 \cdot 10^3$	Basin length
A (m^2)	2.6	1.3	$1500 \cdot 10^5$	$2000 \cdot 10^5$	$7.5 \cdot 10^5$	$7.62 \cdot 10^5$	$439 \cdot 10^5$	Total estuary area
Q ($m^3 \cdot s^{-1}$)	$2.0 \cdot 10^{-5}$	$4.2 \cdot 10^{-5}$	120	66	9	80	500	River discharge
τ (Pa)	0.20	0.28	2.73	1.31	0.50	0.66	1.64	Shear stress
C ($m^{0.5} \cdot s^{-1}$)	22.1	27.9	90.0	88.3	83.7	80.6	77.4	Friction
θ (-)	0.23	0.12	0.84	0.51	0.17	0.23	0.51	Sediment mobility
Fr (-)	0.29	0.40	0.15	0.13	0.10	0.09	0.23	Froude number
Re (-)	1019	1832	$129 \cdot 10^5$	$56 \cdot 10^5$	$21 \cdot 10^5$	$31 \cdot 10^5$	$17 \cdot 10^5$	Reynolds number
Re^* (-)	25.66	17.43	9.00	4.99	3.49	3.98	6.98	Reynolds particle number
L_w^{-1} (m)		3.42	$2.95 \cdot 10^4$	$1.64 \cdot 10^4$	$0.57 \cdot 10^4$	$0.47 \cdot 10^4$	$1.67 \cdot 10^4$	Convergence length width
$(L_w/L)^{-1}$ (-)		0.39	2.71	3.04	0.88	2.12	1.79	Relative convergence
$u_{r\ inlet}$ ($m \cdot s^{-1}$)	0.0025	0.0043	0.0019	0.0016	0.0239	0.0286	0.0556	Velocity river at inlet
u_r/u (-)	0.025	0.028	0.001	0.002	0.040	0.043	0.056	Relative velocity

Sediment mobility is relatively low compared to the large natural systems, but resembles the smaller estuaries in the UK very well. I thus conclude that the combination of a periodically tilting flume with light-weight sediments solved the problem of low sediment mobility in previous experiments (e.g. Stefanon et al., 2010). Froude numbers are well below the transitional value for critical flow and Reynolds numbers indicate turbulent flow in all cases.

The setup of previous experiments of tidal systems resulted in solely ebb-related sediment transport until mobility was below the beginning of motion – static equilibrium (Reynolds, 1889, 1890, 1891; Tambroni et al., 2005; Stefanon et al., 2010). My experiments showed that flood-related sediment transport could also occur. For example in the experiment without river discharge, the upper part of the initial channel filled in (Fig. 24).

Reynolds particle numbers in my experiment are high compared to other experiments of tidal systems (Table 14). Unfortunately, final bed conditions corresponded to hydraulic smooth conditions in the experiments with blasting polymer sediments. The smooth conditions explain the emergence of relatively deep scour holes in the final stage of the experiments (Fig. 35) (Van Dijk et al., 2012). Scours were the most abundant and deepest in the experiment with the highest river discharge. The emergence of scour holes is further discussed in chapter 10.

Spatial scales of the experiments are approximately 10,000-100,000 times smaller than natural systems. The experimental estuaries formed in approximately 3000 tidal cycles, which would correspond to about 4 years in nature. Natural estuaries developed typically 10-1000 times slower: morphodynamics responded faster to hydrodynamics than in nature induced by higher sediment transport rates. One tidal cycle in my experiments thus probably corresponded to about 100 tidal cycles in nature, depending on the system I compare the experiment to. Furthermore, tidal cycles in my experiments were about 1700 times shorter than in nature.

Upscaling of ebb and flood tidal channels in the polystyrene sediments results in very long (± 12 km) and wide (± 2 km) channels that are mutually evasive. The scale of ebb and flood dominance reversal, would correspond to the scale of avulsions in river systems. The explanation for the large dimensions is unclear. Groundwater flow was higher than in natural systems and may be part of the explanation.

The permeability of the sediment affects groundwater flow. Groundwater outflow causes weaker banks and additional channel discharge, which simulated the outflow of small creek systems and tidal marshes (Kleinhans et al., 2014b). Since outflow was too high in the first set of experiments, I controlled groundwater flow in the second set of experiments (with blasting polymer).

Compared to the Tweed, Coquet and Oer-IJ estuary, the amount of river inflow compared to tidal flow seems appropriate in my experiments. For these estuaries, dimensionless numbers are closest to typical experimental values. Estuaries such as the Thames and Western Scheldt appear to be much less influenced by river inflow. Interestingly, these estuaries have the most convergent channels of all estuaries compared here, which is in line with my observation that correlation between river discharge and channel convergence is low.

4.4 Future research

New questions arise from the result that river inflow is important for estuarine morphology. Ideally, I would also investigate the effect of adding river inflow to an initially stable short tidal basin. Furthermore, these experiments showed that river inflow causes dynamic behaviour of channels. Dynamics might change and even increase if the direction of river inflow changes over time, such as was done in meandering river experiments (Van Dijk et al., 2012).

Many estuaries filled up during the Holocene, for example the Dutch estuaries, including the Oer-IJ (Berendsen & Stouthamer, 2000, 2001, 2002; Vos et al., 2011). What caused the filling of these estuaries? Was it a river avulsion that caused a decrease in river discharge and caused infilling or caused estuary infilling the river avulsion? Future model and experimental approaches will probably concern the interplay of estuaries, bifurcations and avulsions.

Also the conditions under which mutually evasive ebb and flood tidal channels evolve in estuaries are still poorly understood. There is a strong desire for a mechanism that describes the occurrence, which can help explaining under which conditions ebb and flood tidal channels are stable and how they will respond under future climate change and human intervention.

So far the tilting flume demonstrated promising results for experimental approach of tidal systems and estuaries (also Kleinhans et al., 2014a, 2014b). Some scaling issues still remain, such as relatively low sediment mobility, low bank stability and the occurrence of scour holes. These problems will be addressed shortly with a larger and more advanced facility, which will also allow experiments with more cohesive floodplains and a sustained dynamic upstream perturbation (Kleinhans, 2013). These factors appeared necessary for dynamic meandering in river experiments (Van Dijk et al., 2012) and might enhance the similarity of experiments to nature.

5. Conclusions

I studied the effects of upstream river discharge on the small-scale channel-shoal dynamics and large-scale equilibrium planform and dimensions of estuaries. A behaviour-oriented model (Townened, 2010) was modified and used together with two sets of tilting flume experiments with light-weight sediments. Typical values of river flow velocity divided by tidal flow velocity in the experiments were 0.015-0.030. This corresponds to small estuaries in the UK, such as the Tweed, Coquet and Oer-IJ estuary. Other scaling parameters – such as sediment mobility and hydraulic rougness – seemed appropriate for these estuaries.

River inflow increases the width of the upper estuary and estuary mouth resulting in (1) larger total estuary surface area, (2) higher width to depth ratios and (3) larger tidal prisms. This conclusion is supported by my model results, experiments and data from UK estuaries. Experiments were inconclusive on the relation between channel convergence and river discharge, while the model results predicted stronger channel convergence.

The set of experiments with polystyrene particles showed that river inflow enhances small scale dynamics of estuaries – particularly migration and shifting of channels and reversals in ebb and flood dominance of channels. The occurrence of tidal bars possibly relates to the increase in width and width to depth ratio, which enhances bar formation according to theories of Schramkowski et al. (2002, 2004) and Kleinhans & Van den Berg (2011). A full explanation for the occurrence of bars associated with mutually evasive ebb and flood tidal channels as described by Van Veen (1950) still lacks.

So far the tilting flume demonstrated promising results for experimental approach of tidal systems and estuaries. Scaling issues remain in laboratory experiments, such as the occurrence of scour holes. Scour holes formed in experiments with blasting polymer sediments. My main conclusions regarding estuary dynamics and equilibrium remain, since scour holes formed after equilibrium set in. However, better understanding of the exact conditions under which scours form is required for further proceedings in laboratory experiments.

Acknowledgements

I wish to thank the following people, without whom this research would have been impossible:

Dr. Maarten Kleinhans – who put all his effort in getting the most out of me and surprised and inspired me every time again with his critical thinking and creative solutions;

Dr. Maarten van der Vegt – who grasped my fascination for tidal systems and challenged me to discover the theoretical background of tidal system physics;

Chris Roosendaal, **Henk Markies** and **Marcel van Maarseveen** – who did their very best to explore the experimental limits with me;

Willem-Bart Bartels, **Lisanne Braat**, **Laura Taal, Carolien Wegman** and **Hugo Lantman** – for thoughtful discussions that mattered for the results in this thesis;

Lisanne Braat and **Renske Terwisscha van Scheltinga** – who carried out the preliminary experiments on which this research could proceed;

Lisanne Braat and **Anne Baar** – who performed the first 121 scour hole experiments;

Tjalling de Haas – for all the lovely coffee breaks and support in all stages of the process;

Lex Dolfing – for the lovely diners and support in all stages off the process;

My parents – for motivating me through all stages and supporting me always in every choice I make.

References

Berendsen, H. J. & Stouthamer, E. (2000). Late Weichselian and Holocene palaeogeography of the Rhine-Meuse delta (The Netherlands). *Palaeogeography, Palaeoclimatology, Palaeoecology, 161*(3/4), 311-335.

Berendsen, H. J. & Stouthamer, E. (2001). *Palaeogeographic development of the Rhine-Meuse delta.* Assen: Van Gorcum.

Berendsen, H. J. & Stouthamer, E. (2002). Palaeogeographic evolution and avulsion history of the Holocene Rhine-Meuse delta, The Netherlands. *Netherlands Journal of Geosciences, 81*(1), 97-112.

Boyd, R., Dalrymple, R. W. & Zaitlin, B. A. (2006). Estuary and incised facies models. In H. W. Posamentier & R. G. Walker (Eds.), *Facies models revisited* (Vol. 84, pp. 171-234). Tulsa: SEPM Special Publication.

Cao, S. & Knight, D. (1996). Regime theory of alluvial channels based upon concepts of stream power and probability. *Water, Maritime and Energy, 118*(3), 160-167.

Cao, S. & Knight, D. (1997). Entropy-based design approach of threshold alluvial channels. *Journal of Hydraulic Research, 35*(4), 505-524.

Chen, M. S., Wartel, S., Van Eck, B. & Van Maldegem, D. (2005). Suspended matter in the Scheldt estuary. *Hydrobiologia, 540*, 97-104.

Chorley, R. J. & Kennedy, B. (1971). *Physical geography: a systems approach.* Englewood Cliffs: Prentice Hall.

Coco, G., Zhou, Z., Van Maanen, B., Olanarroeta, M., Tinoco, R. & Townend, I. (2013). Morphodynamics of tidal networks: Advanced and challenges. *Marine Geology, 346*, 1-16.

Coleman, J. M. & Wright, L. D. (1975). Modern river deltas: variability of processes and sand bodies. In M. L. Broussard (Ed.), *Deltas: models for exploration* (pp. 99-149). Houston Geological Society.

Consortium, E. (2007). *Development and demonstration of systems-based estuary simulators.* Joint Defra/EA Flood and Coastal Erosion Risk Management R&D Programme.

Cowell, P., Stive, M., Niedoroda, A., Swift, D., De Vriend, H., Buijsman, M., Nicholls, R., Roy, P., Kaminsky, G., Cleveringa, J., Reed, C. & De Boer, P. (2003). The coastal-tract (part 2): applications of aggregated modeling of lower-order coastal change. *Journal of Coastal Research, 19*(4), 828-848.

Curray, J. R. (1969). Estuaries, lagoons, tidal fiats, and deltas,. In D. J. Stanley (Ed.), *The new concepts of continental margin sedimentation: application to the geological record* (pp. JC-III-I-JC-III-30). Washington, D.C.: American Geological Institute.

Dalrymple, R. W., Zaitlin, B. A. & Boyd, R. (1992). Estuarine facies models: conceptual basis and stratigraphic implications. *Journal of Sedimentary Petrology, 62*(6), 1130-1146.

Dargahi, B. (1990). Controlling mechanism of local scouring. *Journal of Hydraulic Engineering, 116*(10), 1197-1214.

Davidson, N. C., De Laffoley, D., Doody, J. P., Way, L. S., Gordon, J., Key, R., Drake, C. M., Pienkowski, M. W., Mitchell, R. & Duff, K. (1991). *Nature conservation and estuaries in Great Britain.* Peterborough, UK: Nature Conservancy Council.

Davies, G. & Woodroffe, C. D. (2010). Tidal estuary width convergence: Theory and form in North Australian estuaries. *Earth Surface Processes and Landforms, 35*, 737-749.

De Bok, C., Stam, J. M., Turner, A. K. & Maurenbrecker, P. M. (2001). Relation between tidal prism and cross-section area of the inlet of the Eastern Scheldt. *2nd Symposium on River Coastal Estuarine Morphodynamics* (pp. 483-494). Obihiro: International Association for Hydro-Environment Engineering and Research.

De Jong, H. & Gerritsen, F. (1984). Stability parameters of Western Scheldt estuary. *19th International Conference on Coastal Engineering* (pp. 3078-3093). Houston: Coastal Engineering.

Defra. (2002). Futurecoast, Halcrow, Defra CD-Rom, 3 Vols.

Diab, R., Link, O. & Zanke, U. (2010). Geometry of developing and equilibrium scour holes at bridge piers in gravel. *Canadian Journal of Civil Engineering, 37*, 544-552.

Dyer, K. R. (1995). Sediment transport processes in estuaries. In G. M. Perillo (Ed.), *Geomorphology and Sedimentology of Estuaries* (pp. 423-449). Amsterdam: Elsevier.

Engelund, F. & Hansen, E. (1967). *A monograph on sediment transport in alluvial streams.* Teknisk Forlag, Kobenhavn, Denmark.

Euler, T. & Herget, J. (2011). Obstacle-Reynolds-number based analysis of local scour at submerged cylinders. *Journal of Hydraulic Research, 49*(2), 267-271.

Eysink, W. D. (1990). Morphologic response of tidal basins to changes. In B. L. Edge (Ed.), *Coastal Engineering Proceedings 1990* (pp. 1948-1961). New York: ASCE.

Friedrichs, C. T. (1995). Stability shear stress and equilibrium cross-sectional geometry of sheltered tidal channels. *Journal of Coastal Research, 11*, 1062-1074.

Friedrichs, C. T. (2010). Barotropic tides in channelized estuaries. In A. Valle-Levinson (Ed.), *Contemporary Issues in Estuarine Physics* (pp. 27-61). Cambridge: Cambridge University Press.

Friedrichs, C. T. & Aubrey, D. G. (1996). Uniform bottom shear stress and equilibrium hypsometry of intertidal flats. In C. Pattiaratchi, *Mixing in estuaries and coastal seas* (pp. 405-429). Washington: American Geophysical Union.

Friendrichs, C. T. & Aubrey, D. G. (1994). Tidal propagation in strongly convergent channels. *Journal of Geophysical Research, 99*(C2), 3321-3336.

Galloway, W. E. (1975). Process framework for describing the morphologic and stratigraphic evolution of deltaic depositional systems. In M. L. Broussard (Ed.), *Deltas: models for exploration* (pp. 87-98). Houston Geological Society.

Gourgue, O., Baeyens, W., Chen, M., De Brauwere, A., De Brye, B., Deleersnijder, E., E.; Elskens, M. & Legat, V. (2013). A depth-averaged two-dimensional sediment transport model for environmental studies in the Scheldt Estuary and tidal river network. *Journal of Marine Systems, 128*, 27-39.

Green, M. & Coco, G. (2007). Sediment transport on an estuarine intertidal flat: measurements and conceptual model of waves, rainfall and exchanges with a tidal creek. *Estuarine Coastal Shelf Science, 72*(4), 553-569.

Guilcher, A. (1967). Origin of sediments in estuaries. In G. H. Lauff (Ed.), *Estuaries* (pp. 149-157). American Association for the Advancement of Science.

Hey, R. D. & Thorne, C. R. (1986). Stable channels with mobile gravel beds. *Journal of Hydraulic Engineering, 112*(8), 671-689.

Hibma, A., De Vriend, H. J. & Stive, M. J. F. (2003). Numerical modelling of shoal pattern formation in well-mixed elongated estuaries. *Estuarine, Coastal and Shelf Science, 57(5-6),* 981-991.

Hill, K. (2013). *Scientific American*. Retrieved March 17, 2014, from http://blogs.scientificamerican.com/but-not-simpler/2013/05/24/scour-why-most-bridges-fail/

Hughes, S. (1993). *Physical models and laboratory techniques in coastal engineering.* Advanced Series on Ocean Engineering, Vol. 7, World Scientific.

Hume, T. M. & Herdendorf, C. E. (1988). A geomorphic classification of estuaries and its application to coastal resource management. *Journal of Ocean and Shoreline Management, 11*, 249-274.

Huthnance, J. M., Karynarathna, G., Lane, A., Manning, A., Norton, P. A., Reeve, D. E., Spearman, J., Soulsby, R. L., Townend, I. H. & Wright, A.D. (2007). Development of estuary morphological models, Flood Risk Assessment II. *Institute of Mathe- matics and its Applications, Southend on Sea, UK*, 131-140.

Iwasaki, T., Shimizu, Y. & Kimura, I. (2013). Modelling of the initiation and development of tidal creek networks. *Proceedings of the ICE — Maritime Engineering*, 1-13.

Karunarathna, H. & Reeve, D. (2008). A boolean approach to prediction of long-term evolution of estuarine morphology. *Journal of Coastal Research, 24*(2B), 51-61.

Kirkil, G. & Constantinescu, G. (2010). Flow and turbulence structure around an in-stream rectangular cylinder with scour hole. *Water Resources Research, 46*(W11549).

Kleinhans, M. G. (2005). Flow discharge and sediment transport models for estimating a minimum timescale of hydrological activity and channel and delta formation on Mars. *Journal of Geophysical Research, 110*(E12003).

Kleinhans, M. G. (2013). *Research proposal on estuaries.* Utrecht, The Netherlands.

Kleinhans, M. G., Schuurman, F., Bakx, W. & Markies, H. (2008). Meandering channel dynamics in highly cohesive sediment on an intertidal mud flat in the Westerschelde estuary, the Netherlands. *Geomorphology, 105*, 261-276.

Kleinhans, M. G., Van Dijk, W., Van de Lageweg, W. I., Hoendervoogt, R., Markies, H. & Schuurman, F. (2010a). From nature to lab: scaling self-formed meandering and braided rivers. Braunschweig, Germany: International Conference on Fluvial Hydraulics - Riverflow.

Kleinhans, M. G., Buskes, C. J. & De Regt, H. W. (2010b). Philosophy of earth science. In F. Allhoff (Ed.), *Philosophies of the sciences: a guide* (pp. 213-236). Oxford, UK: Wiley-Blackwell.

Kleinhans, M. G., Bierkens, M. F. P. & Van der Perk, M (2010c). On the use of laboratory experimentation: 'Hydrologists, bring out shovels and harden hoses and hit the dirt'. *Hydrology and Earth System Science*, *14*, 369-382.

Kleinhans, M. G. & Van den Berg, J. H. (2011). River channel and bar patterns explained and predicted by an empirical and physics-based method. *Earth Surface Processes Landforms, 36*, 721-738.

Kleinhans, M. G., Van der Vegt, M., Terwisscha van Scheltinga, R., Baar, A. W. & Markies, H. (2012). Turning the tide: experimental creation of tidal channel networks and ebb deltas. *Netherlands Journal of Geosciences, 91*(3), 311-323.

Kleinhans, M. G., Van Rosmalen, T. M., Roosendaal, C. & Van der Vegt, M. (2014a). Turning the tide: mutually evasive ebb- and flood-dominant channels and bars in an experimental estuary. *Advances in Geosciences* (Submitted).

Kleinhans, M. G., Terwisscha van Scheltinga, R., Van der Vegt, M. & Markies, H. (2014b). Turning the tide: growth and dynamics of a tidal basin and inlet in experiments. *Journal of Geophysical Research* (Submitted).

Kleinhans, M. G., Van Dijk, W., Van de Lageweg, W., Hoyal, D., Markies, H., Van Maarseveen, M., Roosendaal, C., Van Weesep, W.; Van Breemen, D., Hoendervoogt, R. & Cheshier, N. (2014c). Quanti

fiable effectiveness of experimental scaling of river- and delta morphodynamics and stratigraphy. *Earth-Science Reviews, 133*, 43-61.

Lacey, G. (1929). Stable channels in alluvium. *Proceedings, Institution of Civil Engineers, 229*, 259-384.

Lanzoni, S. & Seminara, G. (2002). Long-term evolution and morphodynamic equilibrium of tidal channels. *Journal of Geophysical Research, 107*(C1). doi:10.1029/2000JC000468.

Manning, A. (2012). TR167 - Enhanced UK Estuaries database: explanatory notes and metadata. *HR Wallingford Report, DDY0427-RT002-R02-00*.

Marciano, R., Wang., Z. B., Hibma, A., De Vriend, H. J. & Defina, A. (2005). Modeling of channel patterns in short tidal basins. *Journal of Feophydical Research, 110*(F01001).

Martinius, A. W. & Van den Berg, J. H. (2011). *Atlas of sedimentary structures in estuarine and tidally-influenced river deposits of the Rhine-Meuse-Scheldt system.* Houten, The Netherlands: EAGE Publications.

Maynord, S. T. (2006). Evaluation of the micromodel: an extremely small-scale movable bed model. *Journal of Hydraulic Engineering, 132*(4), 343-353.

Mayor-Mora, R. E. (1977). *Laboratory Investigation of Tidal Inlets on Sandy Coasts.* U.S. Army Coastal Engineering Research Centre.

McCoy, A. (2010). *The stagnation point*. Retrieved March 17, 2014, from http://thestagnationpoint.blogspot.nl/2010/09/scour-hole-platte-river-maxwell.html

Meftah, M. B. & Mossa, M. (2006). Scour holes downstream of bed sills in low-gradient channels. *Journal of Hydraulic Research, 40*(4), 497-509.

Morgan, M. (2003). Experiments without material intervention: model experiments, virtual experiments, and virtually experiments. In H. Radder (Ed.), *The philosophy of scientific experimentation* (pp. 216-235). Pittsburgh: University of Pittsburgh Press.

Nichols, M. M. & Biggs, R. (1985). Estuaries. In R. A. Davis (Ed.), *Coastal sedimentary environments* (pp. 77-186). New York: Springer Verlag.

Oreskes, N., Shrader-Frechette, K. & Belitz, K. (1994). Verification, validation, and confirmation of numerical models in the earth sciences. *Science, 263*, 641-646.

Paola, C., Straub, K., Mohrig, D. & Reinhardt, L. (2009). The 'unreasonable effectiveness' of stratigraphic and geomorphic experiments. *Earth-Science Reviews*, *97*, 1-43.

Parker, G., Wilcock, P. R., Paola, C., Dietrich, W. E. & Pitlick, J. (2007). Physical basis for quasi-universal relations describing bankfull hydraulic geometry of single-thread gravel bed rivers. *Journal of Geophysical Research, 112*(4), F04005.

Peakall, J., Ashworth, P. & Best, J. (1996). Physical modelling in fluvial geomorphology: principles, applications and unresolved issues. In B. Rhoads & C. Thorn (Eds.), *The scientific nature of geomorphology* (pp. 222-253). Chichester: Wiley.

Perillo, G. M. (1995). *Geomorphology and sedimentology of estuaries.* Amsterdam: Elsevier.

Porter-Smith, R., Harris, P., Andersen, O., Coleman, R., Greenslade, D. & Jenkins, C. (2004). Classification of the Australian continental shelf based on predicted sediment threshold exceedance from tidal currents and swell waves. *Marine Geology, 211,* 1–20.

Pritchard, D. W. (1967). What is an estuary? Physical viewpoint. In G. H. Lauff (Ed.), *Publication 83* (pp. 3-5). Estuaries: American Association for the Advancement.

Reeve, D. & Karunarathna, H. (2009). On the prediction of long-term morphodynamic response of estuarine systems to sea level rise and human interference. *Continental Shelf Research, 29*, 938-950.

Reeves, G. (2009). Matlab smooth2a function. Pasadena, California, United States: Division of Biology, Caltech.

Reynolds, O. (1889, 1890, 1891). *First, second and third report of the committee appointed to investigate the action of waves and currents on the beds and foreshores of estuaries by means of working models.* Reprinted in: Papers on mechanical and physical subjects, Technical report I, II and III: British Association Report.

Roy, P. S., Thom, B. G. & Wright, L. D. (1980). Holocene sequences on an embayed high energy coast: an evolutionary model. *Sedimentary Geology, 26*, 1-19.

Schramkowski, G. P., Schuttelaars, H. M. & De Swart, H. E. (2004). Non-linear channel-shoal dynamics in long tidal embayments. *Ocean Dynamics, 54,* 399-407.

Schramkowski, G. P., Schuttelaars, H. M. & De Swart, H. E. (2002). The effect of geometry and bottom friction on local bed forms in a tidal embayment. *Continental Shelf Research, 22(11-13)*, 1821-1833.

Savenije, H. (2005). *Salinity and tides in alluvial estuaries.* Amsterdam: Elsevier.

Schuttelaars, H. M., De Jonge, V. N. & Chernetsky, A. (2013). Improving the predictive power when modelling physical effects of human interventions in estuarine systems. *Ocean and Coastal Management, 79*, 70-82.

Silberman, E., Carter, R., Einstein, H., Hinds, J., Powell, R. & ASCE, t. (1963). Friction factors in open channels. *Journal of Hydraulic Engeneering, 89*(HY2), 97-143.

Soulsby, R. & Clarke, S. (2004). *Bed shear stresses under combined waves and currents on smooth and rough beds.* Wallingford: HR Wallingford.

Stefanon, L., Carniello, L., D'Alpaos, A. & Lanzoni, S. (2010). Experimental analysis of tidal network growth and development. *Continental Shelf Research, 30*, 950-962.

Stefanon, L., Carniello, L., D'Alpaos, A. & Rinaldo, A. (2012). Signatures of sea level changes on tidal geomorphology: experiments on network incision and retreat. *Geophysics Research Letters, 39*(2), L12402.

Stive, M., Capobianco, M., Wang, Z., Ruol, P. & Buijsman, M. (1998). Morphodynamics of a tidal lagoon and the adjacent coast. *Proceedings of the 8th international biennial conference on physics of estuaries and coastal seas, 1996*, 397-407.

Tambroni, N., Bolla Pittaluga, M. & Seminara, G. (2005). Laboratory observations of the morphodynamic evolution of tidal channels and tidal inlets. *Journal of Geophysical Research, 110*, F04009.

Todeschini, I., Toffolon, M. & Tubino, M. (2005). Long-term evolution of self-formed estuarine channels. In G. Parker & M. Garcia (Eds.), *River, Coastal and Estuarine Morphodynamics: RCEM 2005* (pp. 161-170). London: Taylor & Francis Group.

Townend, I. (2010). An exploration of equilibrium in Venice Lagoon using an idealised form model. *Continental Shelf Research, 30*, 984-999.

Townend, I. H., Wright, A. P. & Price, D. M. (2000). *An investigation of the gross properties of UK estuaries, EMPHASYS Consortium, Modelling Estuarine morphology and Process.* Wallingford: HR Wallingford.

Van den Berg, J. H., Boersma, J. R. & Van Gelder, A. (2007). Diagnostic sedimentary structures of the fluvial-tidal transition zone - Evidence from deposits of the Rhine and Meuse. *Netherlands Journal of Geosciences, 86*, 287-306.

Van den Berg, J. & Van Gelder, A. (1993). A new bedform stability diagram, with emphasis on the transition of ripples to plane bed in flows over fine sand and silt. *International Association of Sedimentologists, 17*, 11-21.

Van Dijk, W. M., Van de Lageweg, W. I. & Kleinhans, M. G. (2012). Experimental meandering river with chute cutoffs. *Journal of Geophysical Research, 117*, F03023.

Van Dijk, W., Kleinhans, M., Postma, G. & Kraal, E. (2012). Contrasting morphodynamics in alluvial fans and fan deltas: effect of the downstream boundary. *Sedimentology, 59*, 2125-2145.

Van Maanen, B., Coco, G. & Bryan, K. (2013). Modelling the effects of tidal range and initial bathymetry on the morphological evolution of tidal embayments. *Geomorphology, 191*, 23-34.

Van Veen, J. (1950). Ebb and flood channel systems in the Netherlands tidal waters, reprint of the original text. *Journal of the Royal Dutch Geographical Society, 67*, 303-325.

Van Vliet, M. T., Franssen, W. H., Yearsley, J. R., Ludwig, F., Haddeland, I., Lettenmaier, D. P. & Kabat, P. (2013). Global river discharge and water temperature under climate chang. *Global Environmental Change, 23*(2), 450-464.

Van der Wegen, M. & Roelvink, J.A. (2012). Reproduction of estuarine bathymetry by means of a process-based model: Western Scheldt case study, the Netherlands. Geomorphology, 179, 152-167.

Vlaswinkel, B. M. & Cantelli, A. (2011). Geometric characteristics and evolution of a tidal channel network in experimental setting. *Earth Surface Processes and Landforms, 36*(6), 739-752.

Vollmer, S. & Kleinhans, M. G. (2007). Effects of particle exposure, near-bed velocity and pressure fluctuations on incipient motion of particle-size mixtures. In C. Dohmen-Janssen & S. Hulscher (Eds.), *River, coastal and estuarine morphodynamics* (pp. 541-548). London, UK: Taylor and Francis/Balkema.

Vos, P. C., Bazelmans, J., Weerts, H. J. & Van der Meulen, M. J. (2011). *Atlas van Nederland in het Holoceen* (ISBN 978-90-351-3639-7 ed.). Bert Bakker, Amsterdam.

Wang, Z., Karssen, B., Fokkink, R. & Langerak, A. (1998). A dynamic–empirical model for estuarine morphology. *Proceedings of the 8th international biennial conference on physics of estuaries and coastal seas*, 279-286.

Whitehouse, R. (1995). Observations of the boundary layer characteristics and the suspension of sand at a tidal site. *Continental Shelft Research, 15*(13), 1549-1567.

Yalin, M. (1971). *Theory of hydraulic models.* London, UK: Macmillan.

Zanke, U. C. E. (2003). On the influence of turbulence on the initiation of sediment motion. *International Journal of Sediment Research, 18(1),* 1-15.

Appendix 1: Symbols and units used

Symbol	*Property*	*Units*
a	Tidal amplitude real scale estuaries	m
a	Tidal amplitude experiments	mm
A_m	Cross-sectional area at mouth	m^2
c_d	Drag coefficient	(-)
c_n	Sediment concentration	$kg \cdot m^{-3}$
C	Chézy coefficient	$m^{0.5} \cdot s^{-1}$
C'	Chézy coefficient – grain related	$m^{0.5} \cdot s^{-1}$
D_{10}	Grain size (10th percentile)	mm
D_{50}	Grain size (median)	mm
D_{90}	Grain size (90th percentile)	mm
D_*	Dimensionless grain size	(-)
f	Friction factor	(-)
Fr	Froude number	(-)
g	Gravitational acceleration	$m \cdot s^{-2}$
h	Water depth estuary channel average	m
h_s	Water depth estuary including tidal flats	m
$<h>$	Water depth tidal average	m
h_r	Water depth river	m
HWS	High water slack	(-)
k	Wave number	m^{-1}
k_s	Nikuradse roughness length	m
L_e	Length of estuary	m
L_A	Convergence e-folding length for cross-sectional area	m
L_h	Convergence e-folding length for depth	m
L_w	Convergence e-folding length for width	m
LWS	Low water slack	(-)
m_e	Erosion constant	(-)
P	Tidal prism	m^3
q_s	Suspended sediment transport	$m^2 \cdot s^{-1}$
Q	Discharge	$m^3 \cdot s^{-1}$
r	Friction factor	(-)
R	Relative submerged density	(-)
Re	Reynolds number	(-)
$Re*$	Reynolds particle number	(-)
S_v	Valley slope	(-)
S_{hw}	Surface area at high water	m^2
t	Time	s
T	Tidal period	s
u	Flow velocity	u
$u*$	Shear velocity	$m \cdot s^{-1}$
U	Velocity amplitude	$m \cdot s^{-1}$

w_s	Fall velocity of sediment	$m \cdot s^{-1}$
$W(x)$	Channel width at location x	m
W_m	Channel width at mouth	m
W_r	Reference channel width river	m
x	Location along channel from inlet	m
z_0	Bed roughness length	m
α	Channel geometry constant	$s^{0.5} \cdot m^{-0.5}$
ϑ	Shields number	(-)
ν	Kinematic viscosity of water	$m^2 \cdot s^{-1}$
ρ or ρ_w	Density water	$kg \cdot m^{-3}$
ρ_s	Density sediment	$kg \cdot m^{-3}$
τ	Bed shear stress	Pa
τ_{cr}	Critical bed shear stress	Pa
φ	Phase lag between high water and HWS	Rad
ω	Tidal frequency	s^{-1}
ω_{pv}	Potential specific stream power	$W \cdot m^{-2}$

Appendix 2: Scour hole experiments for sediment selection

Introduction

Scour holes are depressions in the bed surface of a river or other water conducting channel with dimensions independent on channel dimensions and often larger than the water depth (Fig. 40). Scour holes seem to develop under three conditions: (1) around and downstream of an obstacle at the bed such as a bridge pile, groyne or obstruction (Kirkil & Constantinescu, 2010), (2) spontaneous under some critical flow and sediment conditions (Kleinhans et al., 2014c), (3) at convergence of flow.

Scour holes are of interest for this research, because scour holes were found to be unwanted effects of hydraulic smooth conditions in scale experiments (Fig. 40d). Previous experiments of river and tidal systems showed the formation of scour holes (Tambroni et al., 2005; Stefanon et al., 2010; Van Dijk et al., 2012; described by Kleinhans et al., 2014c). When experimental scour holes are scaled to real world cases, they are unrealistically deep. Besides, the scours cause a severe alteration of the hydraulics.

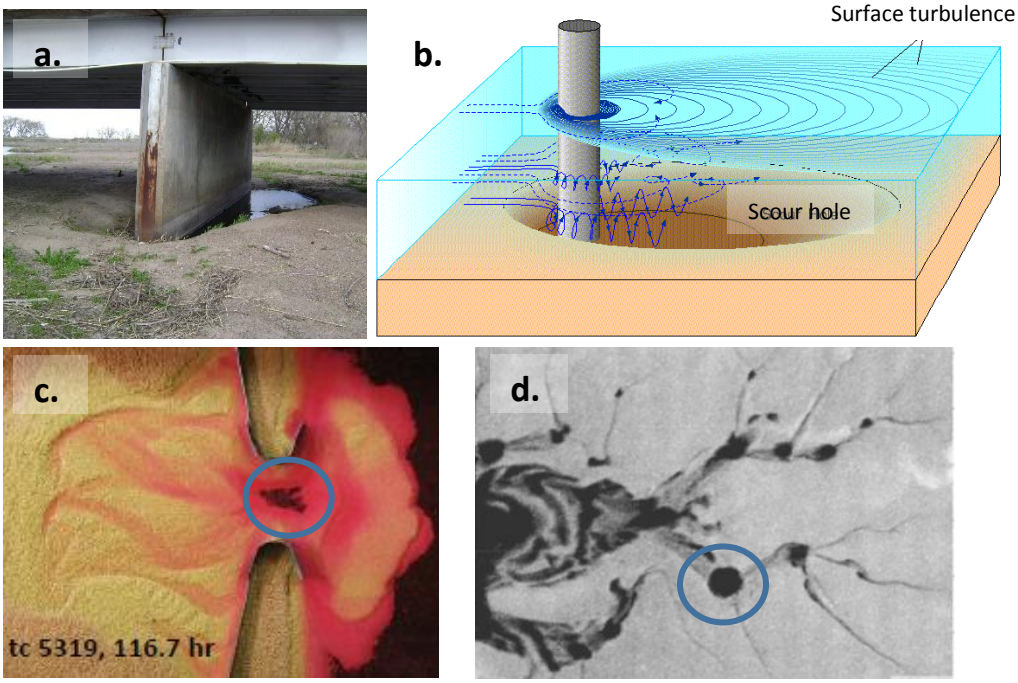

Fig. 40: Examples of scour holes: (a) around a bridge pier (McCoy, 2010); (b) schematic picture (Hill 2013); (c) due to convergence of flow in a laboratory experiment of a tidal system (Kleinhans et al., 2014b); (d) spontaneous in a laboratory experiment of a tidal system (Stefanon et al., 2010).

Dargahi (1990) has described the scour mechanisms at a circular obstacle with an experimental study (later reviewed by Kirkil & Constantinescu (2010)). He described one mechanism for the initiation and one for the later stages of scour holes. First, the scour initiates at the sides of the cylinder due to the strong acceleration of the flow as it passes the cylinder. The later stages are characterised by a vortex in the shape of a horseshoe (Fig. 41), which plays a dominant role in the growth of the scour downstream of the cylinder. Once the scour formed, the horseshoe vortex becomes stable. From then on, most scour takes place around the upstream base of the obstacle.

Other studies elaborated further on the formation of scour holes. Kirkil & Constaninescu (2010) describe the mechanisms that form scour holes and study obstacles of other than round shapes, for which they use both an experimental and numerical model approach. Euler and Herget (2011) investigated the effect of submerged obstacle dimensions on scour hole formation. They created dimensionless relations between equilibrium scour depth and a combination of obstacle turbulence and flow conditions. Other studies concern the geometry of scour holes and the depth of

this phenomenon at equilibrium, which is relevant for management strategies on obstructions in rivers or estuaries (e.g. Meftah & Mossa, 2006; Diab et al., 2010). So far, no results were published about the conditions under which scour holes occur in scaled laboratory experiments.

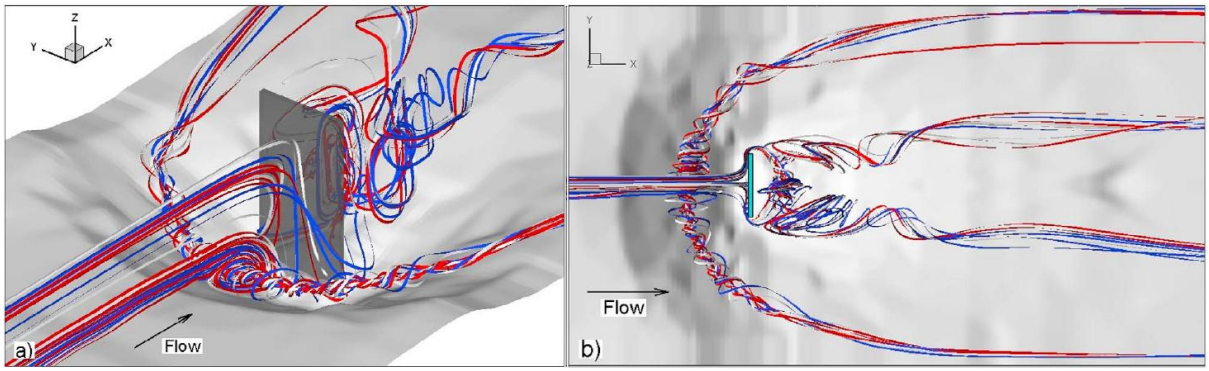

Fig. 41: Visualisation of the (horseshoe) vortices around an obstacle that cause scouring (Kirkil & Constantinescu, 2010). (a) 3-D view; (b) top view.

Past research on scour holes focused mainly on real world applications, such as scouring around bridge piers (Kirkil & Constantinescu, 2010; Euler & Herget, 2011). Scour holes in small scale laboratory experiments have been reported (Maynord, 2006; Stefanon et al., 2010), but the conditions under which these scour holes evolve are poorly understood.

Scouring is one of the major problems of scaled laboratory experiments (Tambroni et al., 2005; Stefanon et al., 2010; Kleinhans et al., 2014c). The scours are unrealistically deep, with dimensions independent of channel depth and often larger than channel depth (Kleinhans et al., 2014). They probably result from the near-bed hydraulic smooth flow conditions.

Particle size, shape and distribution effect roughness and turbulence (Kleinhans et al., 2014c). The occurrence of scour holes can thus be reduced when poorly sorted sediments are used (Van Dijk et al., 2012). When larger particle sizes are used, the Reynolds particle number can be far above the threshold below which scour holes and ripples form (Kleinhans et al., 2014c). Scour holes were prevented in previous experiments by using a poorly sorted unimodal sediment mixture.

Preliminary experiments on the occurrence of scours showed that the actual limit below which scour holes and ripples form is rather at the lower end of the transition from smooth to hydraulic rough conditions (Re* 3.5 – 70) (Kleinhans et al., 2014c). They hypothesised that the transition might be around Reynolds particle numbers of 5-10. Compared to empirical bedform stability diagrams (Van den Berg & Van Gelder, 1993), this transition takes place in the lowest part of the Shields curve (Kleinhans, 2005; Vollmer & Kleinhans, 2007).

When the conditions under which scour holes form are known, it is possible to prevent scour holes in two ways: (1) use hydraulic conditions outside the scour hole regime or (2) use a sediment mixture that does not scour under the required hydraulic conditions.

This research extends on the first experiments reported by Kleinhans et al. (2014c). The goal was to determine the range of hydraulic conditions and grain sizes under which scour holes occur in scaled laboratory experiments. The main target was to identify the sediment mobility, hydraulic roughness and sediment properties (grain size and density) under which scour holes form and are stable.

Method

In total 385 recordings were made on the occurrence of scour holes. All the recordings were classified as one of the following: (1) no motion, (2) no scours, (3) provokable scours that do refill after removal of obstacle, (4) provokable scours that stay after removal of obstacle, (5) self-formed scours, (6) ripples, (7) sheet flow. I used scours that can be provoked and stay after removal of the obstacle to identify the hydraulic conditions under which autogenic scour holes would occur in scaled laboratory experiments.

In a flume water flow was generated (Fig. 42). In the middle of the flume, a plane layer of sediment (0.05 m height) with known properties was located (Fig. 42). During the experiment the flow velocity was increased stepwise. For each flow condition observations were made on the sediment motion and scours or ripples if occurring without any obstacles present. Thereafter, scour holes were provoked by inserting obstacles in the sediment bed. The diameters of the obstacles were 1.5-15 mm. When an obstacle triggered the formation of a scour hole (provocation), the obstacle was removed after equilibrium. I recorded whether the remaining scour hole filled in (provocation and filled) or not (provocation and not filled). A wide range of sediment mixtures was used, including light-weight, uniform and poorly sorted sediments (Table 13).

After classification, I calculated characteristic dimensionless numbers: Reynolds particle number (Re^*, Eq. 26), dimensionless grain size (D^*, Eq. 31) and sediment mobility (ϑ, Eq. 28). For Reynolds particle number, both the values based on D_{50} and D_{90} were calculated. All the data were plotted in a bedform stability diagram (Van den Berg & Van Gelder, 1993). Obstacle diameter was subtracted from the grain size to visualise the measurements with different obstacle sizes. Furthermore, relative obstacle size (obstacle diameter divided by D_{50}) was plotted against thickness the boundary layer (Re^* based on D_{90}).

Table 13: Characteristics of the sediment types used in the scour hole experiments.

Sediment type	Density (kg·m^{-3})	D_{10} (mm)	D_{50} (mm)	D_{90} (mm)
Polystyrene	1042	1.0	2.1	2.8
Blasting polymer mix 1	1200	0.7	1.2	1.5
Blasting polymer mix 2	1200	0.3	0.6	1.2
Blasting polymer (REG 3)	1200	0.5	0.6	0.7
Blasting polymer (REG 2)	1200	-	1.0	1.3
Blasting polymer (REG 1.5)	1200	-	1.1	1.3
Blasting polymer (REG 1)	1200	-	1.6	1.8
Sand (river origin)	2650	-	0.5	1.2
Sand (beach origin)	2650	-	0.2	0.3

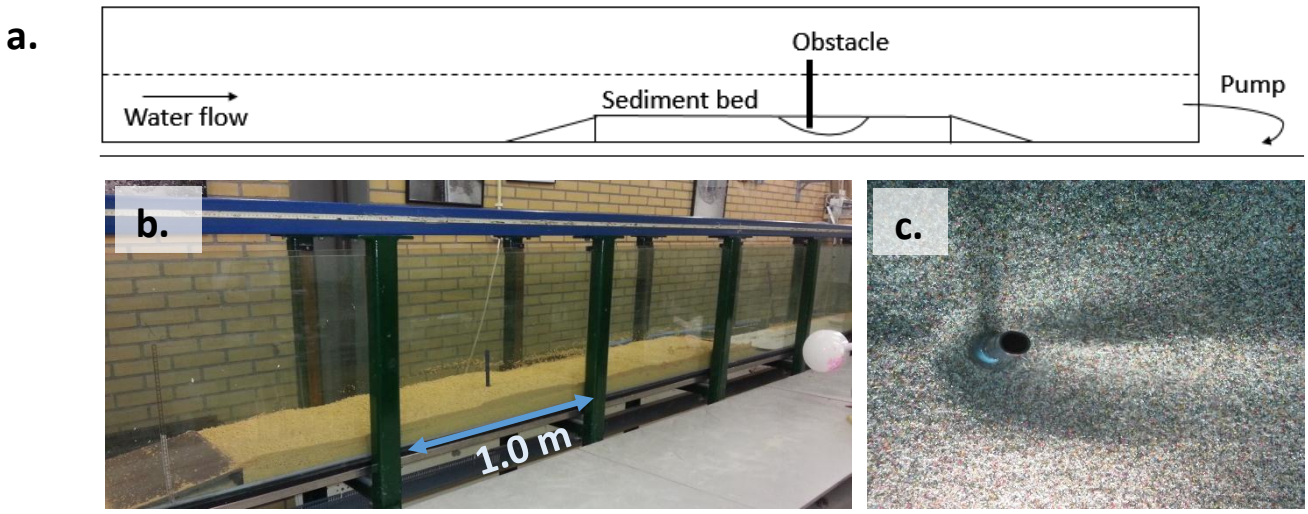

Fig. 42: (a) Schematic overview of the experimental setup for the scour hole experiments. The length of the sediment bed was approximately 3 m. (b) Image of the experimental setup. (c) Example of scour hole provocation. The diameter of the obstacle in both images is 15 mm.

Results

All experiments showed similar trends under increasing flow velocities. However, the absolute transitional flow velocities are dependent on sediment characteristics.

First, the transition from no sediment motion to motion took place. Around this transition, the larger obstacles (± 15 mm) tended to provoke scours. The formed scours generally stay because there is too little sediment motion upstream of the scour hole to fill. With increased flow velocities, scours also form with smaller obstacle diameters. Even higher flow velocities lead in most cases to refilling of scour holes after they had been provoked. The experiments stopped when sediment was so mobile that recordings were impossible – either the sheet flow or ripple regime.

It appears that scour holes occur at the lower end of the ripple regime in the bedform stability diagram (Fig. 43abc). Results for different densities are shown in different figures, since density affects the trend. For higher sediment mobility scour holes refill after provocation. For both sand and blasting polymer (ρ = 1200 kg m^{-3}), scour holes occur with sediment mobility between 0.02 and 0.1 (Fig. 43ab). Only the polystyrene sediment (ρ = 1042 kg m^{-3}) showed no tendency to scour at all (Fig. 43c). The coarser the sediments are, the lower the mobility values are for the transition between scours that stay and scours that refill.

Going from the ripple regime to the dunes regime, sand and polystyrene become unsusceptible for the formation of scours. In contrast, the light-weight blasting polymer sediment still formed scours in the dune regime and at the ripple-dune transition (Fig. 43b). The results show some scatter. Ripples and self-formed scours occur also in the upper end of the provokable scours that stay and in the refilling scour regime.

The effect of a certain obstacle size is dependent on the boundary layer thickness (Re^*_{90}), which is dependent of the grain size and shear stress. For thin boundary layers (Re^*_{90}<10), small obstacles have no effect, while larger obstacles cause autogenic scours (Fig. 43de). Thicker boundary layers (Re^*_{90}>10) form autogenic scours with smaller obstacles and refilling scour holes with larger obstacles. The polystyrene sediment only scours with largest obstacle diameter (Fig. 43f).

There is a trend between dimensionless grain size and Reynolds particle number (Re^*_{50}) under which autogenic scour holes occur (Fig. 44). Autogenic scour holes in sands occur for Re^* between 2 and 8. For light-weight blasting polymer, scour holes occur for Re^* 2-4 in fine sediments and 20-30 in coarse sediments.

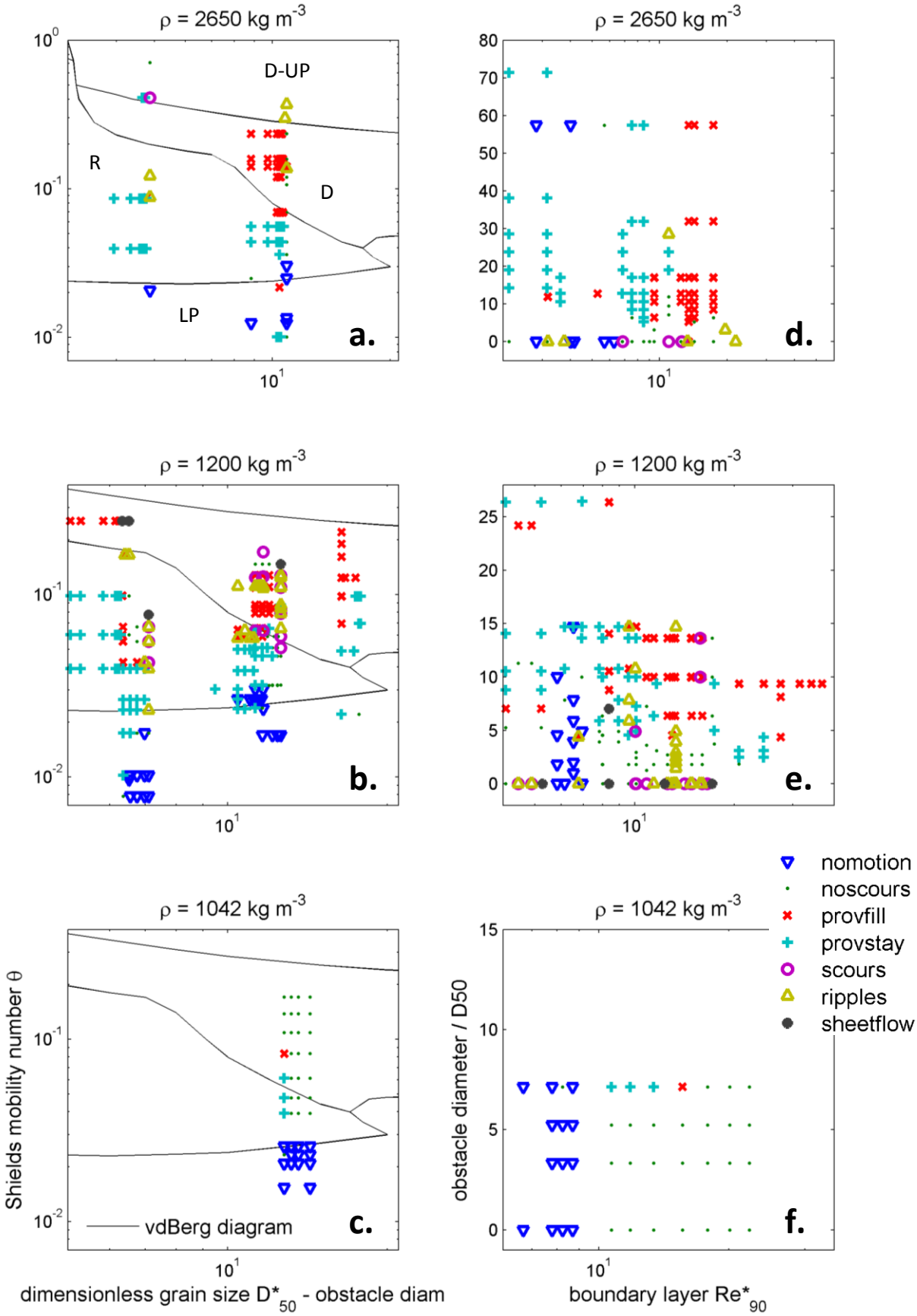

Fig. 43: (left) Shields mobility number (ϑ) against dimensionless grain size (D). Obstacle diameter was subtracted from the grain size to visualise the measurements with different obstacles sizes. LP = lower stage plane bed, R = ripples, D = dunes and D-UP = transition from dunes to upper stage plan bed. (right) Relative obstacle size against thickness the boundary layer (Re* based on D90). Upper figures (a,d) correspond to experiments with quartzite sand, middle (b,e) to blasting polymer sediment and lower (c,f) to polystyrene sediment.*

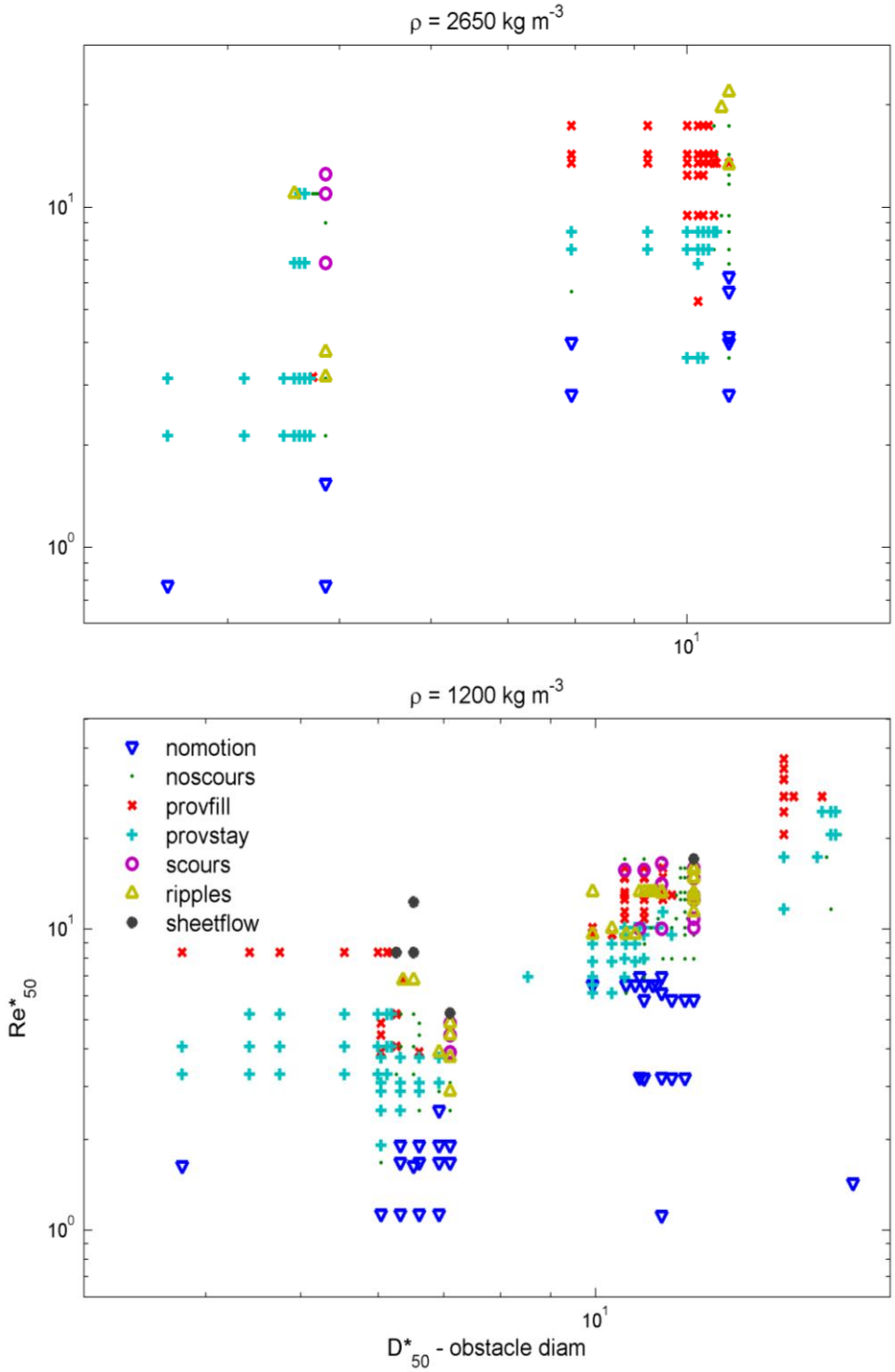

Fig. 44: Reynolds particle number (Re) against dimensionless grain size (D*) for sand (top) and light-weight blasting polymer sediment (bottom).*

Discussion

I found that all sediments used in this study scoured just above the beginning of motion, except for the light-weight polystyrene sediment. Scour holes form in the range of sediment mobility between 0.02 and 0.1. This is in agreement with the hypothesis of Kleinhans et al. (2014c). Since the sediment mobility was around the beginning of motion in most previous scaled laboratory experiments, this partly addresses the formation of scour holes in these experiments.

The hydraulic conditions under which autogenic scours form are dependent on grain size and sediment density. The hypothesis that scours occur at the lower end of the transition from hydraulic smooth to hydraulic rough (Re* 3.5-70) (Kleinhans et al., 2014c) is confirmed for sand and fine grained light-weight blasting polymer. However, for coarser light-weight sediments, scours are stable at higher values (Re* 20-30). So it appears that the laminar boundary layer is thicker for coarser sediments, but that generated turbulence can still penetrate through this layer to create scour under higher shear stresses.

Stefanon et al. (2010) and Tambroni et al. (2005) found scour holes in their laboratory experiments of tidal systems. Experiments with light-weight polystyrene sediment in this study were unsusceptible for scouring (Kleinhans et al., 2014b; this study). While I used the same material as Stefanon et al. (2010), I probably observed no scour holes in my experiments because sediment mobility and Reynolds particle number were higher (Table 14).

The dimensionless grain size (D*), Shields number (θ) and Reynolds particle number (R*) were calculated for previous laboratory experiment of tidal systems and for the estuary experiments of this study (Table 14). The hydraulic conditions of experiments in which scour holes or ripples occurred (Tambroni et al., 2005; Stefanon et al., 2010; blasting polymer in this study) match the range of conditions indicative for autogenic scours.

Table 14: Characteristic properties of sediment and flow in laboratory experiments of tidal systems. Dimensionless grain size (D), Shields number (ϑ) and Reynolds particle number (R*) were calculated from grain size, density, water depth and flow velocity.*

Study	**D_{50} (m)**	**D_{90} (m)**	**ρ (kg·m^{-3})**	**D^*_{50}**	**h (m)**	**u (m·s^{-1})**	**θ**	**Re^*_{50}**	**Re^*_{90}**
Stefanon et al. (2010)	0.0008	0.0013	1041	5.4	0.05	0.05	0.05	2.8	4.5
Tambroni et al. (2005)	0.0003	0.0004	1480	4.8	0.082	0.24	0.14	3.9	5.0
Kleinhans et al. (2014b)	0.0021	0.0028	1042	14.3	0.025	0.25	0.91	51.5	68.6
Exp. 26 polyst. (this study)	0.0021	0.0028	1042	14.3	0.012	0.10	0.23	25.7	34.5
Exp. 39 polymer (this study)	0.0012	0.0016	1200	13.7	0.014	0.15	0.12	17.4	23.7

The experiments that are unsusceptible for scours have both high Reynolds particle numbers and relatively high sediment motilities. The requirement of sufficient sediment mobility conflicts with the requirement for hydraulic rough bed conditions. A poorly sorted mix of blasting polymer sediment was used for the estuary experiments in this study to prevent scours from occurring. However, this might have resulted in opposite effects. An increase in the median (D_{50}) of the sediment might have increased the threshold for hydraulic rough conditions and decreased the sediment mobility. In other words, the theory for sandy sediments, in which a poorly sorted sediment with a coarse tail is used to prevent scouring, might not work for light-weight sediments.

I confirm the hypothesis that autogenic scour holes form at the lower end of the transition from hydraulic rough to hydraulic smooth (Re* 3.5-70) and just above the beginning of motion in the ripple regime of the bedform stability diagram. However, critical Reynolds particle numbers (Re*) for the occurrence of scour holes seem dependent on grain size and sediment density for light-weight sediments. This might explain why the blasting polymer used in the estuary experiments in this research showed scouring tendency. In contrast, the polystyrene sediment was not susceptible for scours at all.

Since lightweight sediment is often used in scaled laboratory experiments, the desire for a solid predictor of scour holes still remains. This might require a new dimensionless number that includes the sediment en hydraulic properties important for scour hole formation, such as grain size and density and a flow properties. Better understanding of the exact conditions under which scours form is required for further proceedings in laboratory experiments.

Appendix 3: Coastal environments in Fig. 4b

Deltas

1 Mississippi Delta, USA
2 Chang Jiang Delta, China
3 Ebro Delta, Spain
4 Sao Francisco Delta, Brazil
5 Mahakam Delta, Indonesia
6 Klang-Langat Delta, Malaysia
7 Fly River Delta, New Guinea
8 Colorado Delta, Mexico

Wave-dominated Estuaries

9 San Antonio Bay, USA
10 Hawksbury Estuary, Australia
11 Lavaca Bay, USA
12 Miramichi River, Canada
13 Lake Macquarie, Australia
14 Mgeni Estuary, South Africa
15 Eastern Shore estuaries, Nova Scotia, Canada

Mixed-energy Estuaries

16 St. Lawrence River, Canada
17 Gironde River, France
18 Raritan River, USA
19 Humber River, GB
20 James River, USA
21 Ogeechee River, USA
22 Chesapeake Bay, USA
23 Delaware Bay, USA
24 Willapa Bay, USA
25 Oosterschelde Estuary, The Netherlands
26 Corio Bay, Australia

Tide-dominated Estuaries

27 Cook Inlet, Alaska
28 Ord River, Australia
29 South Alligator, Daily and Adelaide Rivers, Australia
30 Severn River, GB
31 Broad Sound, Australia
32 Cumberland Basin, Canada
33 Cobequid Bay-Salmon River and Avon River, Canada

Prograding Strand Plains

34 Senegal Delta
35 Shoalhaven River, Australia
36 Yaquina Bay, USA
37 Nayarit, Mexico

Prograding Tidal Flats

38 Mont St. Michel Bay, France
39 Head of the German Bight
40 East coast, Taiwan

Appendix 4: QR-codes for online material

Movie of Experiment 26: first 2280 tidal cycles (approximately 14 hours).
(https://www.youtube.com/watch?v=fgN-F7U-jeA&feature=youtu.be)

Movie of Experiment 32: first 3000 tidal cycles (approximately 18 hours).
(https://www.youtube.com/watch?v=s3VWRXjT16Q&feature=youtu.be)

Movie of Experiment 39: first 6000 tidal cycles (approximately 116 hours).
(https://www.youtube.com/watch?v=DRzt5ZyI4-k&feature=youtu.be)

Appendix 5: List of figures

Appendix 6: List of tables

Appendix 7: Logical explanation structure used in this research

Three types of logical explanation structures are used in science: (1) induction, (2) deduction and (3) abduction (Fig. 45). In this research, deduction is the most dominant logical explanation structure (Fig. 45). In the model approach, I combined initial and boundary conditions with laws of nature to derive the effect of river flow on estuary equilibrium. The laboratory experiments started with an initial situation and boundary conditions, after which behaviour was controlled by the laws of physics.

In some cases, deduction was combined with induction. For example, a large dataset of estuaries in the United Kingdom was used to determine generalisations on the effect of river flow on estuary dimensions. Furthermore, combining al the experimental results to find similar trends is also induction.

All three types of explanations (Fig. 45) have strengths and weaknesses (Kleinhans, 2010b). One of the problems of induction is that the empirical relations found are often only valid for a small range of conditions, for example just for one type of estuaries. This problem of induction was recognised for example in using the dataset of UK estuaries: different subsets of estuary types resulted in different empirical relations.

In deduction, the model outcome depends on the physical laws chosen and on how well these laws describe natural phenomenon. These laws are never perfect, while initial and boundary conditions may be based on a limited amount of measurements and may contain errors. Furthermore, it is impossible to fully verify and validate numerical models of natural systems (Oreskes, 1994), because natural systems are never closed and model results are always non-unique (Kleinhans et al., 2010b; Kleinhans et al., 2010c).

Experimental limitations in deduction are different from those in model approach. While the physics is more real than in models (Morgan, 2003), validity can be restricted by scale effects (Kleinhans, 2010b). Peakall et al. (1996) discussed that proper analysis of dimensionless numbers in combination with experimental and real scale modelling can reduce the limitations of scale experiments. Since induction and deduction are used in this study, it is recommended for further research to add the abduction approach. For example, a unique historical record of estuaries in the Netherlands (Berendsen & Stouthamer, 2000, 2001, 2002; Vos et al., 2011) can be used to complement numerical and physical models in this study.

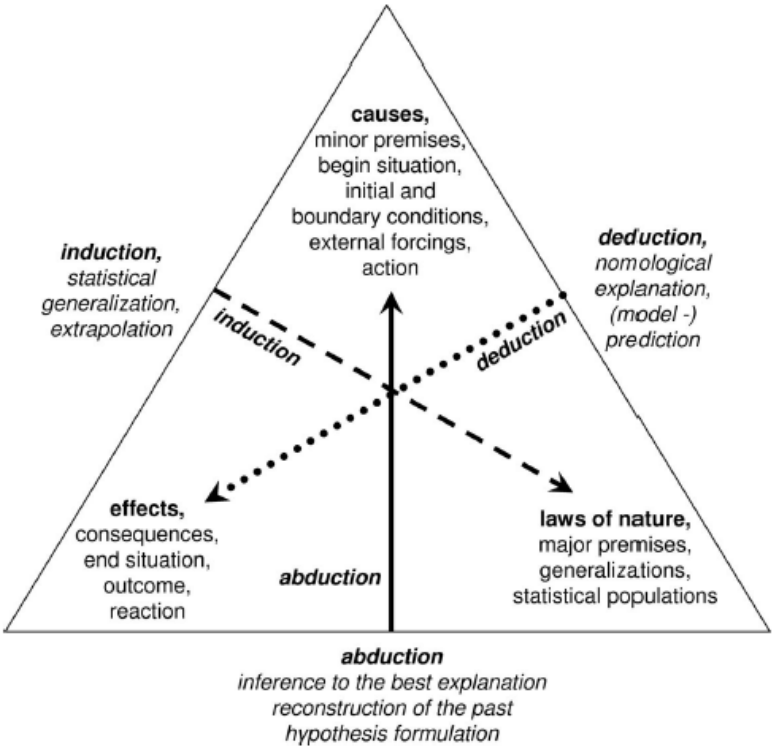

Fig. 45: Source: Kleinhans et al. (2010b). The three logical explanation structures used in science. They are based on the three pillars – causes, effects and laws. Two of these are required to arrive at the third. Each methods has its own weakness.